



Machine Learning on Population Imaging for Mental Health

Kamalaker Dadi

► To cite this version:

Kamalaker Dadi. Machine Learning on Population Imaging for Mental Health. Medical Imaging. Université Paris-Saclay, 2020. English. NNT : 2020UPASG001 . tel-02949546

HAL Id: tel-02949546

<https://theses.hal.science/tel-02949546>

Submitted on 25 Sep 2020

HAL is a multi-disciplinary open access archive for the deposit and dissemination of scientific research documents, whether they are published or not. The documents may come from teaching and research institutions in France or abroad, or from public or private research centers.

L'archive ouverte pluridisciplinaire **HAL**, est destinée au dépôt et à la diffusion de documents scientifiques de niveau recherche, publiés ou non, émanant des établissements d'enseignement et de recherche français ou étrangers, des laboratoires publics ou privés.

Machine learning on population imaging for mental health

Thèse de doctorat de l'université Paris-Saclay

École doctorale n° 580, Sciences et technologies de l'information et de la communication (STIC)
Spécialité de doctorat: Mathématiques et Informatique
Unité de recherche: Université Paris-Saclay, Inria, Inria Saclay-Île-de-France, 91120, Palaiseau, France
Référent: : Faculté des Sciences d'Orsay

Thèse présentée et soutenue à Palaiseau, le 14 septembre 2020, par

Kamalaker Reddy DADI

Composition du jury:

Michel Thiebaut de Schotten	Président
Directeur de recherche, Groupe d'Imagerie Neurofonctionnelle (GIN), Université de Bordeaux, France	
Sylvia Villeneuve	Rapportrice & Examinatrice
Maître assistant, HDR, Department of Psychiatry, McGill University, Canada	
Pierre Bellec	Rapporteur & Examinateur
Maître de conférences, HDR, Centre de recherche de l'institut Universitaire de gériatrie de Montréal, Université de Montréal, Canada	
Camille Maumet	Examinatrice
Chargée de recherche, Empenn INRIA, Université Rennes I, France	
Vincent Frouin	Examinateur
Directeur de recherche, CEA Neurospin, Université Paris-Saclay, France	
Gaël Varoquaux	Directeur de thèse
Directeur de recherche, Parietal Inria, Université Paris-Saclay, France	
Bertrand Thirion	Codirecteur de thèse
Directeur de recherche, Parietal Inria, Université Paris-Saclay, France	
Denis Engemann	Invité
Chargé de recherche, Parietal Inria, Université Paris-Saclay, France	
Josselin Houenou	Invité
Directeur de recherche, Psychiatry Team, UNIACT Lab, Université Paris-Saclay, France	

MACHINE LEARNING ON POPULATION
IMAGING FOR MENTAL HEALTH

KAMALAKER DADI

*Dissertation submitted in partial fulfillment of the
requirements for the degree of Doctor of Philosophy.*

UNIVERSITÉ PARIS-SACLAY
SCIENCES ET TECHNOLOGIES DE L'INFORMATION
ET DE LA COMMUNICATION

October 2017 – September 2020
Parietal team, Inria Saclay / Neurospin, CEA. France

PH.D. COMMITTEE

DIRECTOR:

Dr. Gaël Varoquaux, Parietal Inria, Université Paris-Saclay, France

CODIRECTOR:

Dr. Bertrand Thirion, Parietal Inria, Université Paris-Saclay, France

SUPERVISORS:

Dr. Denis Engemann, Parietal Inria, Université Paris-Saclay, France

Dr. Josselin Houenou, CEA, Neurospin, Université Paris-Saclay, France

REVIEWERS:

Dr. Sylvia Villeneuve, McGill University, Canada

Dr. Pierre Bellec, Université de Montréal, Canada

EXAMINERS:

Dr. Camille Maumet, INRIA, Université Rennes I, France

Dr. Vincent Frouin, CEA Neurospin, Université Paris-Saclay, France

JURY PRESIDENT:

Dr. Michel Thiebaut de Schotten, Université de Bordeaux, France

This thesis was prepared in Parietal team, at Inria Saclay and Neurospin, CEA, from October 2017 to September 2020. It was funded by the Institut national de recherche en informatique et en automatique.

© Kamalaker Dadi, September 2020

ABSTRACT

Mental disorders display a vast heterogeneity across individuals. A fundamental challenge to studying their manifestations or risk factors is that the diagnosis of mental pathological conditions are seldom available in large public health cohorts. Here, we seek to develop brain signatures, biomarkers, of mental disorders. For this, we use machine learning to predict mental-health outcomes through population imaging i. e. with brain imaging (Magnetic Resonance Imaging (MRI)). Given behavioral or clinical assessments, population imaging can relate unique features of the brain variations to these non-brain self-reported measures based on questionnaires. These non-brain measurements carry a unique description of each individual's psychological differences which can be linked to psychopathology using statistical methods. This PhD thesis investigates the potential of learning such imaging-based outcomes to analyze mental health. Using machine-learning methods, we conduct an evaluation, both a comprehensive and robust, of population measures to guide high-quality predictions of health outcomes.

This thesis is organized into three main parts: first, we present an in-depth study of connectome biomarkers, second, we propose a meaningful data reduction which facilitates large-scale population imaging studies, and finally we introduce proxy measures for mental health.

We first set up a thorough benchmark for imaging-connectomes to predict clinical phenotypes. With the rise in the high-quality brain images acquired without tasks, there is an increasing demand in evaluation of existing models for predictions. We performed systematic comparisons relating these images to clinical assessments across many cohorts to evaluate the robustness of population imaging methods for mental health. Our benchmarks emphasize the need for solid foundations in building brain networks across individuals. They outline clear methodological choices.

Then, we contribute a new generation of brain functional atlases to facilitate high-quality predictions for mental health. Brain functional atlases are indeed the main bottleneck for prediction. These atlases are built by analyzing large-scale functional brain volumes using scalable statistical algorithm, to have better grounding for outcome prediction. After comparing them with state-of-the-art methods, we show their usefulness to mitigate large-scale data handling problems.

The last main contribution is to investigate the potential surrogate measures for health outcomes. We consider large-scale model comparisons using brain measurements with behavioral assessments in an

imaging epidemiological cohort, the United Kingdom (UK) Biobank. On this complex dataset, the challenge lies in finding the appropriate covariates and relating them to well-chosen outcomes. This is challenging, as there are very few available pathological outcomes. After careful model selection and evaluation, we identify proxy measures that display distinct links to socio-demographics and may correlate with non-pathological conditions like the condition of sleep, alcohol consumption and physical fitness activity. These can be indirectly useful for the epidemiological study of mental health.

RÉSUMÉ

Les troubles mentaux présentent une grande hétérogénéité entre les individus. Une difficulté fondamentale pour étudier leurs manifestations ou leurs facteurs de risque est que le diagnostic des conditions mentales pathologiques est rarement disponible dans les grandes cohortes de santé publique. Ici, nous cherchons à développer des biomarqueurs, signatures cérébrales de troubles mentaux. Pour cela, nous utilisons l'apprentissage automatique pour prédire les résultats de santé mentale grâce à l'imagerie de population, en se basant sur l'imagerie cérébrale (imagerie par résonance magnétique (IRM)). Compte tenu des évaluations comportementales ou cliniques, l'imagerie de population peut relier les caractéristiques uniques des variations cérébrales à ces mesures autodéclarées non cérébrales basées sur des questionnaires. Ces mesures non cérébrales fournissent une description unique des différences psychologiques de chaque individu qui peuvent être liées à la psychopathologie à l'aide de méthodes statistiques. Cette thèse de doctorat examine le potentiel d'apprentissage de tels résultats basés sur l'imagerie pour analyser la santé mentale. En utilisant des méthodes d'apprentissage automatique, nous effectuons une évaluation, à la fois complète et robuste, des mesures de population pour guider des prévisions de haute qualité des résultats pour la santé.

Cette thèse est organisée en trois parties principales : premièrement, nous présentons une étude approfondie des biomarqueurs du connectome, deuxièmement, nous proposons une réduction significative des données qui facilite les études d'imagerie de population à grande échelle, et enfin nous introduisons des mesures indirectes pour la santé mentale.

Nous avons d'abord mis en place une étude approfondie des connectomes d'imagerie afin de prédire les phénotypes cliniques. Avec l'augmentation des images cérébrales de haute qualité acquises en l'absence de tâche explicite, il y a une demande croissante d'évaluation des modèles prédictifs existants. Nous avons effectué des comparaisons systématiques reliant ces images aux évaluations cliniques dans de

nombreuses cohortes pour évaluer la robustesse des méthodes d'imagerie des populations pour la santé mentale. Nos résultats soulignent la nécessité de fondations solides dans la construction de réseaux cérébraux entre les individus. Ils décrivent des choix méthodologiques clairs.

Ensuite, nous contribuons à une nouvelle génération d'atlas fonctionnels du cerveau pour faciliter des prédictions de haute qualité pour la santé mentale. Les atlas fonctionnels du cerveau sont en effet le principal goulot d'étranglement pour la qualité de la prédiction. Ces atlas sont construits en analysant des volumes cérébraux fonctionnels à grande échelle à l'aide d'un algorithme statistique évolutif, afin d'avoir une meilleure base pour la prédiction des résultats. Après les avoir comparés avec des méthodes de pointe, nous montrons leur utilité pour atténuer les problèmes de traitement des données à grande échelle.

La dernière contribution principale est d'étudier les mesures de substitution potentielles pour les résultats pour la santé. Nous considérons des comparaisons de modèles à grande échelle utilisant des mesures du cerveau avec des évaluations comportementales dans une cohorte épidémiologique d'imagerie, le UK Biobank. Dans cet ensemble de données complexe, le défi consiste à trouver les covariables appropriées et à les relier à des cibles bien choisies. Cela est difficile, car il y a très peu de cibles pathologiques fiables. Après une sélection et une évaluation minutieuses du modèle, nous identifions des mesures indirectes qui sont en corrélation avec des conditions non pathologiques comme l'état de sommeil, la consommation d'alcool et l'activité physique. Ceux-ci peuvent être indirectement utiles pour l'étude épidémiologique de la santé mentale.

ACKNOWLEDGMENTS

I am very grateful to my supervisors Gaël Varoquaux, Bertrand Thirion, Denis Engemann and Josselin Houenou for always being available at any time and for their valuable guidance. I warmly thank Sylvia Villeneuve, Pierre Bellec for reviewing this thesis as well as Camille Maumet, Vincent Frouin, Michel Thiebaut de Schotten for accepting to be part of my defense jury.

I thank all the members of the Parietal team for being great friends and amazing colleagues. I thank Régine Bricquet, Corinne Petitot, Stéphanie Druetta and Anne Vilant for their efficiency at handling administrative issues. Most of all, I thank my family, my parents and my wife for their patience and immense support. Finally, I thank Inria for funding my thesis.

CONTENTS

1	INTRODUCTION	1
1.1	Overview of the thesis	1
1.2	A primer on MRI for Population Imaging	4
1.3	Conclusion	7
2	PIPELINES TO BEST PREDICT PHENOTYPES FROM FUNCTIONAL CONNECTOMES	8
2.1	Population phenotypes studied	9
2.2	Estimating functional connectomes	10
2.3	Many choices of prediction pipeline	12
2.4	Guidelines for optimal modeling choices of prediction pipeline	16
2.5	Discussion	18
2.6	Conclusion	21
3	BRAIN ATLASES TO EXTRACT FUNCTIONAL SIGNALS	22
3.1	Dimensionality reduction	22
3.2	Image-derived phenotypes for population imaging	23
3.3	A scalable model and a very large fMRI dataset	24
3.4	Soft functional modes in practice	26
3.5	Region names: relation to anatomical structures	31
3.6	Validations for population imaging	31
3.7	Discussion	35
3.8	Conclusion	39
4	PREDICTING PROXY MEASURES FOR MENTAL HEALTH	40
4.1	Problem Statement	40
4.2	Proxy measures	41
4.3	Objectives of conceptualizing mental disorders	42
4.4	Brain features and Socio-demographics for predicting modeling	43
4.5	Predictive model comparisons	46
4.6	Brain imaging complements socio-demographics for proxy measures	49
4.7	Classification groups are better discriminated with socio-demographics	50
4.8	Age is best predicted from MRI compared to other proxy measures	52
4.9	Conclusion	53
5	CONCLUSION	55
6	SYNTHÈSE EN FRANÇAIS	57

REFERENCES

REFERENCES 61

APPENDICES

A	REVIEW OF PREDICTIVE METHODS	84
A.1	Practices for imaging-based diagnosis	84
B	TANGENT-SPACE	85
B.1	Computing the tangent-space group average	85
B.2	Transforming covariance matrices	86
C	IMAGING-BASED PREDICTIVE MODELS	88
C.1	Reproduced on high-quality datasets	88
D	DIFUMO EXTRACTION	90
D.1	Implementation details: model parameters	90
D.2	Input fMRI data	90
E	IMAGE-DERIVED PROXY MEASURES	96
E.1	Data acquisition details on UKBB samples	96
E.2	Data processing details on UKBB samples	97
E.3	More experiments	99

ACRONYMS

- ADHD Attention Deficit Hyperactivity Disorder
- ASD Autism Spectrum Disorder
- AD Alzheimer's disease
- ADNI the Alzheimer's Disease Neuroimaging Initiative
- ADNI-DOD the Alzheimer's Disease Neuroimaging Initiative
Department of Defense
- AUC Area Under Curve
- ANOVA Analysis of Variance
- AAL Automated Anatomical Labeling
- ACPI Addiction Connectome Preprocessed Initiative
- ABIDE Autism Brain Imaging Data Exchange database
- BOLD Blood Oxygenation Level Dependent
- BET Brain Extraction Tool
- BASC Bootstrap Analysis of Stable Clusters
- COBRE Center for Biomedical Research Excellence
- CanICA Canonical Independent Component Analysis
- CamCAN The Cambridge Centre for Ageing and Neuroscience
- CSF Cerebro-Spinal Fluid
- dMRI Diffusion Magnetic Resonance Imaging
- dMRI Diffusion Magnetic Resonance Imaging
- DictLearn Dictionary Learning - ℓ_1
- DOD Department of Defense
- DiFuMo Dictionaries of Functional Modes
- EPI Echo Planar Imaging
- FDR False Discovery Rate
- fMRI functional Magnetic Resonance Imaging

FoV	Field of View
FA	Fractional Anisotropy
GNB	Gaussian Naïve Bayes
GLM	General Linear Model
GM	Gray Matter
HCP	Human Connectome Project
i.i.d.	independent identically distributed
IBC	Individual Brain Charting
IDPs	Image-derived Phenotypes
ICA	Independent Component Analysis
ICVF	Intra-Cellular Volume Fraction
ISOVF	Isotropic Volume Fraction
ICBM	International Consortium for Brain Mapping
KNN	K-Nearest Neighbor
MTA	Multimodal Treatment Study
MCI	Mild Cognitive Impairment
MO	Tensor Mode
MEG	Magnetoencephalography
MD	Mean Diffusivity
MPRAGE	Magnetization-Prepared Rapid Acquisition with Gradient Echo
MNI	Montreal Neurological Institute
MRI	Magnetic Resonance Imaging
MIST	Multiresolution Intrinsic Segmentation Template
MODL	Massive Online Dictionary Learning
OD	Orientation Dispersion index
PTSD	Post Traumatic Stress Disorder
TR	Repetition Time
rfMRI	Resting-state functional Magnetic Resonance Imaging

ROC	Receiver Operating Characteristic
RSVP	Rapid-Serial-Visual-Presentation
ROIs	Regions of Interest
RSVP	Rapid-Serial-Visual-Presentation
SOMF	Stochastic Online Matrix Factorization
sMRI	Structural Magnetic Resonance Imaging
SVC	Support Vector Classifier
TR	repetition time
UK	United Kingdom
UKBB	UK Biobank
WM	White Matter

1

INTRODUCTION

1.1 OVERVIEW OF THE THESIS

Brain imaging holds the promise to provide an objective picture of brain states and structure, reflecting individual characteristics and diseases (Bearden and Thompson, 2017; Biswal et al., 2010; Miller et al., 2016). There has thus been an important interest in finding the brain imaging correlates of neurological and psychiatric diseases, in order to provide reliable markers of these diseases (Woo et al., 2017). On the other hand, machine learning is expected to provide powerful inference mechanisms to discover and leverage such markers. Hence, until recently, machine-learning approaches to population imaging studies analysis have focused mostly on predicting individual clinical status from brain images acquired on individuals who are pre-stratified as healthy controls and patients (Arbabshirani et al., 2017). For instance, a typical situation consists in discriminating normal versus major depression - a binary classification problem. These ongoing efforts have led to limited progress in psychiatry research, as manifested by the low accuracy of brain imaging-based predictions of clinical status (Kapur, Phillips, and Insel, 2012). The patho-physiological mechanisms of mental disorders are indeed complex to understand due to their vast heterogeneity in pathological conditions (Insel and Cuthbert, 2015), and therefore too unreliable for clinical translation.

Alternative strategies for understanding mental disorders have put some emphasis on characterizing the underlying biological changes observed through population imaging (Insel et al., 2010). This builds on the observation that complex information embedded in brain imaging requires adequate intermediate representations to overcome noise and be relevant for individual characterization (Smith and Nichols, 2018). Large public health cohorts have emerged to allow the extraction of brain-imaging based signatures with statistical power (Collins, 2012). Yet, this analysis framework is limited by the lack of direct measures relevant to mental health. This challenge calls for studying the impact of risk factors —whether derived from imaging or behavioral data— on generic potential health outcomes. For instance, considering that e.g. personality traits like neuroticism are genetically linked to depression, neuroticism may be a reliable proxy for mental health assessed through depression related questionnaires (Lahey, 2009). We cast this challenge as understanding brain-behavior relationships which can be achieved by linking the large-scale brain measurements to behav-

ioral assessments such as responses to questionnaires on populations (Smith et al., 2015).

Statistical modeling is key in linking these unique population descriptions to psychopathology. The objective of using multivariate statistical methods in population imaging is thus two-fold: *i*) to extract sensible imaging patterns from multiple dimensions useful for personal trait prediction; *ii*) to make predictions about health outcomes at single-subject level.

The following work is organized around three major research directions, which have led to different series of contributions.

1.1.1 Methods for predicting outcomes

Chapter 2 focuses on outlining robust methods for imaging-based predictions. With the rise in population imaging and the many possible modeling pipelines, there is a clear need to benchmark predictive models for clinical phenotypes, in order to select the most accurate and robust methods. This part relies on Resting-state functional Magnetic Resonance Imaging (rfMRI) data and many analytic steps, organized in *pipelines*, required to process rfMRI data. rfMRI is a widely used technique to study functional connectomes, i.e. quantitative functional connectivity models estimated from brain Regions of Interest (ROIs) sampled over the whole brain. A core goal is indeed to predict clinical phenotypes from functional connectomes. Achieving this requires to make several choices regarding modeling steps : brain parcellations schemes, connectomes extraction algorithms and machine learning methods for prediction. After exhaustive comparisons of state-of-the-art methods across diverse brain-imaging cohorts, this part provides guidelines and default choices for connectomes-based predictive modeling.

Published work

Kamalaker Dadi, Mehdi Rahim, Alexandre Abraham, Darya Chyzhyk, Michael Milham, Bertrand Thirion, and Gaël Varoquaux (2019). “Benchmarking functional connectome-based predictive models for resting-state fMRI.” In: *NeuroImage* 192, pp. 115 –134.

1.1.2 Scalable methods for high-quality predictions

Imaging-derived brain parcellations have received great interest and made enormous progress with the availability of large-scale brain image collections. In this Chapter 3, we took the advantage of these large brain data collections to contribute new data-driven fine-grain brain parcellations using Stochastic Online Matrix Factorization (Mensch

et al., 2018), a scalable Dictionary Learning algorithm. We also discuss the usefulness of these atlases from an analytical task standpoint and sketch some guidelines to choose brain parcellations for fMRI analysis, after comparing our atlases to the existing state-of-the-art pre-defined and data-driven functional parcellations. Task- and Rest-fMRI data-analysis, as well as data compression experiments are presented. To complete this contribution, we provide names to these parcels based on neuroanatomical landmarks.

Published work

Kamalaker Dadi, Gaël Varoquaux, Antonia Machlouzarides-Shalit, Krzysztof J. Gorgolewski, Demian Wassermann, Bertrand Thirion, and Arthur Mensch (2020b). "Fine-grain atlases of functional modes for fMRI analysis." In: *NeuroImage*, p. 117126. ISSN: 1053-8119.

1.1.3 Predicting proxy measures for mental health

Finally, Chapter 4 investigates the use of potential proxy measures from an imaging epidemiological cohort aimed at studying mental health. It provides a conceptualization of the use of indirect measures called proxies (self-reported measures to questionnaires) for mental health. This idea is tested through analysis of the UK Biobank cohort from a predictive modeling perspective. We combined both (self-reported) socio-demographic data and brain imaging data of each individual with a Random Forest model to perform the predictive modeling of behavioral outcomes. The outputs of such models combining population imaging and socio-demographic data are evaluated to assess whether there is an advantage in pooling imaging with socio-demographic variables. Finally, the best model comparisons are selected and predicted scores on each individual are gathered to correlate with health outcome variables such as sleep, alcohol consumption and physical fitness to derive endpoints for mental health. This chapter concludes with a brief outline to the elements of an ongoing work that are not part of this manuscript.

Submitted to journal

Kamalaker Dadi, Gaël Varoquaux, Josselin Houenou, Danilo Bzdok, Bertrand Thirion, and Denis Engemann (2020a). "Beyond brain age: Empirically-derived proxy measures of mental health." In: *bioRxiv*. doi: [10.1101/2020.08.25.266536](https://doi.org/10.1101/2020.08.25.266536).

1.2 A PRIMER ON MRI FOR POPULATION IMAGING

1.2.1 Brain connectivity and its relevance to neuroscience

Brain imaging techniques such as functional Magnetic Resonance Imaging (fMRI) or Magnetoencephalography (MEG) are a fundamental tool for systems and cognitive neuroscience (Friston, 2009). These brain mapping methods can be used to understand the principles of brain organization such as brain connectivity, or the spatial organization of the brain networks underlying certain mental functions (Friston, 1994). Brain connectivity encompasses many dimensions: synapses, axonal fiber pathways (anatomical connectivity), statistical relationships in the activity between remote regions (functional connectivity) or model-based interactions (effective connectivity). These relationships are defined among distinct units, where each unit or region is in principle composed of homogeneous neurons (Sporns et al., 2004). Brain connectivity is a central topic of interest to elucidate the interregional connections of the nervous system.

ESTIMATES OF BRAIN CONNECTIVITY Though connectivity can be seen as the core concept in systems neuroscience, brain mapping approaches can be categorized according to the signal that they measure, and according to their goal (Bullmore and Sporns, 2009). A core distinction lies in how they capture the patterns of connectivity and whether these patterns could be used to understand brain function. Anatomical connectivity represents networks of neurons linked together through axonal pathways and synapses, forming distinct structured-like representations of the brain (Sporns, Tononi, and Edelman, 2000). Anatomical connectivity can be investigated using diffusion-weighted imaging techniques such as Diffusion Magnetic Resonance Imaging (dMRI). Such neuroanatomical structures ground our understanding of brain connectivity. Importantly, they do not inform us on how these structures communicate between each other nor regarding how their interaction is modulated by experimental manipulations. By contrast, functional connectivity and effective connectivity are ways to quantify neuronal activations for instance measured at macroscopic level using fMRI – a technique which indirectly measures the evoked or ongoing neural activity depending upon the regional metabolic demands Blood Oxygenation Level Dependent (BOLD) signal changes in time – reveal regional connectivity (static and dynamic interactions) (Rubinov and Sporns, 2010).

Under no strict biological assumptions for e.g. micro-structural properties, functional connectivity estimates functional associations between remote brain locations based on their neurophysiological states or neural activity (Friston, 1994). In contrast to effective connectivity, functional connectivity estimates do not quantify the influence

of one region over another one; instead it provides estimates of temporal associations without assessing directed effects (Friston, 2011). In terms of statistical modeling, given certain measurements of neural activity, functional connectivity analyses find patterns of connectivity that can be used as phenotypes to predict or classify individuals into specific groups e.g. clinical diagnosis (Fox and Greicius, 2010). These phenotypes are most often taken as the linear correlation coefficients among pairs of regions. In a nutshell, functional connectivity is dominantly used for classification problems i.e. attempts to establish a mapping from imaging data to a diagnostic label (consequences to cause) whereas effective connectivity analysis compares models of cause to consequences among brain states (Friston, 2011). The study of brain functional architecture with connectivity methods now spans from simple correlations to complex models (Smith, 2012).

1.2.2 Brain function and structure for population analysis

FUNCTIONAL CONNECTIVITY Task-fMRI is used to map changes in BOLD signal in brain areas that are involved in doing certain behavioral tasks. Functional connectivity may be investigated in regions defined by task-fMRI. In these scenarios, the analyses will be more confined towards task-evoked regions constrained to sparse functional architecture (Cole et al., 2014). However, it may be interesting to study the functional coupling across multiple experimental conditions or across multiple trials (Rissman, Gazzaley, and D'Esposito, 2004).

Beyond task-driven activity, most brain activity can be captured with fMRI even when subjects are not engaged in any of the tasks or simply stay at "rest" (Fox and Raichle, 2007). This ongoing activity is observed as resting-state BOLD signal fluctuations (of frequency < 0.1 Hz), and generally considered as some background activity observable even when the metabolic demands are at baseline level. These temporal fluctuations form coherent networks that are interesting to examine functional connectivity on large-scale populations (Greicius et al., 2008). This ongoing brain activity should not be viewed as a random noise, as it can influence task-evoked activity at the onset of the stimulus (Fox et al., 2006) and is strongly associated with the task-evoked activity (Biswal et al., 1995), actually representing temporal synchronization into networks (Luca et al., 2006; Raichle et al., 2001).

Resting-state functional connectivity thus demonstrates the presence of intrinsic human brain functional architecture even in the absence of behavioral tasks (Fox et al., 2005). Several applications have been developed: *i*) relating functional connectivity to clinical status (Greicius et al., 2004), *ii*) to behavior (Miller et al., 2016), *iii*) predicting psychological traits (Dubois et al., 2018a) and *iv*) deriving data-driven parcellations (Varoquaux et al., 2011; Yeo et al., 2011).

BRAIN STRUCTURAL ANALYSIS There exist other popular methods for population imaging. One is morphometric analysis of the structural neuroimaging, concerned with the quantification of size, volume of brain structures and tissue types and their variations under neuropathologies or behavior (Lerch et al., 2017). For example, volume changes in gray matter areas over lifetime are associated with: brain ageing (Ritchie et al., 2015), brain evolution (Evans, 2006), general intelligence ('g') (Cox et al., 2019) and brain disease (Thompson et al., 2007). Such volumes are calculated within pre-defined ROIs (Desikan et al., 2006) or voxel-wise (Ashburner and Friston, 2000). Another popular method in structural neuroimaging i. e. dMRI, is concerned with the quantification of axonal pathways. Diffusion MRI enables to identify white matter tracts along principal diffusive direction of water molecules, as well as the connections between different gray matter areas (Behrens et al., 2003; Conturo et al., 1999). The study of these local anatomical connections through white matter are relevant to the understanding of neuropathologies and functional organization (Saygin et al., 2016).

1.2.3 Challenges in population imaging

There are however important issues with resting-state based functional connectivity or morphometric analysis, namely the presence of many potential confounds (Smith and Nichols, 2018). Unlike task-based functional connectivity, resting-state does not represent a well-characterized haemodynamic response function. Neural signal is not separated from noise sources, whether physiology- or acquisition-related (Alexander-Bloch et al., 2016; Liu, 2016; Power et al., 2017).

Moreover, subjects e. g. psychiatric patients may feel uncomfortable while undergoing scanning and often move while sampling BOLD time series. This motion-related time series may create spurious functional connectivity (Power et al., 2012) or false positives in group studies (Reuter et al., 2015) if not addressed properly. These population-specific effects are a typical confound when linking functional connectivity or morphological changes to clinical conditions (Pardoe, Hiess, and Kuzniecky, 2016). Another well known issue is subjects falling asleep during acquisition, which strongly corrupts the recorded signal (Laumann et al., 2016).

What can we do about it? Several denoising methods and pipelines have already been proposed for cleaning such noisy BOLD timeseries signals (Behzadi et al., 2007; Caballero-Gaudes and Reynolds, 2017; Ceric et al., 2017; Griffanti et al., 2014a). Following those recommendations, we made choices of confounds such as 10 CompCor (Behzadi et al., 2007) and 6 motion signals to regress them from pre-processed BOLD time series. CompCor confounds are extracted on whole-brain voxels and motion signals are pre-extracted using common data pre-

processing procedure on raw fMRI data as part of data analysis. In addition to confounds regression, signals are also normalized, detrended and bandpass-filtered between 0.01 and 0.1Hz. These cleaning steps are commonly used while studying phenotypes from functional connectivity or during the raw data preprocessing. These non-noisy data are then used for prediction, which is studied in detail in Chapters 2 to 4.

MRI DATA PREPROCESSING STEPS TO MITIGATE CONFOUNDS We use a standard protocol that includes: motion correction, fMRI co-registration to T₁-weighted MRI, normalization to the Montreal Neurological Institute (MNI) template using SPM12¹, Gaussian spatial smoothing (FWHM = 5mm). The SPM based preprocessing pipeline is implemented through pypreprocess²- Python scripts relying on Nipype interface (Gorgolewski et al., 2011). All subjects were visually inspected and excluded from the analysis if they have severe scanner artifacts or head movements with amplitude larger than 2mm. Confounds regression is done at signal extraction level in the functional-connectomes pipeline Section 2.3.1.3 implemented with Nilearn (Abraham et al., 2014a).

1.3 CONCLUSION

In summary, we have sketched the context behind the contributions presented in this manuscript, and target a good use of brain imaging for population studies. We also gave a very brief introduction to MRI for population imaging neuroscience that covers: brain structure and function for predicting population phenotypes and the importance of data preprocessing and introduction of standard preprocessing pipeline. In our thesis, we extensively worked on fMRI datasets. A note on the datasets that we used in preparation of this manuscript is openly-available downloaded under standard terms and conditions. We were not involved in any data acquisition.

¹ www.fil.ion.ucl.ac.uk/spm/

² <https://github.com/neurospin/pypreprocess>

2

PIPELINES TO BEST PREDICT
PHENOTYPES FROM
FUNCTIONAL CONNECTOMES

Functional images acquired during rest is a promising universal marker of brain function (Biswal et al., 2010). It can easily be acquired on many different individuals, as it does not require any task performance, and is applicable to studying diseased populations. Many population-imaging studies use rfMRI to relate brain imaging to neuropathologies or other behavior and population phenotypes (Dubois and Adolphs, 2016; Miller and Alfaro-Almagro, 2016).

A *functional connectome* or shortly connectome – a model characterizing the network structure of the brain (Sporns, Tononi, and Kotter, 2005) – can be extracted from functional interactions in rfMRI data (Varoquaux and Craddock, 2013). The weights of the corresponding brain functional connectome are used to characterize individual subjects behavior and mental health (Dubois et al., 2018a; Milazzo et al., 2014; Smith et al., 2015).

Machine-learning pipelines are key to turning functional connectomes into biomarkers that *predict* the phenotype of interest (Woo et al., 2017). On rfMRI, such a pipeline typically comprises of 3 crucial steps as depicted in Fig. 2.2, linking functional connectomes to the target phenotype (Craddock, Tungaraza, and Milham, 2015; Varoquaux and Craddock, 2013).

PROBLEM STATEMENT There exist many variations of this prototypical pipeline, even for classification from edge-weights of brain functional connectomes, as revealed by reviews of the field (Arbabshirani et al., 2017; Brown and Hamarneh, 2016; Wolfers et al., 2015). These various choices have a sizable impact on the accuracy of population studies, and are seldom discussed (Carp, 2012). The cost of such analytical variation is twofold. First, it puts the burden on the practitioner to explore many options and make choices without systematic guidance. Second, methods variations create researchers degrees of freedom (Simmons, Nelson, and Simonsohn, 2011) that can compromise the measure of the prediction accuracy of biomarkers (Varoquaux, 2017). Guidelines on optimal modeling choices are thus of great value for imaging-based biomarker research.

In this chapter we introduce a prediction pipeline that estimates connectivity weights to relate them to phenotypes and thereafter review practices and methods used for prediction of psychiatric diseases from functional connectomes. Then, we present and benchmark different

methodological choices involved in the classification pipelines. Finally, we report experimental results and the best performing methods, as revealed by our experiments.

2.1 POPULATION PHENOTYPES STUDIED

Population phenotypes are individual assessments, characterized through clinical diagnostic systems or questionnaires. We can study prediction from functional connectomes of various phenotypes – clinical and non-clinical outcomes that includes: neuro-degenerative and neuro-psychiatric disorders, drug abuse impact, fluid intelligence. Studies can then focus either on discriminating between two or more groups i. e. binary values or predicting on a continuous integers, for instance brain-aging (Liem et al., 2017a). Thanks to the open science (Poldrack and Gorgolewski, 2014), several openly-accessible rfMRI datasets exists to study diseased populations (Biswal et al., 2010). This could be useful to apply our connectome-classification pipeline to benchmark various predictive modeling choices. Some of the diverse phenotypes which could be interesting to study on populations who are pre-stratified into binary groups are listed below.

1. Center for Biomedical Research Excellence (COBRE)¹, comprising rfMRI data to study schizophrenia and bipolar disorder (Calhoun et al., 2012). We focus on predicting schizophrenia diagnosis versus normal control.
2. the Alzheimer's Disease Neuroimaging Initiative (ADNI)² database studies neuro-degenerative diseases (Mueller et al., 2005). We focus on using rfMRI to discriminate individuals with Mild Cognitive Impairment (MCI) from individuals diagnosed with Alzheimer's disease (AD) (Trzepacz et al., 2014).
3. the Alzheimer's Disease Neuroimaging Initiative Department of Defense (ADNI-DOD), funded by the US Department of Defense (DOD) to study brain aging in Vietnam War Veterans, includes rfMRI data of individuals with Post Traumatic Stress Disorder (PTSD) or brain traumatic injuries. We focus on discriminating PTSD condition from normal controls.
4. Addiction Connectome Preprocessed Initiative (ACPI)³, a longitudinal study to investigate the effect of cannabis use among adults with a childhood diagnosis of Attention Deficit Hyperactivity Disorder (ADHD). In particular, we use readily-preprocessed rfMRI data from Multimodal Treatment Study (MTA) of ADHD.

¹ <http://schizconnect.org/>

² www.adni-info.org

³ http://fcon_1000.projects.nitrc.org/indi/ACPI/html/

We attempt to discriminate whether individuals have consumed marijuana or not.

5. Autism Brain Imaging Data Exchange database (ABIDE), investigates the neural basis of autism (Di Martino et al., 2014). We use the data from Preprocessed Connectome Project (Craddock et al., 2013) to discriminate individuals with Autism Spectrum Disorder (ASD) from normal controls.

We also perform extra benchmarks including the Human Connectome Project (HCP) rfMRI datasets to discriminate individuals with high vs low intelligence score. These additional light-weight benchmarks are to investigate the consistency of analytical choices while probing high-quality datasets.

2.2 ESTIMATING FUNCTIONAL CONNECTOMES

A functional connectome is estimated from a set of brain ROIs, *nodes* Fig. 2.1 that altogether form brain parcellations, by measuring their pairwise interactions termed as functional connectivity, *edges* Fig. B.1. This section describes standard methods to estimate such nodes and edges from the rfMRI data.

2.2.1 Definition of brain regions of interest (ROIs)

For functional connectomes, the hypothesis is that the definition of ROIs should capture well the relevant functional units (Smith et al., 2011). ROIs selection is an important difficult choice, as the optimal may vary for different conditions or pathologies. Studies define *nodes* to estimate functional connectomes with a variety of approaches:

- balls⁴ of radius varying from 5mm to 10mm centered at coordinates from the literature (Dosenbach et al., 2010; Power et al., 2011);
- Pre-defined reference anatomical atlases such as Automated Anatomical Labeling (AAL) (Tzourio-Mazoyer et al., 2002), sulci-based atlases (Desikan et al., 2006; Perrot et al., 2009), or connectivity-based cortical landmarks (Zhu et al., 2013);
- data-driven approaches based on k-means or Ward clustering (Thirion et al., 2014), as well as Independent Component Analysis (ICA) approaches (Beckmann and Smith, 2004a; Calhoun et al., 2001) or dictionary learning (Mensch, Varoquaux, and Thirion, 2016).

⁴ We used the term ball rather a sphere. From a mathematical standpoint, A “ball” is the inside of a sphere.

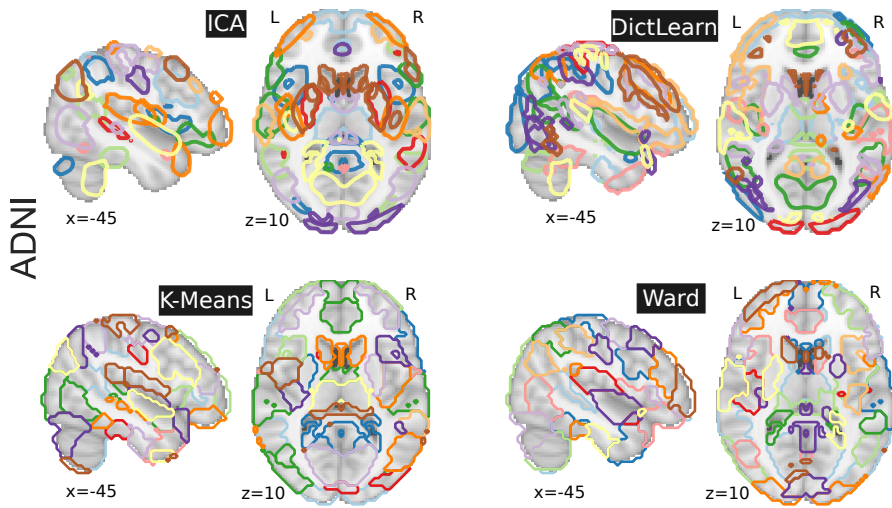


Figure 2.1: Brain regions extracted with ICA, DictLearn, KMeans, and Ward For ICA and dictionary learning, the dimensionality is of 80 and 60 resting-state networks – which are then broken up into more regions – yielding 150 regions, and 120 for KMeans and Ward clustering. Colors are arbitrary. Regions are data-driven on ADNI dataset (Mueller et al., 2005).

The number of nodes which range from dozens to several hundreds and the formation of nodes either as local regions or distributed networks are tied to the choice of definition of ROIs. For pre-defined atlases, these are certainly fixed.

We contribute further to this problem of selecting good analytical choices in brain parcellations at Chapter 3.

2.2.2 Representation of brain functional connectomes

Studies define functional interactions from second-order statistics – based on signal covariance– using Pearson’s correlation or partial correlations estimated mostly either with the maximum-likelihood formula for the covariance or the Ledoit-Wolf shrinkage covariance estimator (Brier et al., 2015; Ledoit and Wolf, 2004a; Varoquaux and Craddock, 2013). Partial correlation between nodes is useful to rule out indirect effects in the correlation structure, but calls for shrunk estimates (Smith et al., 2011; Varoquaux et al., 2010b). Mathematical arguments have also led to representations tailored to the manifold-structure of covariance matrices (Colclough et al., 2017; Dodero et al., 2015; Ng et al., 2014; Varoquaux et al., 2010c). We benchmark the simplest of these, a *tangent* representation of the manifold which underlies the more complex developments (see Appendix B for a quick introduction to this formalism). Fig. B.1 shows the representation of functional connectomes estimated on ADNI dataset (Mueller et al., 2005).

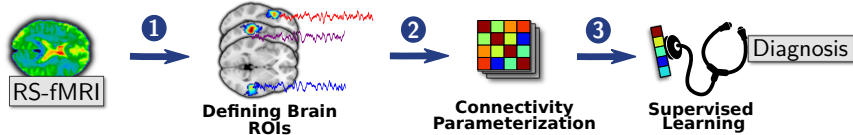


Figure 2.2: Functional connectome prediction pipeline with three main steps: 1) definition of brain regions ROIs from rfMRI images or using already defined reference atlases, 2) quantifying functional interactions from time series signals extracted from these ROIs and 3) comparisons of functional interactions across subjects using supervised learning.

Some studies employ complex-graph network modeling approaches –e. g. network modularity or centrality (Rubinov and Sporns, 2011)– (Arbabshirani et al., 2017; Brown and Hamarneh, 2016; Wolfers et al., 2015).

2.3 MANY CHOICES OF PREDICTION PIPELINE

Fig. 2.2 shows the standard prediction pipeline considered for functional connectomes-based predictions. It typically comprises 3 crucial steps: definition of brain ROIs from rfMRI data, estimation of connectomes from time series signals extracted upon on these ROIs, and comparison of connectomes across subjects using machine learning. In Appendix A.1, we list some studies that have used rfMRI to study diverse psychiatric diseases as well as the choices selected at the each step.

The current practice is very diverse, without standard modeling choices. To open the way toward informed decisions, we explore popular variants of the classic machine-learning pipeline to predict on connectomes. We measure the impact of choices at each step on prediction for diverse targets across multiple datasets as on Table 2.1 and Section 2.1. We detail below the specific modeling choices included in our benchmarks.

Dataset	Prediction task	Groups
COBRE	Schizophrenia vs Control	65/77
ADNI	AD vs MCI	40/96
ADNIDOD	PTSD vs Control	89/78
ACPI	Marijuana use vs Control	62/64
ABIDE	Autism vs Control	402/464

Table 2.1: Datasets and prediction tasks, as well as the number of subjects in each group. COBRE - 142 subjects, ADNI - 136 subjects, ADNIDOD - 167 subjects, ACPI - 126 subjects, ABIDE - 866 subjects.

2.3.1 A selection of methods for definition of brain ROIs

2.3.1.1 *Pre-defined atlases*

Pre-defined atlases defined based on brain anatomy: AAL (Tzourio-Mazoyer et al., 2002), a structural atlas defined from the anatomy of a reference subject, Harvard Oxford (Desikan et al., 2006), a probabilistic atlas of anatomical structures, contains of cortical & sub-cortical ROIs.

Another category is defining ROIs from rfMRI data which we call as functional atlases. Such atlases include Bootstrap Analysis of Stable Clusters (BASC)(Bellec et al., 2010), a multi-scale functional atlas built with clustering on rfMRI; Power, a coordinate-based atlas consisting of coordinates which can be positioned by the balls of 5mm radius (Power et al., 2011).

For a pre-computed functional atlas with dictionary learning, we can use an atlas⁵ computed by Mensch et al., 2016 with a very scalable sparse dictionary-learning algorithm on the HCP900 dataset (Van Essen et al., 2012). This algorithm, Stochastic Online Matrix Factorization (SOMF), solves the ℓ_1 dictionary-learning problem with an algorithm fast on very large datasets that converges to the same solution as standard on-line solvers (Mensch et al., 2018).

2.3.1.2 *Data-driven methods*

Moving away existing pre-defined atlases, brain ROIs can also be defined using popular data-driven methods from intrinsic brain activity of the rfMRI a. k. a. data-driven (Abraham et al., 2013; Beckmann and Smith, 2004a; Calhoun et al., 2001; Kahnt et al., 2012; Thirion et al., 2014; Yeo et al., 2011). We choose to define ROIs using two clustering methods: K-Means (Hastie, Tibshirani, and Friedman, 2009), and hierarchical agglomerative clustering using Ward's algorithm (Ward, 1963) with spatial connectivity constraints (Michel et al., 2012); and two linear decomposition methods: Canonical Independent Component Analysis (CanICA) (Varoquaux et al., 2010a), Dictionary Learning - ℓ_1 (DictLearn) (Mensch, Varoquaux, and Thirion, 2016).

2.3.1.3 *Time-series signals extraction*

After defining brain ROIs, we extract a representative time-series for each ROI in each subject. For atlases composed of non-overlapping ROIs as can be seen in Fig. 2.1 (bottom row), we simply compute the weighted average of the fMRI time series signals over all voxels within that specific region. For fuzzy overlapping ROIs, such as the atlases driven by CanICA and DictLearn as shown in Fig. 2.1 (top row), we use ordinary least squares regression to unmix the signal in each voxel as

⁵ Pre-computed sparse dictionaries with the Massive Online Dictionary Learning (MODL) approach of Mensch et al., 2016 are available from https://team.inria.fr/parietal/files/2018/10/MODL_rois.zip

the additive decomposition of signals over several overlapping ROIs. Let $\mathbf{Y} \in \mathbb{R}^{n \times p}$ be the subject-specific signals, written as p voxels by n timepoints, and $\mathbf{V} \in \mathbb{R}^{k \times p}$ the atlas of k maps supported on p voxels. We estimate $\hat{\mathbf{U}} \in \mathbb{R}^{n \times k}$, the set of time series for each ROI, using:

$$\hat{\mathbf{U}} = \arg \min_{\mathbf{U}} \|\mathbf{Y} - \mathbf{U}\mathbf{V}\|^2$$

At the signal-extraction level, we regress out confounds or non-neural information (Varoquaux and Craddock, 2013). As confounding time-series we use: 10 CompCor (Behzadi et al., 2007) on the whole brain and 6 motion related. We remove motion-related signal only for COBRE, ADNI and ADNIDOD as they are provided as raw data. We have not done any additional preprocessing steps on already preprocessed public datasets like ABIDE⁶, ACPI⁷. The signal of each region is also then normalized, detrended and bandpass-filtered between 0.01 and 0.1Hz. All these steps are done with Nilearn v0.3.

2.3.2 Connectivity parametrization

To estimate functional interactions efficiently from time series signals extracted from these ROIs, we use the Ledoit-Wolf regularized shrinkage estimator (Brier et al., 2015; Ledoit and Wolf, 2004a; Varoquaux and Craddock, 2013), which gives a closed form expression for the shrinkage parameter. This estimator yields well-conditioned estimators despite the variation in length of time series across rfMRI datasets. With this covariance structure, we study three different parametrizations of functional interactions: full correlation, partial correlation (Smith et al., 2011; Varoquaux and Craddock, 2013) and the tangent space of covariance matrices. The latter is less frequently used but has solid mathematical foundations and a variety of groups have reported good decoding performances with this framework (Barachant et al., 2013; Dodero et al., 2015; Ng et al., 2014; Qiu et al., 2015; Rahim, Thirion, and Varoquaux, 2017; Varoquaux et al., 2010c; Wong et al., 2018). Note that computing partial correlation or tangent space require inverting covariance matrices, hence these must be well conditioned. Non regularized covariance estimation is thus not useable for these parametrizations.

For each parametrization, we vectorize the functional connectome, using the lower triangular part of the connectomes matrix for classification.

⁶ <http://preprocessed-connectomes-project.org/abide/>

⁷ http://fcon_1000.projects.nitrc.org/indi/ACPI/html/

2.3.3 Supervised learning: Classifiers

The final step of our pipeline predicts a binary phenotypic status from connectivity features extracted from previous step. We consider several linear and non-linear classifiers for prediction i. e. both sparse and non-sparse methods. For non-linear methods, we consider K-Nearest Neighbor (KNN) (Cover and Hart, 1967) with $K=1$ and Euclidean distance metric, Gaussian Naïve Bayes (GNB) and Random Forests Classifier (Breiman, 2001a). For linear classifiers we consider sparse ℓ_1 regularization for Support Vector Classifier (SVC), and Logistic Regression (Hastie, Tibshirani, and Friedman, 2009). For non-sparse linear classifiers – i. e. ℓ_2 regularization – we consider Ridge classification, SVC, Logistic regression. For SVC, we also considered 10% feature screening with univariate Analysis of Variance (ANOVA). With regards to the regularization parameter (e. g. soft margin parameter in SVC), we use the default $C = 1$ or $\alpha = 1$, which has been found to be a good default (Varoquaux et al., 2017).

2.3.4 Cross validation and error measure

We perform cross-validation (CV) by randomly shuffling and splitting each dataset over 100 folds, forming two sets of subjects: 75% for training the classifier and learning brain atlases with data-driven models and the remaining 25% for testing on unseen data (Varoquaux et al., 2017). We create *stratified* folds, preserving the ratio of samples between groups. For each split, we measure the Area Under Curve (AUC) from the Receiver Operating Characteristic (ROC) curve: 1 is a perfect prediction and .5 is chance. The final prediction scores in AUC (> 120 scores, see Section 2.3.5) are used to measure the impact of various choices in our prediction pipeline outlined below in results section.

2.3.5 Computations and implementation

Our experimental study consists of more than 240 types of pipelines (8 atlases \times 3 connectivity measures \times 10 classifiers). These pipelines were run on each of 5 datasets for 100 CV folds. As a result, there are more than 50 000 pipeline fits, from the raw data to the supervised step, a heavy computational load. Technically, we rely on efficient implementations open-source scientific computing packages using Python 2.7: Nilearn v0.3 (Abraham et al., 2014b) to define brain atlases, extract representative timeseries, and build connectivity measures. All machine-learning methods used for prediction *i.e.*, classifiers and cross-validation are implemented with scikit-learn v0.18.1 (Pedregosa, Varoquaux, and Gramfort, 2011). For visualization, we rely on Nilearn

for brain-related figures while matplotlib is used (Hunter, 2007) for generating other figures.

2.4 GUIDELINES FOR OPTIMAL MODELING CHOICES OF PREDICTION PIPELINE

We now outline which modeling choices have an important impact on predicting over diverse phenotypes from all rfMRI datasets as mentioned on Table 2.1. We use high-quality HCP dataset to investigate whether analytical choices which showed an impact on clinical questions will carry forward its consistency on a non-clinical behavioral task prediction. Below, we study comparisons based on clinical questions and that behavioral task included comparisons on 6 datasets with pre-computed atlases are summarized at Appendix C.1.

IMPACT OF METHODOLOGICAL CHOICES We study the prediction score of each pipeline *relative to the mean across pipelines* on each fold. This relative measure discards the variance in scores due to folds or datasets. From these relative prediction scores, we study the impact of the choice of each step in the prediction pipeline: choice of classifiers, connectivity parametrizations, and definition of brain ROIs. This is a multifactorial set of choices and there are two points of view on the impact of a choice for a given step. First, the impact of the choice for one step may be considered when the other steps are optimal, or close to optimal. Second, the impact of one step may be considered for all other choices for the other steps –marginally on the choice of other steps. In the following figures, we study the first situation, focusing on “good choices”: given a choice for one step, we report data for top third highest performing scores (quantiles 0.666) for the choices in the other steps.

2.4.1 Choice of classifier

Figure 2.3 summarizes the performances of classifiers on prediction scores for all rfMRI datasets. The results display a certain amount of variance across folds and datasets (*i.e.*, prediction targets). However, they show that non-sparse (ℓ_2 -regularized) linear classifiers perform better, with a slight lead for logistic- ℓ_2 . Using non-linear classifiers does not appear useful; neither does sparsity. The results in Figure 2.3 are conditional on a good choice for the other steps of the pipeline.

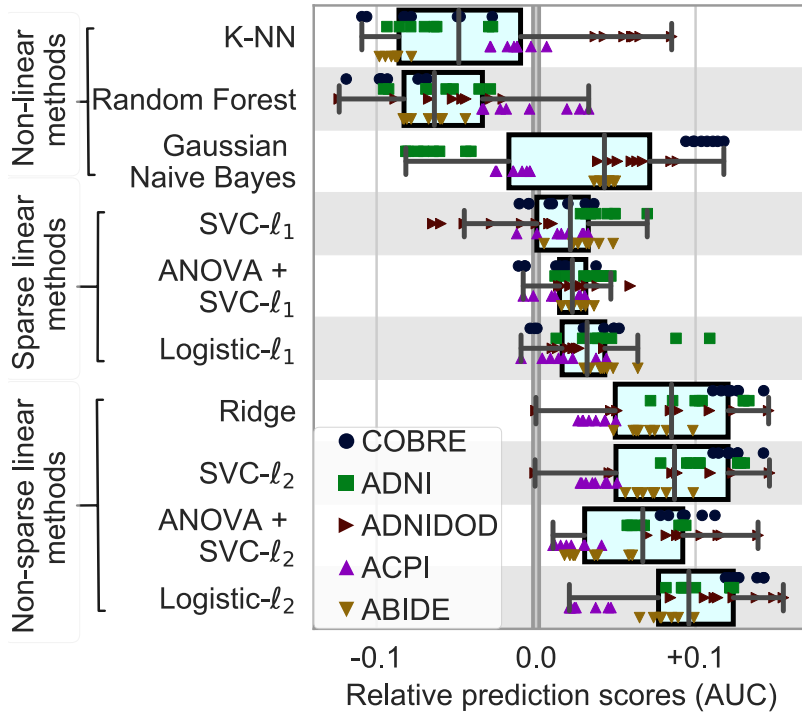


Figure 2.3: Impact of classifier choices on prediction accuracy, for all rfMRI datasets and all folds. For each classifier choice, only the top third highest performing scores are represented when varying the modeling choices for other steps in the pipeline: brain-region definition and connectivity parametrization. Overall, ℓ_2 -regularized linear classifiers perform better, with a slight lead for ℓ_2 logistic regression. The box plot gives the distribution across folds ($n=100$) and datasets (denoted by markers) of prediction score for a given choice (classifier) relative to the mean across all choices (regions-definition and connectivity parametrizations, classifiers). The box displays the median and quartiles, while the whiskers give the 5th and 95th percentiles.

2.4.2 Choice of connectivity parameterization

Figure 2.4 summarizes the impact of covariance matrix parametrization on the relative prediction scores for all rfMRI datasets. Tangent-space parametrization tends to outperform full correlations or partial correlations. Indeed, it performs better on average, but also has less variance across datasets (prediction targets) or folds.

2.4.3 Choice of regions definition method

Figure 2.5 summarizes the relative prediction performance of all choices of region-definition methods. While the systematic effects are small compared to the variance over the folds and the datasets, the general trend is that regions defined from functional data lead to better prediction than regions defined from anatomy. Using ℓ_1 dictionary learning to define regions from rfMRI data appears to be

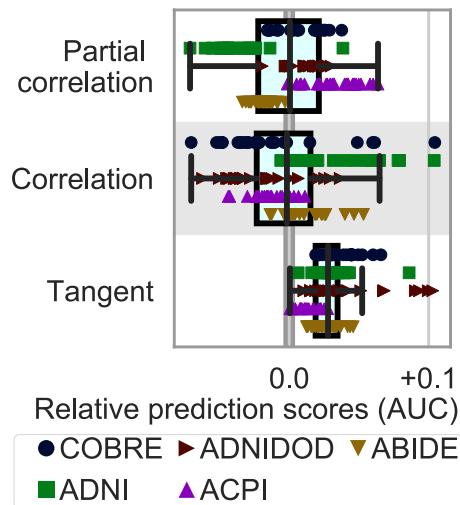


Figure 2.4: Impact of connectivity parameterization on prediction accuracy, for all rfMRI datasets and folds. For each parametrization choice, only the top third highest performing scores are represented when varying the modeling choices for other steps in the pipeline: brain-region definition and classifier. Prediction using tangent space based connectivity parameterization displays higher accuracy with relatively lower variance than using full or partial correlation. The box displays the median and quartiles, while the whiskers give the 5th and 95th percentiles.

the best method, closely followed by ICA, which is also based on a linear decomposition model. Interestingly, BASC, an atlas pre-defined on unrelated rfMRI datasets using data-driven clustering technique, performs almost as well as the best regions-extraction method applied to the rfMRI data of interest. Unlike other pre-defined atlases, like Harvard Oxford or AAL, that lack some crucial functional regions. The BASC atlas (Bellec et al., 2010) is readily available online, and is thus easy to apply to data. Figure 2.5 shows the impact of region-definition approach conditional on good choices in the other steps of the pipeline. Overall, comparisons highlight that defining regions from functional data gives the best-performing pipelines, and that linear-decomposition methods are to be preferred.

2.5 DISCUSSION

An increasing amount of studies use predictive models on functional connectomes, for instance in population-imaging settings to relate brain activity to psychological traits or to build biomarkers of pathologies. While the basic steps of a pipeline are fairly universal –definition of brain regions, construction of an interaction matrix, and supervised learning– studies in the literature show many methodological variants (Appendix A.1). Recommendations on methods that perform well can increase practitioner’s productivity and limit vibration effects that

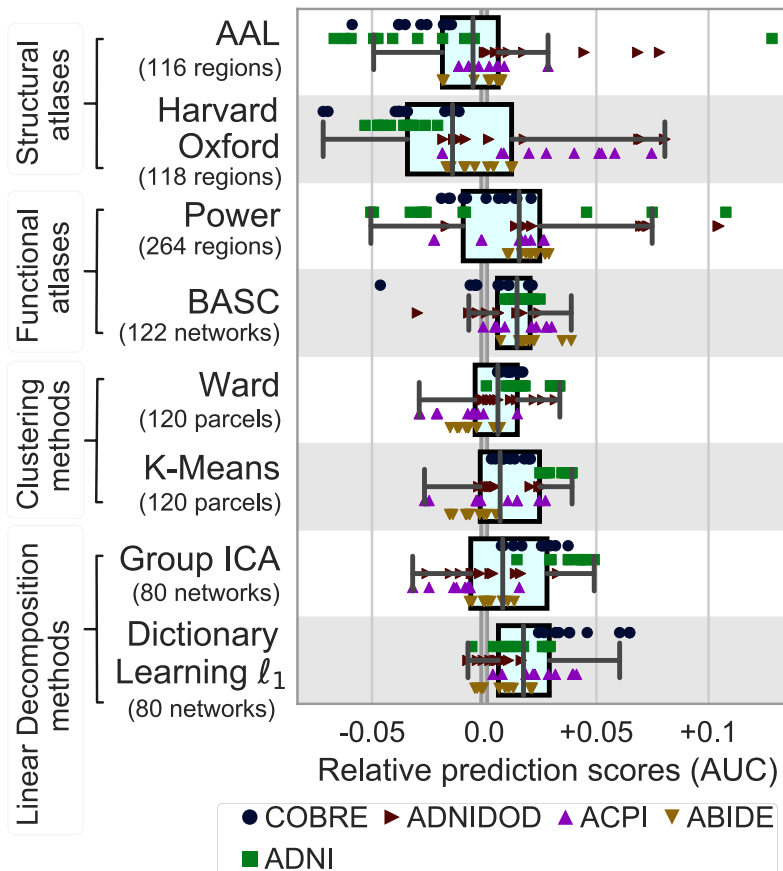


Figure 2.5: Impact of region-definition method on prediction accuracy, for all rfMRI datasets and folds. For each region-definition choice, only the top third highest performing scores are represented when varying the modeling choices for other steps in the pipeline: classifier and connectivity parametrization. Learning atlases from rfMRI data tends the prediction for all tasks. By contrast anatomical atlases perform poorly over diverse tasks. The box displays the median and quartiles, while the whiskers give the 5th and 95th percentiles.

risk undermining the reliability of biomarkers (Varoquaux, 2017). A challenge to such recommendations is the heterogeneity of prediction settings, for instance across different acquisition centers or clinical questions.

SUMMARY OF MODELS FOR PREDICTING OUTCOMES Here, we investigate methodological choices across 6 databases covering different clinical questions and behavioral task. We systematically compare commonly used functional connectome-based prediction methods. We find that some trends emerge, despite a large variance due to variability across subjects –visible across the folds– and across cohorts and clinical questions. Non-sparse linear models, such as logistic regression, appear as a good default choice of classifier. The lack of success of sparse approaches suggests that the discriminant signal is

Step	Recommendation
1: region extraction	Functional regions, eg Dictionary learning or ICA
2: connectivity matrix	Tangent-space embedding
3: supervised learning	Non-sparse linear model, eg logistic regression or SVM

Table 2.2: Recommendations for imaging-based based prediction pipeline.

distributed across the functional connectome for the tasks we study. The tangent-space parametrization of functional connectomes brings improvements to prediction accuracy. With regards to nodes of the functional connectomes, defining them from rfMRI data gives slight benefits in prediction. Linear decomposition methods, such as dictionary learning or ICA, are good approaches to define these nodes from the rfMRI data at hand. Unlike clustering methods based on “hard” assignment, they provide a soft assignment to regions, enabling to capture a form of uncertainty in the definition of regions.

Alternatively, the MODL⁸ (Mensch et al., 2016) or BASC (Bellec et al., 2010) atlases based predictions as shown on Fig. C.1, provide good readily-available nodes that simplify the process and alleviate computational cost. The good analytic performance of pre-computed atlases is promising and calls for further study. Establishing standard atlases brings significant computational benefits, as the definition of regions and the extraction of signal is the most computation-intensive part of the pipeline –in particular when performed inside a nested cross-validation loop.

To enable comparison across different cohorts, we focused on 2-class classification problems. However, the results in terms of regions definition and connectivity parametrization should extend to other supervised learning settings, such as regression –e.g. for age prediction (Liem et al., 2017a)– multi-output approaches as with Canonical Correlation Analysis popular in large-scale population imaging settings (Miller and Alfaro-Almagro, 2016; Smith et al., 2015) for dimensional approaches to psychology.

⁸ https://team.inria.fr/parietal/files/2018/10/MODL_rois.zip

2.6 CONCLUSION

rfMRI-based predictive models bring the promise of robust and reliable biomarkers: given new brain imaging data, they should give accurate predictions of clinics or behavior (Woo et al., 2017).

Our study reveals trends that can provide good defaults to practitioners, summarized on Table 2.2: regions defined from functional data, for instance with ICA or dictionary learning as in the pre-computed MODL atlas, representing connectivity with the tangent embedding of covariance matrices, and using a non-sparse linear model, such as a logistic regression. In particular, good defaults can limit the combinatorial explosion of analytic pipelines, which decreases the computational cost of running a study and makes its conclusion more robust statistically. Yet, as it is well known in machine learning (Wolpert, 1996), there cannot be a one-size-fits-all solution to data analysis: optimal choices will differ on datasets with very different properties from the datasets studied here.

3

BRAIN ATLASES TO EXTRACT FUNCTIONAL SIGNALS

Chapter 2, has shown the benefits of functionally-defined brain parcellations with ICA (Varoquaux et al., 2010a), dictionary learning (Mensch, Varoquaux, and Thirion, 2016) or clustering (Bellec et al., 2010). Whether they are obtained from the data at hand or pre-defined from other functional rfMRI datasets, these atlases overall showed higher predictive accuracy. They extract better statistical links from brain data to target outcomes as they capture the functional structure of the brain. This finding motivates deriving high-resolution functional atlases for better predictions and making them readily available to plug into the prediction pipeline. This not only alleviates the computation burden but also satisfies the cross-validated supervised learning criterion i. e. learning ROIs only on training data.

In this chapter, we focus on the derivation of high-resolution functional brain parcellations for population imaging. We define this need in the context of dimensionality reduction as a consequence of growth in the population imaging. We discuss the limitations of existing algorithms in terms of their scalability to large-scale brain volumes and thereafter deploy efficient and scalable statistical algorithm for high-resolution functional brain parcellations. We extend the validation of these new finely-grained brain ROIs to many varieties of analytical tasks beyond rfMRI data. After comprehensive evaluation against existing state-of-the-art pre-defined brain parcellations, we conclude by showing the validation results and the need of such ROIs for high-quality predictions.

3.1 DIMENSIONALITY REDUCTION

Population imaging has been collecting terabytes of high-resolution functional brain images, uncovering the neural basis of individual differences (Elliott and Peakman, 2008). While these great volumes of data enable fitting richer statistical models, they also entail massive data storage (Gorgolewski et al., 2017; Poldrack, Barch, and Mitchell, 2013) and challenging high-dimensional data analysis. A popular approach to facilitate data handling is to work with Image-derived Phenotypes (IDPs), i. e. low-dimensional signals that summarize the information in the brain images (high-dimensional) while keeping meaningful representations of the brain (Miller and Alfaro-Almagro, 2016). Then, these reduced representations are the starting point for asking research questions.

Brain parcellations are suitable and widely used for data reduction in functional imaging (Craddock et al., 2012; Thirion et al., 2006). For applications like IDPs, the choice of brain parcellations conditions the signal captured in the data analysis. To define regions well suited to brain-imaging endeavors, there is great progress in building atlases from the neuroimaging data itself (Eickhoff, Yeo, and Genon, 2018). There are two prominent data-driven approaches to define well-suited structures. These can strive to select *homogenous* neural populations, typically via clustering approaches (Bellec et al., 2010; Craddock et al., 2012; Goutte et al., 1999; Schaefer et al., 2017; Thirion et al., 2014). They can also be defined via continuous *modes* that map intrinsic brain functional networks (Damoiseaux et al., 2006; Harrison et al., 2015; Varoquaux et al., 2011). As showed on Fig. 2.5 on Chapter 2 and consistent with Abraham et al., 2017, the functional modes have been shown to capture well functional connectivity, with linear decomposition techniques such as ICA or sparse dictionary learning.

PROBLEM STATEMENT High-resolution atlases can give a fine-grained division of the brain and capture more functionally-specific regions and rich descriptions of brain activity (Schaefer et al., 2017). Yet, there is to date no highly-resolved set of “soft” functional modes available, presumably because increasing the dimensionality raises significant computational and statistical challenges (Mensch et al., 2016; Pervaiz et al., 2019). “Soft” regions take continuous non-negative values, in contrast with hard parcellation atlases.

In this chapter, we address this need with high-order Dictionaries of Functional Modes (DiFuMo) extracted at a large scale both in terms of data size (3 million volumes of total data size 2.4TB) and resolution (up to 1024 modes). For this, we leverage the wealth of openly-available functional images (Poldrack, Barch, and Mitchell, 2013) and efficient dictionary-learning algorithms to fit on large data. This is unlike ICA which is hard to use for a high number of modes (Pervaiz et al., 2019).

3.2 IMAGE-DERIVED PHENOTYPES FOR POPULATION IMAGING

While analysis of brain images has been pioneered at the voxel level (Friston et al., 1995), IDPs are increasingly used in the context of population imaging. Trading voxel-level signals for IDPs has several motivations. First and foremost, it greatly facilitates the analysis on large cohorts: the data are smaller, easier to share, requiring less disk storage, computer memory, and computing power to analyze. It can also come with statistical benefits. For instance, in standard analysis of task responses, e.g. in mass-univariate brain mapping, the statistical power of hypothesis test at the voxel level is limited by multiple

comparisons (Friston et al., 1995), while working at the level of IDPs mitigates this problem (Thirion et al., 2006). For predictive modeling, e.g. in multi-variate decoding (Mourão-Miranda et al., 2005), the high-dimensionality of the signals is a challenge to learning models that generalize well—a phenomenon known as the curse of dimensionality in machine learning (Hastie, Tibshirani, and Friedman, 2009). Finally, for functional connectomes, working at voxel-level is computationally and statistically intractable as it entails modeling billions of connections. The standard approach is therefore to average signals on regions or networks (Varoquaux and Craddock, 2013).

3.3 A SCALABLE MODEL AND A VERY LARGE FMRI DATASET

The most popular model in neuroimaging is ICA (Hyvärinen and Oja, 2000), which optimizes spatial independence between extracted maps. It has been extensively used to define resting-state networks (Beckmann et al., 2005; Calhoun et al., 2001; Kiviniemi et al., 2003) and implicitly outlines soft parcellations of the brain at high order (Kiviniemi et al., 2009; Varoquaux et al., 2010a). ICA-defined networks are used to extract the official IDPs of UK Biobank (UKBB), the largest brain-imaging cohort to date; these have been shown to relate to behavior (Miller and Alfaro-Almagro, 2016).

We rely on another decomposition model, dictionary learning (Olshausen and Field, 1997), that enforces sparsity and non-negativity instead of independence on the spatial maps. While less popular than ICA in neuroimaging, sparsity brings the benefit of segmenting well functional regions on a zeroed-out background (Lee, Tak, and Ye, 2010; Varoquaux et al., 2011). For our purposes, an important aspect of sparse models is that they have computationally-scalable formulations even with high model order and on large datasets (Mensch et al., 2016, 2018).

3.3.1 Stochastic Online Matrix Factorization SOMF

We consider BOLD time-series from fMRI volumes, resampled and registered to the MNI template. After temporal concatenation, those form a large matrix $\mathbf{X} \in \mathbb{R}^{p \times n}$, where p is the number of voxels of the images (around $2 \cdot 10^5$), and n is the number of brain images, of the order of 10^6 in the following. To extract DiFuMos, each brain volume is modeled as the linear combination of k spatial functional networks, assembled in a dictionary matrix $\mathbf{D} \in \mathbb{R}^{p \times k}$. We thus assume that \mathbf{X} approximately factorizes as \mathbf{DA} , where the matrix $\mathbf{A} \in \mathbb{R}^{k \times n}$ holds in every column the loadings α_i necessary to reconstruct the brain image x_i from the networks \mathbf{D} . The *dictionary* \mathbf{D} is to be *learned* from data. For

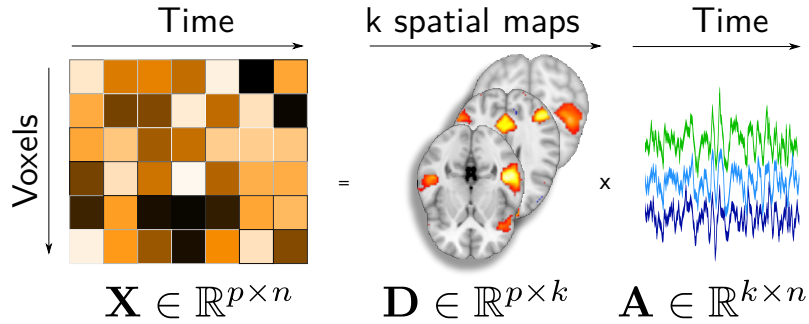


Figure 3.1: Linear decomposition model of fMRI time-series for estimating brain networks: The fMRI time series \mathbf{X} are factorized into a product of two matrices, \mathbf{D} which contain spatial modes and \mathbf{A} temporal loadings of each mode. p - number of features, n - number of volumes in fMRI image, k - number of dictionaries.

this, we rely on *Stochastic Online Matrix Factorization*¹ (Mensch et al., 2018, SOMF), that is computationally tractable for matrices large in both directions, as with high-resolution large-scale fMRI data. SOMF solves the constrained ℓ_2 reconstruction problem

$$\min_{\substack{\mathbf{D} \in \mathbb{R}^{p \times k}, \mathbf{A} \in \mathbb{R}^{k \times n} \\ \mathbf{D} \geq 0, \forall j \in [k], \|\mathbf{d}_j\|_1 \leq 1}} \|\mathbf{X} - \mathbf{DA}\|_F^2 + \lambda \|\mathbf{A}\|_F^2, \quad (3.1)$$

where λ is a regularization parameter that controls the sparsity of the dictionary \mathbf{D} , via the ℓ_1 and positivity constraints². Encouraging sparsity in spatial maps is key to obtaining well-localized maps that outline few brain regions. The parameter λ is chosen so that the union of all maps approximately covers the whole brain with minimum overlap between maps. We provide an exhaustive description of the methodological choices made for extracting DiFuMos in Appendix D. In particular, we provide more details on selecting the optimum λ , on the brain coverage of the DiFuMo atlases (see Table D.1) and overlaps between the modes (see Fig. D.2).

3.3.2 Input fMRI data

Most functional brain atlases have been extracted from rfMRI (Bellec et al., 2010; Craddock et al., 2012; Miller and Alfaro-Almagro, 2016; Power et al., 2011; Schaefer et al., 2017; Yeo et al., 2011). Brain networks can also be extracted from task-fMRI data (Calhoun, Kiehl, and Pearlson, 2008; Lee, Tak, and Ye, 2010), and segment a similar intrinsic large-scale structure (Smith et al., 2009). In our work, we build functional

¹ Available at: <https://arthurmensch.github.io/modl/>

² Eq. (3.1) admits multiple local solutions: the obtained atlases may slightly vary across training runs, although similar regions are recovered, and all atlas perform similarly. Mensch, Varoquaux, and Thirion (2016) further discuss reproducibility of matrix factorization across runs.

modes from datasets with different experimental conditions, including task and rest. Our goal is to be as general as possible and capture information from different protocols. Indeed, defining networks on task-fMRI can help representing these brain images and predicting the corresponding psychological conditions (Duff et al., 2012). We note that appending rest data to the already large task-fMRI corpus gives marginal improvement (Figure D.3).

We build the input data matrix \mathbf{X} with BOLD time-series from 25 different task-based fMRI studies and 2 resting state studies, adding up to 2192 functional MRI recording sessions. We gather data from OpenNeuro (Gorgolewski et al., 2017) –Appendix D.2 lists the corresponding studies.

We use *fMRIprep* (Esteban et al., 2019) for minimal preprocessing: brain extraction giving as a reference to correct for head-motion (Jenkinson et al., 2002a), and co-registration to anatomy (Greve and Fischl, 2009). All the fMRI images are transformed to MNI template space. We then use *MRIQC* (Esteban et al., 2017) for quality control.

MULTI-DIMENSIONAL DIFUMO ATLASES We estimate dictionaries of dimensionality $k \in \{64, 128, 256, 512, 1024\}$. This is useful as the optimal dimensionality for extracting IDPs often depends on the downstream data analysis task. The obtained functional modes segment well-localized regions, as illustrated in Figure 3.2 1a.

3.4 SOFT FUNCTIONAL MODES IN PRACTICE

This section bares a resemblance to Section 2.3.1.3 in Chapter 2. Here, we briefly summarize in this chapter as it is an important step for IDPs to lead high-quality predictions. The functional modes decomposed from ICA or SOMF algorithms take continuous values (we refer to them as *soft*) and can have some overlap –though in practice this overlap is small. As a consequence, signal extraction calls for more than averaging on regions. The natural formulation is that the extracted signals (the IDPs) should best approximate the brain image $\mathbf{x} \in \mathbb{R}^p$ as a linear combination $\boldsymbol{\alpha} \in \mathbb{R}^k$ of the set of modes in the dictionary $\mathbf{D} \in \mathbb{R}^{p \times k}$. This is solved by linear regression:

$$\boldsymbol{\alpha} = \underset{\boldsymbol{\alpha} \in \mathbb{R}^k}{\operatorname{argmin}} \|\mathbf{x} - \mathbf{D}\boldsymbol{\alpha}\|_2^2, \quad \text{i.e.} \quad \boldsymbol{\alpha} = \mathbf{D}^\dagger \mathbf{x}, \quad (3.2)$$

where $\mathbf{D}^\dagger = (\mathbf{D}^\top \mathbf{D})^{-1} \mathbf{D}^\top \in \mathbb{R}^{k \times p}$ is the pseudo-inverse of \mathbf{D} . For atlases composed of non-overlapping regions, such as classic brain parcellations—e.g. BASC (Bellec et al., 2010) or normalized cuts (Cradock et al., 2012)—linear regression simply amounts to averaging the images values in every cluster of \mathbf{D} . For overlapping modes as the ones of DiFuMo or the ICA maps used in UKBB (Miller and Alfaro-Almagro,

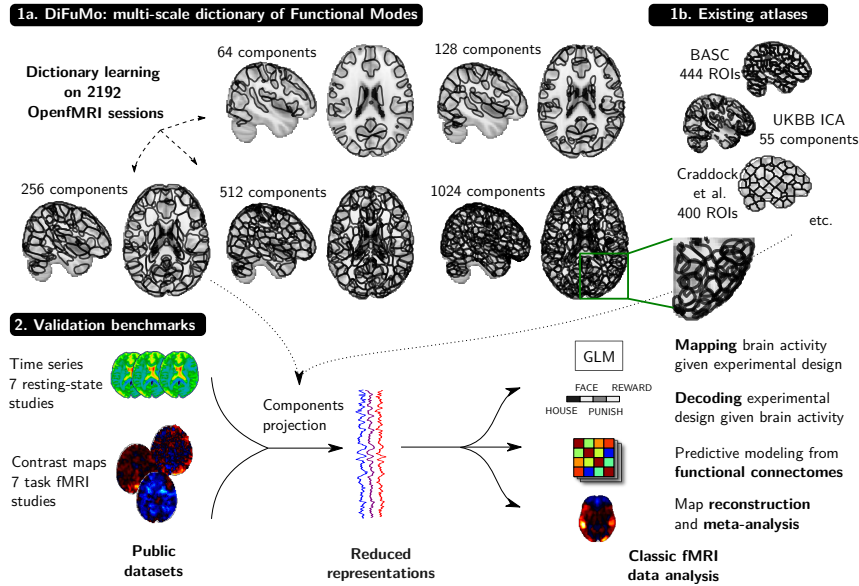


Figure 3.2: Schema of DiFuMo atlases and their usage in typical fMRI analyses. DiFuMo atlases are extracted from a massive concatenation of BOLD time-series across fMRI studies, using a sparsity inducing matrix factorization algorithm. We compute the DiFuMo atlases at different resolutions, up to 1024 components. We assess our atlases in 2 benchmarks that measure suitability to classic fMRI analyses. Those are performed on reduced and non-reduced data, with different atlas sizes and a comparison between atlases. The easiest way to view and download DiFuMo atlases is via the online interactive visualizations: parietal-inria.github.io/DiFuMo.

2016), the linear regression formulation caters for the overlap and softness of the regions.

We use the reduced representations IDPs introduced above for various functional-imaging analytic tasks: decoding mental processes from brain activity (Section 3.4.2); predicting phenotypes from functional connectomes (Section 3.4.3); standard mass-univariate analysis of brain responses (Section 3.4.4); finally, we measure the quality of signal reconstruction after dimension reduction, illustrated on meta-analyses (Section 3.4.5).

3.4.1 Benchmarking several functional atlases

To gauge the usefulness of the DiFuMos for IDPs extraction, we compare each analysis pipeline across several functional atlases: DiFuMo and reference atlases are used to compute functional IDPs. We use the same signal-extraction function (3.2), but vary the spatial components D. As a baseline, we also perform the voxel-level analyses, though it entail significantly larger computational costs.

We consider other functional atlases that are multi-resolutions, accessible to download, and volumetric (Table 3.1):

Name	# subjects	Data type	Dimensionality	Soft	Method
BASC	200	rest	64, 122, 197, 325, 444	No	Hierarchical clustering
MIST ATOM ^a	200	rest	1095	No	Region growing
Craddock	41	rest	200, 400	No	Spectral clustering
FIND ^b	15	rest	90, 499	Yes	ICA; Ward clustering
Gordon	120	rest	333	No	Local-gradient approach
UKBB ICA	4100	rest	21, 55	Yes	Selected ICA components ^c
Schaefer	1489	rest	100, 200, 300, 400 500, 600, 800, 1000	No	Gradient-weighted Markov Random Field (gwMRF)
DiFuMo^d	2192	task, rest	64, 128, 256, 512, 1024	Yes	Sparse dictionary learning

^a https://figshare.com/articles/_/5633638

^b https://findlab.stanford.edu/functional_ROIs.html

^c <https://www.fmrib.ox.ac.uk/ukbiobank/>

^d <https://parietal-inria.github.io/DiFuMo>

Table 3.1: Functional atlases that we benchmark; they define IDPs for population imaging

3.4.2 Decoding experimental stimuli from brain responses

Decoding predicts psychological conditions from task-related z-maps (Haynes and Rees, 2006). The validity of a decoding model is evaluated on left-out data (following Varoquaux et al., 2017), e.g. left-out subjects for inter-subject decoding (Poldrack, Halchenko, and Hanson, 2009). We use linear decoding models: ridge regression for continuous target and SVC (Hastie, Tibshirani, and Friedman, 2009) for classification. For each study, we separate sessions (for intra-subject decoding) or subjects (for inter-subject decoding) into randomly-chosen train and test folds (20 folds with 30% test size), and measure the test accuracy. We compare the performance of predictive models using voxel-level z-maps or data reduced with functional atlases.

3.4.2.1 Data

We use 6 open-access task-fMRI studies. We perform *inter-subject* decoding in the emotional and sensitivity to pain experiences from Chang et al., 2015, and in three studies from HCP900 (Van Essen et al., 2012): working memory, gambling (Delgado et al., 2000), and relational processing (Smith, Keramatian, and Christoff, 2007). We perform *intra-subject* decoding using the several sessions of left and right button press responses in Individual Brain Charting (IBC) (ARCHI protocol, Pinel et al., 2007). The unthresholded z-maps used in the decoding pipeline are either obtained from Neurovault (Gorgolewski et al., 2015), or computed with the General Linear Model (GLM) following Section 3.4.4.

3.4.3 Predicting phenotype from functional connectomes

Resting-state fMRI can be used to predict phenotypic traits (Richiardi et al., 2010). For this, each subject is represented by a functional connectivity matrix capturing the correlation between brain signals at various locations. Our functional-connectome prediction pipeline comprises three steps: 1) we extract a reduced representation of the BOLD signal³, projecting voxel-level data onto a functional atlas as in Section 3.4.4; 2) we compute a *functional connectome* from the reduced BOLD signals; 3) we use it as input to a linear model. We compute a connectome from activations with the Ledoit and Wolf (2004a) covariance estimator as Brier et al. (2015) and Varoquaux and Craddock (2013). We then derive single-subject features from covariance matrices using their tangent space parametrization (Barachant et al., 2013; Pervaiz et al., 2019; Varoquaux et al., 2010c), as advocated by the benchmarks at Section 2.4.2 in Chapter 2. Those are used to fit an ℓ_2 -penalized logistic regression for classification and a ridge regression for continuous targets. We assess predictive performance with 20 folds, random splits of subjects in train and test sets, with 25% test size.

3.4.3.1 Data

We use 7 openly-accessible datasets with diverse phenotypic targets, as summarized in Table D.3. We predict diagnostic status for Alzheimer’s disease on ADNI (Mueller et al., 2005), PTSD on ADNI-DOD; Autism Spectrum Disorder on ABIDE (Di Martino et al., 2014) and schizophrenia on COBRE (Calhoun et al., 2012); drug consumption on ACPI; fluid intelligence measures on HCP (Van Essen and Smith, 2013); and age (with a regression model) in normal aging with The Cambridge Centre for Ageing and Neuroscience (CamCAN) (Taylor et al., 2017).

3.4.4 Mapping brain response: standard task-fMRI analysis

Standard analysis in task-fMRI relates psychological manipulations to brain activity separately for each voxel or region. It models the BOLD signal as a linear combination of experimental conditions—the General Linear Model (GLM, Friston et al., 1995). The BOLD signal forms a matrix $\mathbf{Y} \in \mathbb{R}^{n \times p}$, where p is the number of voxels. With data reduction, we use as input the reduced signal $\mathbf{Y}_{\text{red}} = \mathbf{Y}_{\text{voxel}}(\mathbf{D}^\dagger)^\top \in \mathbb{R}^{n \times k}$ (Equation 3.2). The GLM models \mathbf{Y} or \mathbf{Y}_{red} as $\mathbf{Y} = \mathbf{X}\boldsymbol{\beta} + \boldsymbol{\epsilon}$ where $\mathbf{X} \in \mathbb{R}^{n \times q}$ is the design matrix formed by q temporal regressors of interest or nuisance and $\boldsymbol{\epsilon}$ is noise (Friston et al., 1998). In our experiments, we use the *Nistats* library⁴, and compute a common brain

³ We handle site differences by casting all data in the MNI template space. Abraham et al. (2017) shows the robustness to site difference of predictors based on functional connectomes.

⁴ <https://nistats.github.io/>

mask from data covering brain areas with International Consortium for Brain Mapping (ICBM) grey matter mask.

With reduced input \mathbf{Y}_{red} , we obtain one signal per region, as $\boldsymbol{\beta} \in \mathbb{R}^{q \times k}$. The full β -maps can then be reconstructed by setting $\boldsymbol{\beta}_{\text{rec}} = \boldsymbol{\beta}\mathbf{D}^T \in \mathbb{R}^{q \times p}$. We transform the reconstructed β -maps into *z-maps* $\mathbf{z} \in \mathbb{R}^{q \times p}$ using base contrasts, before thresholding them with Benjamini and Hochberg (1995) False Discovery Rate (FDR) correction for multiple comparisons. We then compare the *z-maps* obtained using voxels as input, and *z-maps* using reduced input and reconstructed β -maps, using the **dice** similarity coefficient.

3.4.4.1 Data

We consider the Rapid-Serial-Visual-Presentation (RSVP) language task of IBC (see Pinho et al., 2018, for experimental protocol and pre-processing). We model six experimental conditions: complex meaningful sentences, simple meaningful sentences, jabberwocky, list of words, lists of pseudowords, consonant strings. β -maps are estimated for each subject using a fixed-effect model over 3 out of the 6 subject's sessions. We randomly select 3 sessions 10 times to estimate the variance of the Dice index across sessions. As a baseline, we evaluate the mean and variance of the Dice index across *z-maps* when varying the sessions used in voxel-level GLM.

3.4.5 Quality of image reconstruction

The signals extracted on a brain atlas can be seen as a compression, or simplification, of the original signal. Indeed, a full image can be reconstructed from these signals. We quantify the signal loss incurred by this reduction. For this, we project a brain map \mathbf{x} (obtained with the ICBM whole brain mask) onto an atlas (solving Eq. (3.2)), and compute the best reconstruction of \mathbf{x} from the loadings $\boldsymbol{\alpha}$, namely $\hat{\mathbf{x}} = \mathbf{D}\boldsymbol{\alpha} \in \mathbb{R}^p$. We compare original and reconstructed images through the R^2 coefficient,

$$R^2(\mathbf{x}, \hat{\mathbf{x}}) = 1 - \frac{\|\mathbf{x} - \hat{\mathbf{x}}\|_2^2}{\|\mathbf{x} - \bar{\mathbf{x}}\|_2^2}, \quad (3.3)$$

where $\bar{\mathbf{x}} \in \mathbb{R}$ is the spatial mean of map \mathbf{x} . The R^2 coefficient is averaged across all images. Higher R^2 coefficients means that the reduced signals IDPs explain more variance of the original images, where $R^2 = 1$ corresponds to no signal loss. The larger the number of signals used, the easier it is to explain variance; it is therefore interesting to compare this measure across atlases with similar number of components. For a fixed number of component in the DiFuMo atlases, R^2 increases with brain coverage.

3.4.5.1 Data

We use **NeuroVault** (Gorgolewski et al., 2015), the largest public database of statistical maps. To avoid circularity, we exclude maps derived from the studies used to extract the DiFuMo atlases, along with maps that fail semi-automated quality inspection (filtering out thresholded or non-statistical maps), resulting in 15,542 maps.

3.4.5.2 Meta-analysis of contrasts maps

Ideally, the extracted IDPs should allow to compute meta-analytical summaries of brain activity maps. In this setting, a single map, corresponding to a certain cognitive concept, is computed from many z-maps across different studies, associated to conditions that involve this cognitive concept. We compare the summaries obtained at voxel-level, i.e. averaging the maps $\{x\}$, with the ones obtained using reconstructed images, i.e. averaging the maps $\{\tilde{x}\}$ used in Eq. (3.3). We use maps from our curated subset of NeuroVault annotated with terms *motor*, *language* and *face recognition*.

3.5 REGION NAMES: RELATION TO ANATOMICAL STRUCTURES

Relating IDPs to known brain structures facilitates interpretation and discussion of results. Though the DiFuMo atlases are defined from functional signal, we choose to reference their regions by their anatomical location, as it is a common and well-accepted terminology in neuroscience. For each resolution, we match the modes with regions in references of brain structure: the Harvard-Oxford atlas (Desikan et al., 2006), Destrieux atlas (Destrieux et al., 2010), the MIST atlas (Uuchs et al., 2019), Johns Hopkins University (JHU) atlas (Hua et al., 2008), and the Dierdrichsen cerebellum atlas (Diedrichsen et al., 2009). We name each mode from the anatomical structure that it most overlaps with. When the overlap was weak, a trained neuroanatomist (AMS) looked up the structure in standard classic anatomy references (Catani and Schotten, 2012; Henri, 1999; Ono, Kubik, and Abernathey, 1990; Rademacher et al., 1992; Schmahmann et al., 1999).

3.6 VALIDATIONS FOR POPULATION IMAGING

3.6.1 Decoding mental state from brain responses

[Figure 3.3](#) shows the impact on decoding performance of reducing signals with various functional atlases. It reports the performance relative to the median across methods for each of the 6 tasks. These

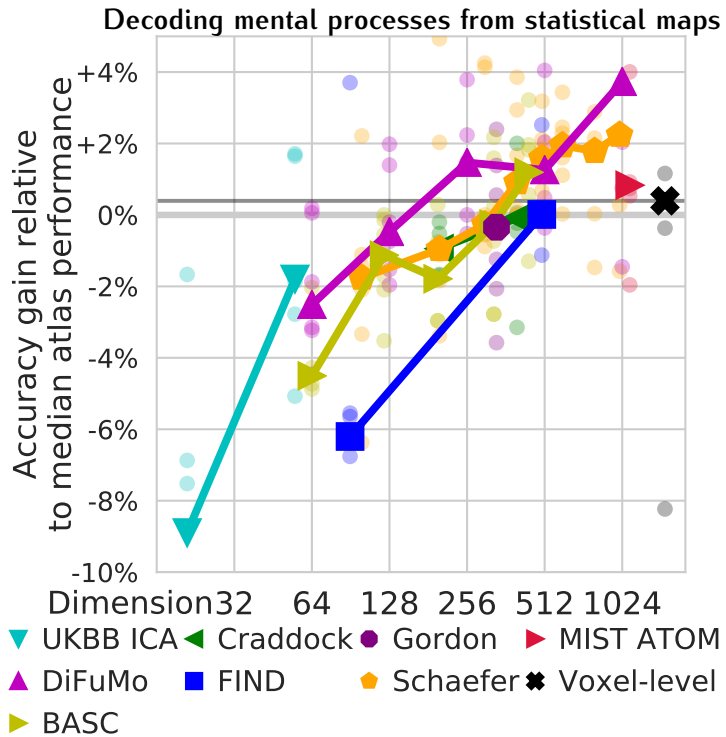


Figure 3.3: Impact of the choice of atlas on decoding performance. Each point gives the relative prediction score, over 6 different task-fMRI experiments. The thick lines give the median relative score per atlas. The baseline (black) is the relative score. High-order resolutions increase prediction accuracy. Using high-order DiFuMo ($k = 1024$) and Schaefer parcellations ($k = 1000$) gives the best performance and, on average, outperforms voxel-level prediction.

results clearly show the importance of high-dimensional functional modes for decoding. Indeed, the higher the atlas resolution, the better the predictions. Using DiFuMo $k = 1024$ or Schaefer $k = 1000$ gives the best performance. In addition, as these functional atlases segment sufficiently-fine regions, prediction from the corresponding signals tends to outperform voxel-level prediction. Indeed, applying multivariate models to a larger number of signals with a limited amount of data is more prone to overfitting—data reduction acts here as a welcome regularization. Qualitatively, brain maps containing decoding weights can be reconstructed. With high-dimensional atlases, they are interpretable and capture information similar to voxel-level analysis (Figure 3.4).

3.6.2 Predicting traits from functional connectomes

Figure 3.5 shows the impact of the choice of functional atlas when predicting phenotypes from functional connectomes. We report the relative prediction accuracy for 7 different prediction problems (each

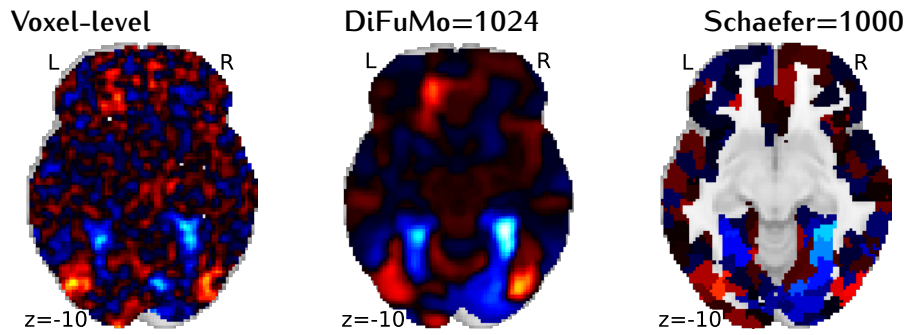


Figure 3.4: Decoding maps of the working memory task, face versus rest, showed for Voxel-level analysis, DiFuMo, and Schaefer. The maps are highly interpretable with high-dimensional soft modes (DiFuMo 1024) compared to voxel-level analysis. Brain areas important in the visual working memory task –fusiform gyrus and lateral occipital cortex– are clearly visible.

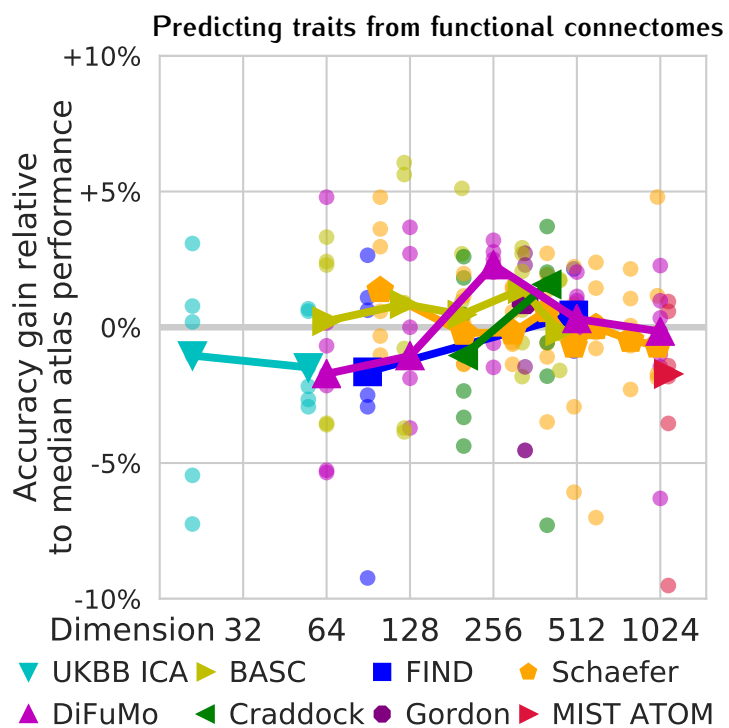


Figure 3.5: Impact of the choice of atlas for predictions based on functional connectomes. Each data point gives the prediction accuracy relative to the median for one of the 7 phenotypic prediction targets, i.e. each point a dataset. The thick line shows the median over the datasets. While the results are noisy, the optimal dimensionality seems to lie around 300 nodes, and the best-performing atlas is DiFuMo $k = 256$, followed by Craddock $k = 400$ and BASC $k = 444$.

composed of a dataset and a target phenotype); the lines give the median across the prediction problems. Here, we do not report a voxel-level baseline, as it requires to compute covariance matrices of dimensions around $100,000 \times 100,000$ and is therefore computa-

tionally and statistically intractable. In contrast with previous results, high-resolution atlases do not provide the best performance, likely because the complexity of the statistical models increases with the square of the number of nodes. The best prediction overall is achieved using DiFuMo $k = 256$, followed by Craddock $k = 400$ and BASC $k = 444$ atlases.

3.6.3 Brain mapping: standard task-fMRI analysis

[Figure 3.6](#) reports the results of standard analysis of task-fMRI GLM, comparing analysis at the voxel-level with analyses on signals extracted from functional atlases. Best correspondence is obtained at highest dimensionality, as the regions are finer. Notably, analysis with DiFuMo of dimensionality 1024 is markedly closer to voxel-level analysis than using the best-performing alternatives, i.e. the 1000-dimensional Schaefer parcellation and the 1095 MIST atoms. In addition, the Dice index relative to the voxel-level gold standard is comparable to the Dice index between runs of voxel-level GLM estimated across folds. We note that using soft functional modes from only 55 ICA components shows excellent results, comparable to those obtained using the 1000 components Schaefer atlas. This stresses the benefit of *continuous functional modes* for the analysis of task responses. Overall, standard task-fMRI analysis on signals derived from 512 or 1024-dimensional DiFuMo gives results close to the voxel-level gold standard ([Figure 3.6](#) shows that the maps are also qualitatively similar).⁵ Dimension reduction has the additional benefit of alleviating the burden of correcting for multiple comparisons.

3.6.4 Fraction of the original signal captured

[Figure 3.7](#) (left) displays the R^2 scores summarizing the loss of information when data are reduced on an atlas and reconstructed back to full images. Unsurprisingly, reducing the images with lower-order dimensions (atlases with fewer regions) yields a high loss of information across all methods. DiFuMo $k = 1024$ captures 70% of the original voxel-level signal. Qualitatively, the benefits of functional modes can be seen by comparing the meta-analytic maps related to motor tasks ([Figure 3.7](#) right). The DiFuMo have clear visual benefits over brain discrete parcellations, such as BASC, as they better capture gradients.

⁵ We note that using too coarse atlases may fail at detecting statistically significant voxel activations, yielding a Dice index of 0.

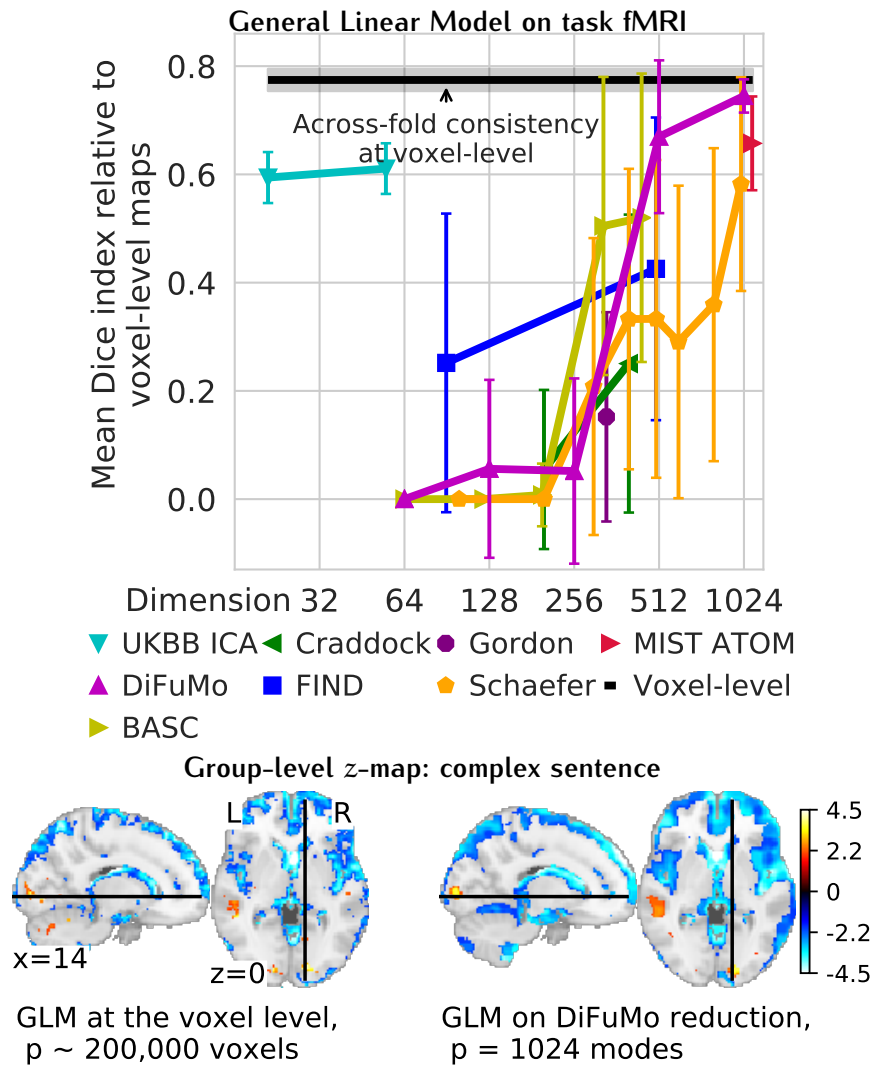


Figure 3.6: Overlap between GLM maps obtained with functional atlases and voxel-level analysis. **Top:** The overlap is measured with the Dice similarity coefficient. The black line gives a baseline the mean overlap between voxel-level contrast maps over several random selections of sessions per subject. The figure gives Dice similarity scores between the GLM maps computed with signals extracted on functional atlases and at the voxel-level, after reconstruction of full z-maps and voxel-level thresholding with FDR control. The best similarity is achieved for highest dimensionality, though 1024-dimensional DiFuMo atlas largely dominates 1000-dimensional Schaefer parcellation and 1095 Multiresolution Intrinsic Segmentation Template (MIST). Each point is the mean and the error bar denotes the standard deviation over contrast maps. **Bottom:** The activity maps encoded on 1024-dimensional space capture the same information as voxel-level analysis, while being smoother.

3.7 DISCUSSION

This chapter introduces brain-wide soft functional modes, named DiFuMos and made of a few hundreds to a thousand of brain sub-

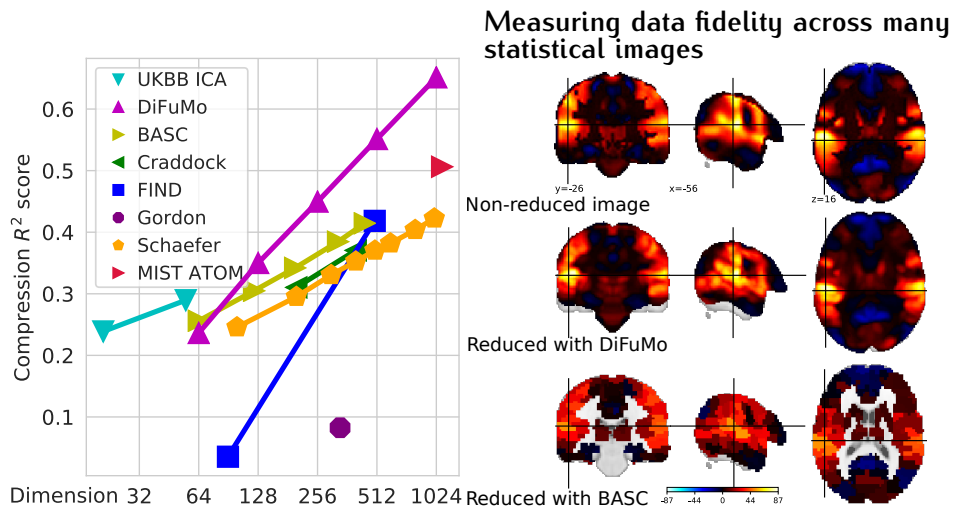


Figure 3.7: Image reconstruction quality. **Left:** Quantitative comparison on 15542 statistical images. The R^2 loss between the true and recovered images after compression with brain atlases of multiple resolutions. In general, higher-order atlases capture more signal. **Right:** Meta-analysis summaries for the motor task. High R^2 score (left) correspond to better capturing fine structures of images, as visible on the qualitative images. DiFuMo atlases better capture the gradients and smooth aspects of the original images than hard parcellations, as BASC.

divisions. They are derived from BOLD time-series across many studies to capture well functional images with a small number of signals. In the context of population imaging, these signals are known as image-derived phenotypes (IDP, Miller and Alfaro-Almagro, 2016) and are crucial to easily scale statistical analysis, building a science of inter-individual differences by relating brain signals to behavioral traits (Dubois and Adolphs, 2016). Reducing the dimensionality of the signals not only come with a $1000\times$ gain in storage, but also with $100\times$ computational speed-up for the analysis (Table 3.2). Even small-scale studies may need functional nodes, e.g. for computing functional connectomes (Varoquaux and Craddock, 2013; Zalesky et al., 2010). There already exist many functional brain atlases; yet DiFuMos have the unique advantage of being both soft and highly resolved. These features are important to capture gradients of functional information.

GROUNDING BETTER IMAGE-DERIVED PHENOTYPES FOR HIGH-QUALITY PREDICTIONS Signals extracted from a functional atlas should enable good statistical analysis of brain function. We considered quantitative measures for typical neuroimaging analytic scenarii and compared the fitness of extracting signal on DiFuMo with using existing functional brain atlases. The biggest gains in analysis come from increasing the dimensionality of brain sub-divisions, aside for functional connectome studies where an optimal is found around 200 nodes. Choosing the number of nodes then becomes a tradeoff be-

Task	# samples	Representation	Time (sec)	Speedup
Emotion	4924	Voxel-level	77.7	46×
		Reduced	1.7	
Pain	84	Voxel-level	1.5	250×
		Reduced	0.006	
Working memory	3140	Voxel-level	874.7	240×
		Reduced	3.7	
Gambling	1574	Voxel-level	298.7	270×
		Reduced	1.12	
Relational	1572	Voxel-level	263.1	405×
		Reduced	0.65	

Table 3.2: The comparison in computational times while predicting mental state on two set of brain features space: voxel-level $\approx 200,000$ and reduced voxels to DiFuMo 1024. We report the averaged time over 20 cross-validation folds for several task-fMRI conditions. Clearly, there are benefits trading for reduced representations in terms of computation time. On high-resolution brain images like HCP, these are decreased by a factor 200.

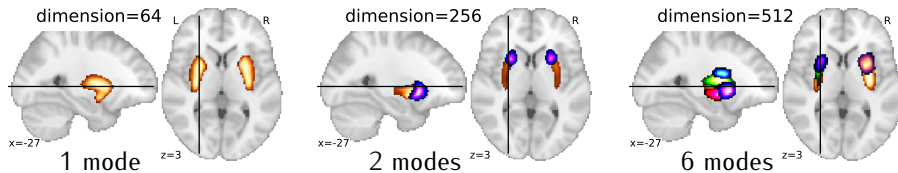


Figure 3.8: Modes around the putamen, for DiFuMo dimensionality 64, 256, and 512. As dimensionality increases: sub-divisions are more refined, modes are split into right and left hemisphere and antero-posterior direction. Each color represents a single mode.

tween complexity of the representation and analytic performance. Importantly, the gains in analytic performance continue way beyond the dimensionality typically used for IDPs (e.g. 55 components from Miller and Alfaro-Almagro, 2016). These results extend prior literature emphasizing the importance of high-dimensional parcellations for fMRI (Abou Elseoud et al., 2011; Arslan et al., 2017; Sala-Llonch et al., 2019; Thirion et al., 2014). To foster good analysis, the second most important aspect of a parcellation appears that it be soft, i.e. continuously-valued. For a given dimensionality, soft modes tend to outperform hard parcellations, whether they are derived with ICA or dictionary learning.

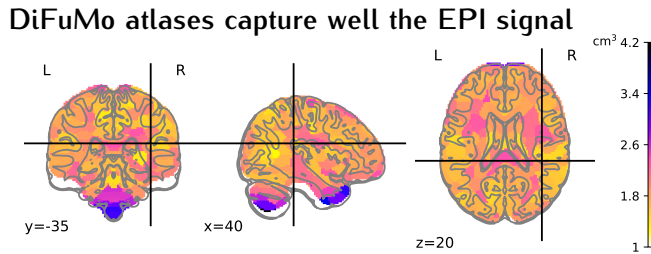


Figure 3.9: Region volume (cm^3) of modes on the brain with 1024 dictionary of DiFuMo. The volume of the modes tends to be larger corresponding to white matter when compared with the cortical gray matter. This justifies the adaptation of DiFuMo atlas to the fMRI signal.

MODES WELL-ADAPTED TO THE EPI SIGNAL The functional modes are optimized to fit well a large number of Echo Planar Imaging (EPI) images: 2,192 sessions across 27 studies. As a result, they form a division of the brain well adapted to the signal. For instance, they define regions larger in the white matter and in the CSF than in the grey matter (Figure 3.9). A large dataset is needed to capture such implicit regularities of the signal with high-dimensional spatial decompositions. Indeed, running the same model on less data extracts modes with less spatial regularity (Mensch et al., 2016). The combination of high dimensionality and large dataset leads to significant computational demands. The extraction of DiFuMos was possible thanks to fast algorithms for huge matrix factorization (Mensch et al., 2018), and gathering data representative of a wide variety of scanning protocols via openfMRI (Poldrack, Barch, and Mitchell, 2013).

We did not limit the DiFuMo modes to gray matter, as measures outside gray matter can be useful in subsequent analysis, for instance to remove the global signal (Murphy and Fox, 2017). In addition, distributed modes extracted from full-brain EPI can separate out noise –such as movement artifacts– and help rejecting it in a later analysis (Griffanti et al., 2014b; Perlberg et al., 2007; Pruim et al., 2015). Some DiFuMo modes indeed segment ventricles or interfaces. Depending on the application, practitioners can choose to restrict signal extraction to a grey-matter mask.

THE FUNCTIONAL MODES ARE SHARP AND ANATOMICALLY RELEVANT To extract structures defined by brain anatomy or microstructure, atlasing efforts have used anatomical or multimodal imaging (Desikan et al., 2006; Eickhoff et al., 2007; Glasser et al., 2016; Mori et al., 2005). The DiFuMo atlases capture a different signal: brain activity. Yet, thanks to the sparsity and non-negativity constraint, they are made of localized modes which often have a natural anatomical interpretation. Consequently, we have labeled the modes with a unique name based on the most relevant anatomical structure, following Urchs et al., 2019 who also give anatomical labels to functional regions. Indeed, using

a common vocabulary of brain structures is important for communication across the neuroimaging community. As visible on [Figure 3.8](#), the modes are well anchored on anatomical structures such as the putamen and the thalamus. They are however not constrained to contain only one connected region. Smaller dimension DiFuMos indeed capture distributed networks, often comprising bilateral regions. As the dimensionality increases, the networks progressively separate in smaller networks which eventually form single regions. For instance, the left and right putamen appear in the same mode at dimension 64, and are first sub-divided along the anterio-posterior direction, and later the left and right putamen are separated ([Figure 3.8](#)). Dimension choice is data driven: it should best explain the functional signal.

3.8 CONCLUSION

With this chapter, we provide multidimensional atlases of functional modes for population imaging to extract functional signals: parietal-inria.github.io/DiFuMo. They give excellent performance for a wide variety of analytic tasks: mental-process decoding or functional-connectivity analysis. Their availability reduces computational burdens: practitioners can readily perform analyses on a reduced signal, without a costly ROI-definition step. In addition, working on common functional modes across studies facilitates comparison and interpretations of results. To help communication, we have labeled every functional mode to reflect the neuroanatomical structures that it contains. To date, these are the only high-dimensional soft functional modes available. As they have been extracted from a variety of data (more than 2,000 sessions across 27 studies, 2.4TB in size) and improve many analytic tasks, the rich descriptions of neural activity that they capture is well suited for a broad set of fMRI studies.

4

PREDICTING PROXY MEASURES FOR MENTAL HEALTH

In this Chapter, we combine socio-demographic information and brain images to derive end points for mental health. We study these to bring complementary information to the challenging problem of understanding complex brain and mind disorders. An epidemiological approach to mental health may benefit from candidate measures extracted from machine learning. We discuss these measures and comparatively learn to predict them from epidemiological data. We evaluate the importance of socio-demographics (non-imaging) and imaging in deriving surrogate endpoints for mental disorders.

4.1 PROBLEM STATEMENT

Individual assessments in psychology and psychiatry rely on observing behavior. Using biological insight to diagnose and treat mental disorders remains a hard problem despite substantial research efforts (Kapur, Phillips, and Insel, 2012). The field of psychiatry has struggled with purely descriptive and unstable diagnostic systems (Insel et al., 2010), small sample sizes (Szucs and Ioannidis, 2017), and reliance on dichotomized groups, *i.e.*, patients vs controls (Hozer and Houenou, 2016). Compared to somatic medicine, mental-health research faces the additional roadblock that mental pathologies cannot be measured the same way diabetes can be assessed through plasma levels of insulin or glucose. Psychological constructs, e.g., depressiveness or anxiety can only be probed indirectly through expert-built procedures such as specially-crafted questionnaires and structured interviews. Measuring reliably a given construct is difficult, and questionnaires often remain the best option (Enkavi et al., 2019). While the field of psychometrics has thoroughly studied the validity of psychological constructs and their measures (Borsboom, Mellenbergh, and Heerden, 2004; Cronbach and Meehl, 1955; Eisenberg et al., 2019), the advent of new biophysical measurements on the brain brings new promises (Engemann et al., 2020a; Kievit et al., 2018; Nave et al., 2018). In particular, the growth of biobanks as well as the advances in statistical-learning techniques opens the door to large-scale validation of psychological constructs and measures for neuropsychiatric research (Collins, 2012).

4.1.1 Motivating example

In clinical neuroscience, machine learning is increasingly popular, driven by the hope to develop more generalizable models (Woo et al., 2017).

Chapter 2 studies the required statistical tools. Yet, the availability of large high-quality neuropsychiatric cohorts is a practical obstacle for applied machine learning in psychiatry (Varoquaux, 2018). Rather, there have been successes developing brain-derived measures on populations without neuropsychiatric conditions, capturing proxy information on mental health such as aging (Liem et al., 2017b). Accordingly, the hope is to learn general measures of individual differences in large datasets with high fidelity, to then enhance a prediction task in a small dataset by exploiting the links between the actual clinical endpoint of interest, e. g. diagnosis or drug response, with those general measures.

4.1.2 Contributions

In this Chapter, we systematically benchmarked distinct proxy-measures of individual differences in three psychological constructs, i. e. brain age, fluid intelligence and neuroticism on the UKBB, the largest epidemiological resource gathering various health-related, social and somatic and neuroimaging data. Contrary to prior studies using similar constructs (Cox et al., 2019; Maglanoc et al., 2020; Nave et al., 2018), our analyses focused on extending the predictive modeling across all domains of MRI and, importantly, performing model comparisons with and against socio-demographic variables. This approach allowed us to investigate, in both regression and classification analyses, the redundancies between these different sources of information and to assess when combining neuroscientific information with socio-demographics variables helped improve learning.

4.2 PROXY MEASURES

In the past years, brain age has received significant interest as one such proxy measure, giving rise to the so called brain age delta defined as the difference between predicted and actual age (Smith et al., 2019). The delta has been shown to reflect physical and cognitive impairment in adults and gives an index of neurodegenerative processes (Liem et al., 2017b). Can the successful strategy pursued with the brain age as a brain-derived proxy-measure be extended beyond the construct of pathological aging?

Intelligence, one of the most extensively studied concepts from psychology, may be such one potential candidate. Fluid intelligence (Cattell, 1963; Cattell and Scheier, 1961) refers to the putatively culture-

free, physiological component of intelligence and has been robustly associated with maturation but also differences in cognitive-processing speed and working-memory capacity (Shelton et al., 2010). It may thus serve as a more specific surrogate measure and, indeed, has been associated with psychiatric disorders such as psychosis, bipolar disorder and substance abuse (Keyes et al., 2017; Khandaker et al., 2018).

Neuroticism, on the other hand, is a traditional concept from personality psychology intrinsically related to anxiety, depression and negative emotions and has been interculturally validated (Cattell and Scheier, 1961; Lynn and Martin, 1997). However, neuroticism has so far been a more elusive trait. Neuroticism has turned out to be useful in psychometric screening and supports predicting real-world behavior (Lahey, 2009; Tyrer, Reed, and Crawford, 2015). Moreover, despite strong heritability at the population level (Power and Pluess, 2015; Vukasović and Bratko, 2015; Yarkoni, 2015), the link with brain function at the level of large-scale network dynamics or the level of molecular mechanisms remains ambiguous given a large body of contradictory results (Yarkoni, 2015). This raises the question of what neuroimaging data it should be related to.

The advent of large MRI datasets has revealed the complexity of anchoring personality traits in the brain. Current attempts to predict fluid intelligence or neuroticism from thousands of MRI scans, argue in favor of overwhelming heterogeneity and rather subtle effects that do not generalize well to unseen data (Dubois et al., 2018b,c). This stands in contrast to the remarkable performance obtained when predicting intelligence or neuroticism from other psychometric measures or semantic data qualitatively similar to psychometric questionnaires, e.g. Twitter and Facebook posts (Quercia et al., 2011; Youyou, Kosinski, and Stillwell, 2015). As MRI acquisitions can be expensive and difficult in clinical settings or population, the success of social-media data is appealing. Reusing such data for medical research and treatment may neither be ethically nor practically feasible while, potentially, susceptible to complex and difficult to control selection bias. On the other hand, background sociodemographic characteristics of individuals can be easily accessible and may help inform in similar ways on the heterogeneity of psychological traits, for instance capturing that fluid intelligence decreases with age. An important question is then whether they bring redundant or complementary information to brain data.

4.3 OBJECTIVES OF CONCEPTUALIZING MENTAL DISORDERS

An intensified focus on sociodemographics calls into attention the diversity of measurement scales, that are often categorical,

e.g. education degree, or quantitative, yet, on arbitrary non-physical units, e.g. monthly income. In fact, society treats individual differences as categorical or continuous, depending on the practical context. Personality has been proposed to span a continuum (Eysenck, 1958). Nevertheless, psychiatrists treat certain people as patients, not others (Perlis, 2011). The utility of any proxy-measure, therefore, depends on its practical context: When learning boundaries between qualitatively distinct groups, a measure that performs globally poorly for regression analysis can, nevertheless, be sufficient for classification analysis. In fact, a measure may be solely informative around the boundary region between certain classes, e.g. pilots who should fly and who should not. Importantly, the utility of any proxy-measure ultimately depends on its signal-to-noise ratio, which may be driven by measurement noise, heterogeneity, as well as variability intrinsic to the particular psychometric instrument chosen, e.g. the type of test to assess intelligence. It is therefore important to assess the limits of what can be learnt with state-of-the-art general purpose machine learning from large-scale datasets.

4.4 BRAIN FEATURES AND SOCIO-DEMOGRAPHICS FOR PREDICTING MODELING

4.4.1 Dataset

We focused on the UKBB database which is openly accessible and has extensive data acquired on 500 000 individuals aged 40-70 years covering rich phenotypes, health-related information, brain-imaging and genetic data (Collins, 2012). UKBB is a prospective cohort where participants across Great Britain who have provided informed consent will follow: Initial assessment visit, first repeat assessment visit, imaging visit (brain image acquisition) and first repeat imaging visit¹.

4.4.2 Participants

In this analysis², we used data mostly based on the initial assessment and the imaging visit (i.e. first and third visit) gathering around 10 000 individuals. We found 11175 individuals who have responded to fluid intelligence questionnaires with 51.6% female (5572) and 48.3% male (5403); and have an age range between 40-70 years (with a mean of 55 years and standard deviation of 7.5 years). Out of these, 5587 individuals are included in the analysis to train the model and

¹ <http://biobank.ctsu.ox.ac.uk/crystal/instance.cgi?id=2> UKBB assessment centre visit and its instances denoted as number

² We undertook this analysis dated December 2017, and we used the data that was available by then, the 10,000 samples release.

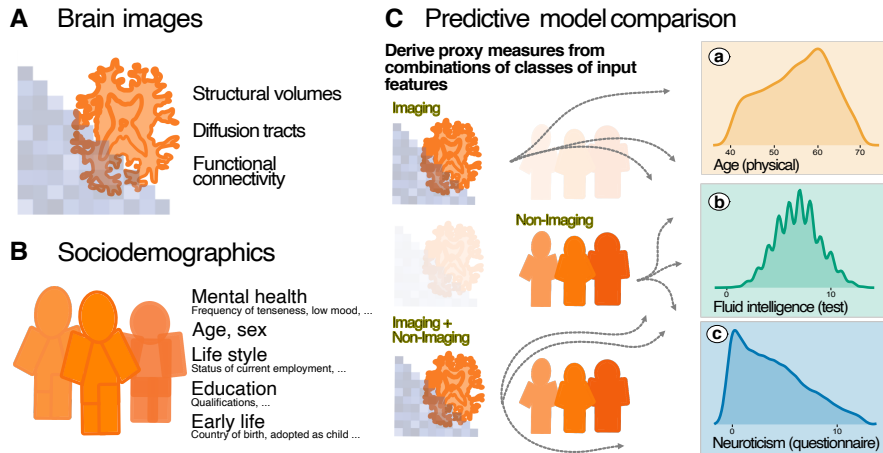


Figure 4.1: Approximating health-related psychological constructs from brain imaging and sociodemographics. In this work we combined multiple classes of brain images (A) with sociodemographic data (B) to approximate health-related biomedical and psychological constructs situated at distinct levels of measurement (C), *i.e.*, the brain age (accessed through prediction of chronological age), cognitive performance (accessed through a test for fluid intelligence) and the tendency to report negative emotions (accessed through the neuroticism questionnaire). We included 10 000 subjects imaging data release from the UK biobank. Among imaging data (A) we considered features related to cortical and subcortical volumes, functional connectivity from rMRI based on ICA networks and white-matter molecular tracts from diffusive directions (see Table 4.1 for an overview about multiple classes of brain images). We then grouped the sociodemographic data (B) into five different blocks of variables related to self-reported responses of health issues, primary demographics, lifestyle, education and early life events (Table 4.2 lists the number of variables in each block). Subsequently, we conducted systematic comparisons between the approximations of all three targets based on either brain images and sociodemographics in isolation or combined (C) to evaluate the relative contribution of these distinct inputs. Models were developed on 50% of the data (randomly drawn) based on random forest regression guided by Monte Carlo cross-validation with 25 splits. For simplicity, we refer to the target-approximations as prediction of proxy measures.

remaining subjects were kept aside for later generalization testing. Also, there were 86 non-imaging variables in our download related to lifestyle, early life, smoking habits and complaints about mental health which we used as additional health-related and sociodemographic predictors in statistical modeling. The present study was supported by application number 23827.

4.4.3 Data processing

The full details about MRI data preprocessing to feature extraction are explained at Appendix E. Here, we briefly outline about the brain features.

4.4.4 Brain features

We conducted predictive modeling combining several sources of input data: Structural Magnetic Resonance Imaging (sMRI), rfMRI, dMRI and non-imaging data.

4.4.4.1 *Structural MRI*

We included 157 sMRI features consisting of volume of total brain and grey matter along with brain subcortical structures.³ All these features are pre-extracted by UKBB brain imaging team (Miller et al., 2016) and are part of data download. We use them as is to stack with other MRI features for predictive analysis.

4.4.4.2 *Diffusion weighted MRI*

We included 432 dMRI skeleton features of Fractional Anisotropy (FA), Tensor Mode (MO) and Mean Diffusivity (MD), Intra-Cellular Volume Fraction (ICVF), Isotropic Volume Fraction (ISOVF) and Orientation Dispersion index (OD) modelled on many brain white matter structures extracted from Neuroanatomy ⁴. The skeleton features we included were from category 134 shipped by the UKBB brain imaging team and we used them without modification.

4.4.4.3 *Functional MRI*

We also included resting-state connectivity features based on the time-series extracted from 55 ICA components representing various brain networks. These included the default mode network (red), extended default mode network and cingulo-opercular network (light red), executive control and attention network (green), visual network (blue), and sensorimotor network (orange) as shown on Fig. E.1. We measured functional connectivity in terms of the between-network covariance. To account for the fact that covariance matrices live inside a particular manifold, i. e. a curved non-Euclidean space, we used the tangent-space embedding to transform the matrices into a Euclidean space (Abraham et al., 2014a; Varoquaux et al., 2010d). Then, we vectorized the connectivity matrices to 1485 features by taking the lower triangular part for predictive modeling.

³ Regional grey matter volumes <http://biobank.ctsu.ox.ac.uk/crystal/label.cgi?id=1101> Subcortical volumes <http://biobank.ctsu.ox.ac.uk/crystal/label.cgi?id=1102>

⁴ Diffusion MRI skeleton measurements <http://biobank.ctsu.ox.ac.uk/crystal/label.cgi?id=134>

Index	Name	# variables	# groups
1	brain volumes (sMRI)	157	1
2	white matter (dMRI)	432	1
3	functional connectivity (fMRI)	1485	1
4	sMRI, dMRI	589	2
5	sMRI, fMRI	1642	2
6	dMRI, fMRI	1917	2
7	sMRI, dMRI, fMRI (full MRI)	2074	3

Table 4.1: Imaging-based models.

4.4.5 Socio-demographics

Also often called as Non-imaging variables in this chapter. We included 86 non-imaging data which are the collection of variables reflecting each participant demographic and social factors i. e. sex, age, date and month of birth, body mass index, ethnicity, exposures at early life such as – breast feeding, maternal smoking around birth, adopted as child – education, exposures of lifestyle related to – occupation, household family income, household people living at the same place, smoking habits – mental health conditions. All these data consist of self-assessments available as part of data download along with imaging data. The whole collection of 86 variables are clustered into 5 groups, where each group consists of variables having correlation associations with each other as shown on Fig. E.2. We name these groups as 1) age, sex (primary demographics) see Table E.1 for the list, 2) early life see Table E.3, 3) education see Table E.2, 4) lifestyle see Tables E.4 and E.5 and 5) mental health see Tables E.6 and E.7.

4.5 PREDICTIVE MODEL COMPARISONS

4.5.1 Imaging-based models

First, we focused on purely imaging-based models based on exhaustive combinations of the three types of MRI modalities (see Table 4.1 for an overview). This allowed us to study potential overlap and additive effects between the modalities. For simplicity, we only focused on the full MRI model in subsequent analyses.

4.5.2 Socio-demographic models

We then composed predictive models based on non-exhaustive combinations of different types of socio-demographic variables. We then performed model comparisons to learn about the importance of each of these types. We were particularly interested in studying the relative

Index	Name	# variables	# groups
1	Mental health (MH)	25	1
2	Age, Sex (AS)	5	1
3	Life style (LS)	45	1
4	Education (EDU)	2	1
5	Early Life (EL)	9	1

Table 4.2: Non-imaging baseline models or socio-demographic models based on single group. Variables in each group are listed on Tables E.1 to E.7 respectively.

contributions of early life factors as compared to factors related to more recent life events such as education as well as factors related to current circumstances such as mental health and life-style. Therefore, we first considered baseline models based on one group of socio-demographic variables and then progressively extended the models to a full model based on all socio-demographic variables. The resulting one group models are listed in Table 4.2.

4.5.3 Combined imaging and socio-demographic models

Importantly, we were interested in how brain-related information would interact with sociodemographics for each of these models. We therefore considered an alternative variant for each of the models in Table 4.2 that included all MRI-related features (2074 additional features) as described at Section 4.4.4.

4.5.4 Predictive model

The choice of learning algorithm is an important concern when performing predictive modeling. As studied on Fig. 2.3 at Chapter 2, linear models have turned out to be good default choices in neuroimaging research, yet they may not be optimal when dealing with heterogeneous data on large-scale samples. To combine imaging data with socio-demographics, we relied on the non-parametric random forest (RF) algorithm that can be readily used on data of different units for regression and classification (Breiman, 2001b). Moreover, random forests enable learning non-linear interaction effects without explicit modeling, which makes them an interesting tool to explore the relationship between different modalities. We used cross-validation to train RF on 90% samples and test on the remaining 10%. We repeat this process for 25 cross-validation splits. For each split, we used in-built cross-validation of the model to tune the maximum depth of the tree and minimum number of samples required at leaf node for split point with two fixed parameters; variance reduction criterion as “mse” for 250 number of trees. For the list of parameters see Table 4.3. After

Parameter	Values
Impurity criterion	Mean squared error
Maximum tree depth	5, 10, 20, 40, full depth
Fraction of features for split	1, 5, "log2", "sqrt", "complete"
Number of trees	250

Table 4.3: Random forest model parameters tuned with in-built cross-validation. Number of trees is set by stabilization of out-of-bag (OOB) error rate after trying from a range of values in 250, 350, 500, 800, 1000, 2000, 3000, 5000.

tuning the parameter selection, the coefficient of determination (R^2) is the metric used for the assessment of prediction performance of the model on test data.

4.5.5 Statistical hypothesis testing

To establish the null-hypothesis baseline of the model, the prediction targets are permuted within each fold where the optimal model is trained on permuted targets and predicted on test data. This process is repeated for 10 random permutations on prediction targets. Finally, the distribution of R^2 scores from these 10 random permutations for 25 splits are used for comparisons against the distributions of the true model. This allows us to assess the significance of model prediction accuracy.

4.5.6 Classification analysis

We also performed classification analysis on the continuous targets. For this purpose, we discretized the targets into three groups based on the 33% and 66% percentiles. Then we performed binary classification on these three groups i.e. group 1 vs group 2; group 2 vs group 3; group 1 vs group 3. We were particularly interested in understanding whether model performance would increase when moving toward classifying extreme groups. For this analysis, we considered all three types of models (see Sections 4.5.1 to 4.5.3 and Tables 4.1 and 4.2). To assess the performance of classification analysis, we use AUC ROC as an evaluation metric.

4.5.7 Ranking statistics to assess paired differences of combined models

To assess the statistical significance in the benefits of combining brain images with socio-demographics for proxy measures, we followed the ranking statistics procedure as in Engemann et al., 2020b. First, we estimate paired differences by relying on pair-wise per split esti-

Features space	# groups	Age	Fluid intelligence	Neuroticism
Imaging and Non-imaging	1	1335	1108	1054
	2	1668	2197	1476
	3	1200	898	1020
Non-imaging	1	1764	1515	1388
	2	2223	2906	1959
	3	1600	1166	1350

Table 4.4: Number of samples for classification analysis (N). N varies on the feature space as not all individuals have completed the imaging visit.

mates of combined models (see Section 4.5.3) and socio-demographics models (see Section 4.5.2). Then, we extracted the mean, the standard deviation, the 5 and 95 percentiles on those paired-wise estimates on distribution of 25 splits to determine the combined models prediction performances.

4.6 BRAIN IMAGING COMPLEMENTS SOCIO-DEMOGRAPHICS FOR PROXY MEASURES

We first performed model comparisons across socio-demographic models Table 4.2 to evaluate the relative performance of each model composed of distinct groups of sociodemographic variables for predicting proxy measures. Fig. 4.2 (in red) summarizes these model comparisons for predicting three targets: age, fluid intelligence and neuroticism. The analysis revealed that for each target there was one principal block of variables explaining most of the prediction performance. For age prediction, variables related to current life-style (LS) showed by far the highest performance. For fluid intelligence, education (EDU) performed by far best. Finally, for neuroticism, mental health clearly showed the strongest performance. This pattern persisted when considering exhaustive model comparisons based on all possible combinations of variable blocks (supplement Figs. E.3 and E.4).

We then repeated the analysis including brain images (full MRI composed of 2074 variables, Table 4.1 to investigate potential synergies and redundancies between socio-demographics and brain imaging Fig. 4.2(in blue). The results suggest that age prediction improved as sociodemographics and MRI were combined. This effect was visible on all four blocks of variables. As the performance distributions between the purely sociodemographic and the combined model were overlapping for the lifestyle model, we considered the paired differences across cross-validation splits. The analysis revealed that the combined model performed better in 24 out of 25 folds than the purely sociodemographic model ($M=0.059$, $SD=0.03$, $P(5,95)=[0.006,$

0.116]), suggesting that the observed differences should reproduce on future data and is unlikely to be due to chance. The potential benefit of including brain imaging features, however, was less consistent for prediction of fluid intelligence and neuroticism. For fluid intelligence, average performance was enhanced through brain images in poorly performing sociodemographic models, i.e. early life (better in 22/25 folds, $M=0.025$, $SD=0.022$, $P(5,95)=[-0.005, 0.06]$), but not the best performing model (education) where distributions were virtually identical. Similarly, for neuroticism, higher average performance with brain images emerged for education (better in all 25 folds, $M=0.023$, $SD=0.014$, $P(5,95)=[0.002, 0.045]$) but not the best model (mental health). Nevertheless, we found significant average prediction based on brain images only for, both, fluid intelligence and neuroticism. This suggests that variance in lifestyle and mental health is reflected in neurobiological variance. For neuroticism current mental health variables were strongly informative for prediction, suggesting that mental health is a reasonable proxy of neuroticism. Overall, predicting fluid intelligence or neuroticism was clearly more successful based on socio-demographic data as compared to brain images.

4.7 CLASSIFICATION GROUPS ARE BETTER DISCRIMINATED WITH SOCIO-DEMOGRAPHICS

The scale and units of psychological proxy-measure are often unknown. In practice, clinicians and educators aim at specific thresholds for decision-making. How do predictive models compare across proxy measures when considering discrete extreme-groups? To address this question, we performed binary classification analysis on three diverse groups i.e. low vs high, low vs middle, middle vs high dichotomized on the continuous values of three prediction targets: age, fluid intelligence and neuroticism. Moreover, we focused on the AUC as a performance metric which, other than accuracy, is only sensitive to ranking while ignoring the scale of the error. The analysis revealed model-ranking comparable to the previous regression analysis. Classification-performance was better than chance for all models as shown on Figs. 4.3, E.5 and E.6. We observed the highest scores when discriminating between the extreme groups, i.e. low vs high Fig. 4.3. Overall, a similar picture emerged as for the regression analysis. Across proxy measures, models including sociodemographics performed best. Combining sociodemographics and brain imaging led to slight benefits for age prediction in 23/25 folds ($M=0.012$, $SD=0.01$, $P(5,95)=[-0.002, 0.027]$). For fluid intelligence and neuroticism a weak opposite trend was visible in which the combined model performed worse on about 2 thirds of the folds. But overall, performance differences between the sociodemographic and combined models were

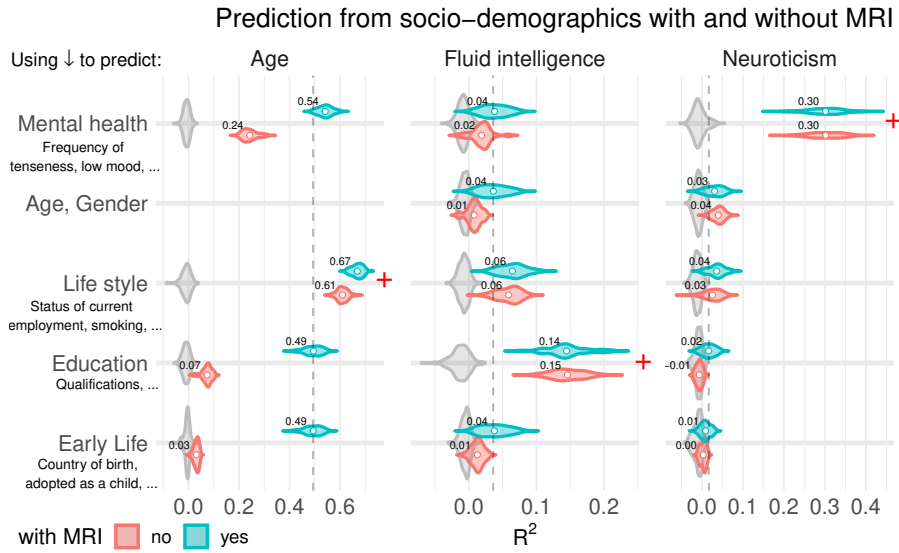


Figure 4.2: Prediction of psychological proxy measures from socio-demographic data combined with and without MRI. Prediction of age, fluid intelligence and neuroticism from socio-demographic one group models Table 4.2. Color indicates whether MRI (blue) was included for prediction or not (red). We used the R^2 score to facilitate comparisons across prediction targets. The estimated null-distribution is depicted by gray violin plots (across permutations and folds). The expected prediction performance is depicted by colored violin plots. Vertical dotted lines indicate the average performance of the full MRI model introduced in Fig. 4.4. For convenience, the mean performance is annotated for each plot. One can readily see that prediction with socio-demographics (red) was markedly stronger than with only the brain-based model (dotted vertical lines) for three targets. The most important blocks of sociodemographic predictors (annotated with red cross) were lifestyle for age, education for fluid intelligence and mental health for neuroticism. Moreover, the effect of combining socio-demographics with brain-data depended on the prediction target. For age, overall performance improved beyond the previous analyses. The picture was less consistent for fluid intelligence and neuroticism showing weaker additive effects, if any.

low on the order of one or two AUC units on average. It is noteworthy that for both types of models prediction performance reached levels above 0.8, which is considered clinically useful for biomarker candidates (Perlis, 2011). Low vs middle and middle vs high groups based classification are shown on Figs. E.5 and E.6. Overall, the results suggest that moving from the more difficult full-scale regression problem to extreme-group classification problem with purely ranking-based loss functions, the relative differences between brain-based and socio-demographics-based prediction gradually fade away.

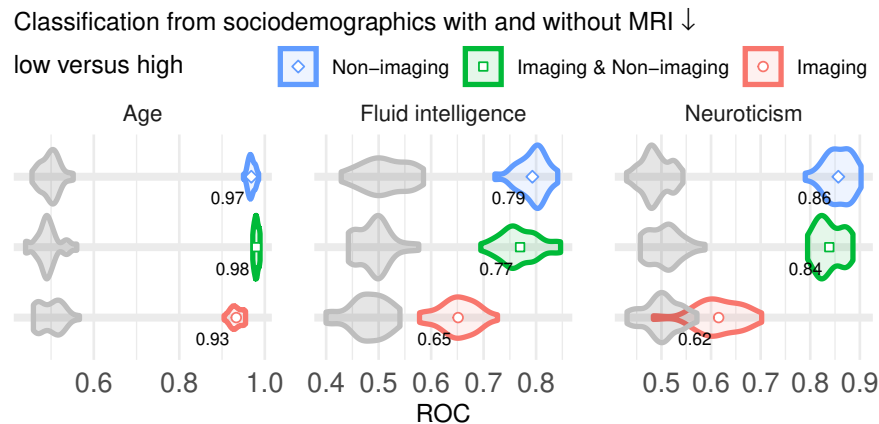


Figure 4.3: Classification analysis from imaging, socio-demographics and combination of both data. Classification of extreme groups i.e. low vs high where split was on the basis of age, fluid intelligence and neuroticism scores. This analysis is a complementary model comparison as compared to Fig. 4.2. Shape and color indicates the type of data used for model comparison on each of two binary groups. We report the accuracy in AUC. The estimated null-distribution is shown in gray violin plots whereas colored violin plots depict the distribution of classification accuracies per model. The mean value is shown on each violin plot to facilitate comparisons across classification groups. The model comparisons reveal that higher classification accuracies were achieved with low vs high when compared to other groups on Figs. E.5 and E.6. Models including socio-demographics performed visibly better than models purely based on brain imaging. Differences between brain-imaging and sociodemographics were reduced as compared to the fully-fledged regression analysis.

4.8 AGE IS BEST PREDICTED FROM MRI COMPARED TO OTHER PROXY MEASURES

We perform imaging-based model comparisons to identify the links between measures of the brain and surrogate targets, also check if there exists any additive effects between brain imaging modalities that could potentially improve these links. Fig. 4.4 summarizes the comparisons of predicting three targets – fluid intelligence, neuroticism and brain age – from the combination of imaging-based models Table 4.1. The analysis revealed weak associations linking targets like fluid intelligence or neuroticism to brain images whereas on the other hand strong associations were found linking age to brain images. In terms of additive learning, the maximum performance for fluid intelligence and neuroticism is achieved while using more than one imaging modality such as the full MRI model. This emphasizes the benefits of combining many sources of brain images for additive effects. For fluid intelligence and neuroticism, we can see that the additive effects are weak but significantly better than chance. Overall, model comparisons

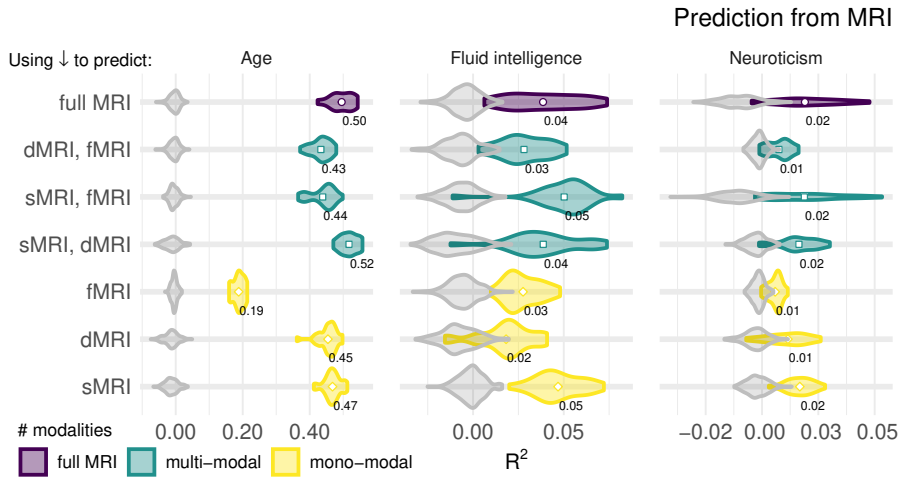


Figure 4.4: Prediction of individual differences from brain-imaging data. Prediction of age, fluid intelligence and neuroticism based on three MR modalities: sMRI, dMRI and rfMRI. Different models are based on exhaustive combinations between modalities. Shape and color indicate the number of modalities per model. We used the R^2 score to facilitate comparisons across prediction targets. The estimated null-distribution is depicted by gray violin plots. The expected prediction performance is depicted by colored violin plots. For convenience, the mean performance is annotated for each plot. Prediction of age was markedly stronger than prediction of fluid intelligence or prediction of neuroticism. Nevertheless, significant prediction was achieved for all targets. As a general trend, models based on multiple MRI modalities tended to yield better prediction.

suggests that combining multiple sources of brain imaging yields better prediction.

4.9 CONCLUSION

A fundamental challenge of mental-health research is that the quantities of interest are not directly observable: psychological traits that have to be inferred. In this work, we systematically compared MRI and socio-demographics data to derive proxy measures for mental health. We build these measures by applying machine learning on the largest brain-imaging cohort to date, UK Biobank, with 10 000 subjects multimodal MRI and rich socio-demographics information. As these measures are based on data of different nature, brain imaging (2074 variables), socio-demographics, and questionnaires (summed to 86 variables), we compare them objectively by assessing which aspects of individual traits they capture, in isolation and both combined (brain & socio-demographics). All brain-derived proxy measures captured the constructs of interest, however the association between the brain imaging and socio-demographics was most pronounced for aging. On the other hand, for intelligence and neuroticism, we did

not find evidence that brain-derived information was independent from sociodemographic information. Overall, brain imaging complement nicely socio-demographic information and self-assessments that are robust to cultural dimensions of distinct constructs of interest. For instance, education variables predict fluid intelligence, mental health complaints predict neuroticism. As such, the combined proxy measures may be promising for epidemiological studies of mental health.

ONGOING WORK Currently in the upcoming work, we investigate how subject-specific derived proxy measures can be linked to lifestyle habits such as alcohol or sleep to test the relevance of proxy measures for health outcomes. We establish brain age delta, the difference between the predicted age and the chronological age, fluid intelligence and neuroticism predictions and their associations with the health-related habits (alcohol and tobacco consumption, sleep duration, physical activity) using multiple linear regression. With best performing models, multiple linear regression reveal specific and additive associations with health outcomes. Furthermore, we extend our model comparisons to 100 cross-validation splits and introduce a new test set which we call generalization set (5 000 samples). Using the trained RF model on 90% samples as described at Section 4.5.4, we evaluate predictions that is independent from the previously left-out data (validation set of equal size 5 000 samples).

This test set is held-out within the same cohort UKBB that accounts for 50% of complete samples size used in this analysis. The idea of keeping aside this generalization set is to assess the generalization performance under new samples. Also importantly, generalization set allowed us to estimate proper permutation-based p-values and bootstrap-based confidence intervals. The fraction of UKBB data held-out for generalization test was not used until June 2020. We prefered to test on the samples within the same cohort, as investigating other data sources would bring undesirable differences in terms of cognitive measures, age range and imaging protocols. The ongoing work we described is presented in

Kamalaker Dadi, Gaël Varoquaux, Josselin Houenou,
Danilo Bzdok, Bertrand Thirion, and Denis Engemann
(2020a). "Beyond brain age: Empirically-derived proxy mea-
sures of mental health." In: *bioRxiv*. DOI: [10.1101/2020.08.25.266536](https://doi.org/10.1101/2020.08.25.266536).

5 | CONCLUSION

More and more cohorts are being built in the general and pathological population, grounding high-quality predictive analysis in mental health. Analyzing such datasets requires benchmarking predictive methods on real and high-dimensional brain-imaging data. This thesis describes a comprehensive and robust evaluation of predictive methods conducted over many brain-imaging cohorts, contributes a family of functional atlases for fMRI analysis, and finally, investigates the potential of imaging epidemiology to analyze behavioural factors for mental health.

In Chapter 2, we benchmarked several analysis pipelines for predicting population phenotypes from Resting-state functional connectomes. rfMRI has proved to be a great tool to study intrinsic brain organization and diseases through brain functional connectivity characterized at “rest”. Transforming the conceptual ideas into practice requires statistical modeling on rfMRI data. Here, the challenge lies in settling on a standard modeling framework to turn complex rfMRI data into regions, connectomes and predictive markers. The availability of many statistical models makes the selection harder and represents a burden on researchers for computational exploration. We ran more than 50 000 analysis pipelines that cover exploration of numerous methods on many openly available imaging cohorts to recommend a robust analysis pipeline. Defining continuously-valued regions with sparse linear decomposition methods, comparing connections estimated on those regions in manifold space, and using linear classifiers were shown to dominate other solutions.

Chapter 2 sheds light on the data-driven brain parcellations that provide the support of functional connectivity (brain phenotypes) to predictions. Given its role in predictions, in Chapter 3, we further explore continuous functional brain parcellations. We took the advantage of the amount of openly-accessible fMRI brain records and existing sparse matrix factorization technique that have been developed to scale to large-scale high-dimensional brain imaging functional records. We extracted dictionaries of 1024 components from OpenfMRI data hosting repository, which opens new perspectives for brain-imaging derived phenotypes – an emerging trend for easier access to non-experts in fMRI data processing. We are the first to provide multi-scale (64, 128, 256, 512, 1024) continuous functional networks learned on such large data (2192 fMRI records). Extensive validation of these functional networks revealed that “soft” probabilistic atlases are beneficial

and more components are crucial for reducing the dimensionality of raw fMRI data.

Proposed atlases and anatomical labels assigned to each atlas component are ready to view and download via the online interactive visualizations website: parietal-inria.github.io/DiFuMo.

The work presented in Chapter 3 relied on a Python package called *modl*, that is publicly available¹ with an easy to use documentation that can be applied to brain-imaging cohorts.

Imaging epidemiological cohorts provide large-scale data resources that challenge the identification of appropriate measures to relate to health outcomes. In Chapter 4, we investigated proxy measures that could be interesting in predicting or understanding complex mental disorders. To do this, we compared three targets – age, fluid intelligence and neuroticism – at large-scale to potentially uncover epidemiologically relevant associations through behavioral assessments and brain measurements. So far, this study used large sample size of 10 000 individuals, on which we performed systematic predictive model comparisons by individuals socio-demographic measures with multi-modal brain images and showed that the combination enhanced predictions. Out of many model comparisons, there exists a predominant model that showed distinct predictive performance linked to each target e.g. mental health variables predicting neuroticism and education is linked to fluid intelligence test scores. This suggests that the models captured the quantitative and objective information from both socio-demographics and brain images. On the other hand, brain images were best at age but less well-suited for predicting psychological constructs such as fluid intelligence and neuroticism questionnaires. This last study opened a new perspective of how proxy measures could be defined as surrogate end points for mental disorders from an epidemiological standpoint.

As part of the non-PhD activity, I was lucky enough to participate in an exciting international project called Neuroimaging Analysis Replication and Prediction Study (NARPS) as one of the analysis team on behalf of the Parietal team. This project involves estimating the variability of neuroimaging results across analysis teams that test nine specific a priori hypotheses (regarding activation in specific brain areas recruited while performing mixed-gambling task). My contribution involved statistical modeling on the raw task-fMRI data towards nine specific hypotheses testing.

During these three years of my PhD, I underwent many non-technical courses that fall under the category of scientific mediation and foreign languages that are the most interesting tools for enhancing my profession as a doctoral student. I also had the joy to attend summer schools, international conference or workshops to present my thesis work.

¹ <https://github.com/arthurmensch/modl>

6

SYNTÈSE EN FRANÇAIS

Les troubles mentaux présentent une grande hétérogénéité entre les individus. Une difficulté fondamentale pour étudier leurs manifestations ou leurs facteurs de risque est que le diagnostic des conditions mentales pathologiques est rarement disponible dans les grandes cohortes de santé publique. Ici, nous cherchons à développer des biomarqueurs, signatures cérébrales de troubles mentaux. Pour cela, nous utilisons l'apprentissage automatique pour prédire les résultats de santé mentale grâce à l'imagerie de population, en se basant sur l'imagerie cérébrale (imagerie par résonance magnétique (IRM)). Compte tenu des évaluations comportementales ou cliniques, l'imagerie de population peut relier les caractéristiques uniques des variations cérébrales à ces mesures autodéclarées non cérébrales basées sur des questionnaires. Ces mesures non cérébrales fournissent une description unique des différences psychologiques de chaque individu qui peuvent être liées à la psychopathologie à l'aide de méthodes statistiques. Cette thèse de doctorat examine le potentiel d'apprentissage de tels résultats basés sur l'imagerie pour analyser la santé mentale. En utilisant des méthodes d'apprentissage automatique, nous effectuons une évaluation, à la fois complète et robuste, des mesures de population pour guider des prévisions de haute qualité des résultats pour la santé.

Cette thèse est organisée en trois parties principales: premièrement, nous présentons une étude approfondie des biomarqueurs du connectome, deuxièmement, nous proposons une réduction significative des données qui facilite les études d'imagerie de population à grande échelle, et enfin nous introduisons des mesures indirectes pour la santé mentale.

Nous avons d'abord mis en place une étude approfondie des connectomes d'imagerie afin de prédire les phénotypes cliniques. Avec l'augmentation des images cérébrales de haute qualité acquises en l'absence de tâche explicite, il y a une demande croissante d'évaluation des modèles prédictifs existants. Nous avons effectué des comparaisons systématiques reliant ces images aux évaluations cliniques dans de nombreuses cohortes pour évaluer la robustesse des méthodes d'imagerie des populations pour la santé mentale. Nos résultats soulignent la nécessité de fondations solides dans la construction de réseaux cérébraux entre les individus. Ils décrivent des choix méthodologiques clairs: régions définies à partir de données fonctionnelles, par exemple avec l'analyse des composants indépendants ou l'apprentissage par dictionnaire, représentant la connectivité avec l'incorporation tangente des matrices de covariance et utilisant un modèle linéaire non

clairsemé, comme une régression logistique. Ce travail est publié dans la revue *NeuroImage* (Dadi et al., 2019).

Ensuite, nous contribuons à une nouvelle génération d'atlas fonctionnels du cerveau pour faciliter des prédictions de haute qualité pour la santé mentale. Les atlas fonctionnels du cerveau sont en effet le principal goulot d'étranglement pour la qualité de la prédiction. Ces atlas sont construits en analysant des volumes cérébraux fonctionnels à grande échelle à l'aide d'un algorithme statistique évolutif, afin d'avoir une meilleure base pour la prédiction des résultats. Après les avoir comparés avec des méthodes de pointe, nous montrons leur utilité pour atténuer les problèmes de traitement des données à grande échelle. Ils offrent d'excellentes performances pour une grande variété de tâches analytiques: décodage de processus mental ou analyse de connectivité fonctionnelle. Leur disponibilité réduit les charges de calcul: les praticiens peuvent facilement effectuer des analyses sur un signal réduit, sans étape coûteuse de définition du retour sur investissement. De plus, travailler sur des modes fonctionnels communs à travers les études facilite la comparaison et l'interprétation des résultats. Pour faciliter la communication, nous avons étiqueté chaque mode fonctionnel pour refléter les structures neuroanatomiques qu'il contient. Nous les avons rendus disponibles pour téléchargement à partir de parietal-inria.github.io/DiFuMo. Ce travail est publié dans la revue *NeuroImage* (Dadi et al., 2020b).

La dernière contribution principale consiste à étudier les mesures de substitution potentielles des résultats pour la santé. Un défi fondamental de la recherche en santé mentale est que les quantités d'intérêt ne sont pas directement observables: des traits psychologiques qui doivent être déduits. Nous considérons des comparaisons de modèles à grande échelle utilisant des mesures du cerveau avec des évaluations comportementales dans une cohorte épidémiologique d'imagerie, le UK Biobank avec 10 000 sujets. Sur cet ensemble de données complexe, le défi consiste à trouver les covariables appropriées et à les relier à des résultats bien choisis, car ces mesures sont basées sur des données de nature différente, l'imagerie cérébrale, la sociodémographie et des questionnaires. Après une sélection et une évaluation soigneuses du modèle à l'aide de l'apprentissage automatique, nous identifions des mesures de substitution qui affichent des liens distincts avec les données sociodémographiques et peuvent être en corrélation avec des conditions non pathologiques. Par exemple, toutes les mesures indirectes dérivées du cerveau ont capturé les construits d'intérêt, mais l'association entre l'imagerie cérébrale et les données sociodémographiques était plus prononcée pour le vieillissement. Par contre, pour l'intelligence et le névrosisme, nous n'avons pas trouvé de preuves que les informations dérivées du cerveau étaient indépendantes des informations sociodémographiques. Dans l'ensemble, l'imagerie cérébrale complète bien

les informations sociodémographiques et les auto-évaluations qui sont robustes aux dimensions culturelles de différents concepts d'intérêt. En tant que telles, les mesures substitutives combinées peuvent être prometteuses pour les études épidémiologiques de la santé mentale. Ce travail est soumis à la publication de revue disponible à <https://doi.org/10.1101/2020.08.25.266536>.

REFERENCES

REFERENCES

- Abou Elseoud, Ahmed, Harri Littow, Jukka Remes, Tuomo Starck, Juha Nikkinen, Juuso Nissilä, Osmo Tervonen, Markku Timonen, and Vesa Kiviniemi (2011). "Group-ICA Model Order Highlights Patterns of Functional Brain Connectivity." In: *Frontiers in Systems Neuroscience* 5, p. 37.
- Abraham, Alexandre, Elvis Dohmatob, Bertrand Thirion, Dimitris Samaras, and Gael Varoquaux (2013). "Extracting brain regions from rest fMRI with Total-Variation constrained dictionary learning." In: *MICCAI*, p. 607.
- Abraham, Alexandre, Fabian Pedregosa, Michael Eickenberg, Philippe Gervais, Andreas Mueller, Jean Kossaifi, Alexandre Gramfort, Bertrand Thirion, and Gael Varoquaux (2014a). "Machine learning for neuroimaging with scikit-learn." In: *Frontiers in Neuroinformatics* 8.
- Abraham, Alexandre, Fabian Pedregosa, Michael Eickenberg, Philippe Gervais, Andreas Mueller, Jean Kossaifi, Alexandre Gramfort, Bertrand Thirion, and Gaël Varoquaux (2014b). "Machine learning for neuroimaging with scikit-learn." In: *Frontiers in neuroinformatics* 8.
- Abraham, Alexandre, Michael P Milham, Adriana Di Martino, R Cameron Craddock, Dimitris Samaras, Bertrand Thirion, and Gaël Varoquaux (2017). "Deriving reproducible biomarkers from multi-site resting-state data: An Autism-based example." In: *NeuroImage* 147, pp. 736–745.
- Alexander-Bloch, Aaron, Liv Clasen, Michael Stockman, Lisa Ronan, Francois Lalonde, Jay Giedd, and Armin Raznahan (2016). "Subtle in-scanner motion biases automated measurement of brain anatomy from in vivo MRI." In: *Human Brain Mapping* 37, pp. 2385–2397.
- Alfaro-Almagro, Fidel et al. (2018). "Image processing and Quality Control for the first 10,000 brain imaging datasets from UK Biobank." In: *NeuroImage* 166, pp. 400–424.
- Alvarez, R. and R.A. Poldrack (2011). "Cross-language repetition priming." In: *Stanford Digital Repository*.
- Anderson, Ariana, Pamela K. Douglas, Wesley T. Kerr, Virginia S. Haynes, Alan L. Yuille, Jianwen Xie, Ying Nian Wu, Jesse A. Brown, and Mark S. Cohen (2014). "Non-negative matrix factorization of multimodal MRI, fMRI and phenotypic data reveals differential changes in default mode subnetworks in ADHD." In: *NeuroImage* 102, pp. 207–219.
- Andersson, J. L. R., M. Jenkinson, S. Smith, M. Jenkinson, S. Smith, J. L. R. Andersson, J. L. R. Andersson, P. a. E. S. Smith, J. L. Anders-

- son, and S. W. Smith (2007). "Non-Linear Registration aka Spatial Normalisation FMRIB Technical Report TR07JA2." In: Andersson, Jesper L. R. and Stamatios N. Sotiroopoulos (2015). "Non-parametric representation and prediction of single- and multi-shell diffusion-weighted MRI data using Gaussian processes." In: *NeuroImage* 122, pp. 166–176.
- Arbabshirani, Mohammad R, Sergey Plis, Jing Sui, and Vince D Calhoun (2017). "Single subject prediction of brain disorders in neuroimaging: Promises and pitfalls." In: *NeuroImage* 145, pp. 137–165.
- Aron, Adam R., Mark A. Gluck, and Russell A. Poldrack (2006). "Long-term test-retest reliability of functional MRI in a classification learning task." In: *NeuroImage* 29.3, pp. 1000 –1006.
- Aron, Adam R., Tim E. Behrens, Steve Smith, Michael J. Frank, and Russell A. Poldrack (2007). "Triangulating a Cognitive Control Network Using Diffusion-Weighted Magnetic Resonance Imaging (MRI) and Functional MRI." In: *Journal of Neuroscience* 27.14, pp. 3743–3752.
- Arslan, Salim, Sofia Ira Ktena, Antonios Makropoulos, Emma C. Robinson, Daniel Rueckert, and Sarah Parisot (2017). "Human brain mapping: A systematic comparison of parcellation methods for the human cerebral cortex." In: *NeuroImage*.
- Ashburner, John and Karl J. Friston (2000). "Voxel-based morphometry—The methods." In: *Neuroimage* 11, pp. 805–821.
- Barachant, Alexandre, Stéphane Bonnet, Marco Congedo, and Christian Jutten (2013). "Classification of covariance matrices using a Riemannian-based kernel for BCI applications." In: *Neurocomputing* 112, pp. 172 –178.
- Bassett, Danielle S., Brent G. Nelson, Bryon A. Mueller, Jazmin Camchong, and Kelvin O. Lim (2012). "Altered resting state complexity in schizophrenia." In: *NeuroImage* 59.3, pp. 2196–2207.
- Bearden, C.E. and P.M. Thompson (2017). "Emerging Global Initiatives in Neurogenetics: The Enhancing Neuroimaging Genetics through Meta-analysis (ENIGMA) Consortium." In: *Neuron* 94, pp. 232–236.
- Beckmann, C. F. and S. M. Smith (2004a). "Probabilistic independent component analysis for functional magnetic resonance imaging." In: *Trans Med Im* 23, p. 137.
- (2004b). "Probabilistic independent component analysis for functional magnetic resonance imaging." In: *IEEE Transactions on Medical Imaging* 23.2, pp. 137–152.
- Beckmann, C.F., M. DeLuca, J.T. Devlin, and S.M. Smith (2005). "Investigations into resting-state connectivity using independent component analysis." In: *Philos Trans R Soc Lond B* 360, p. 1001.
- Behrens, T.E.J., M.W. Woolrich, M. Jenkinson, H. Johansen-Berg, R.G. Nunes, S. Clare, P.M. Matthews, J.M. Brady, and S.M. Smith (2003). "Characterization and propagation of uncertainty in diffusion-weighted MR imaging." In: *Magnetic Resonance in Medicine* 50, pp. 1077–1088.

- Behzadi, Y., K. Restom, J. Liau, and T.T. Liu (2007). "A component based noise correction method (CompCor) for BOLD and perfusion based fMRI." In: *Neuroimage* 37, p. 90.
- Bellec, P., P. Rosa-Neto, O.C. Lyttelton, H. Benali, and A.C. Evans (2010). "Multi-level bootstrap analysis of stable clusters in resting-state fMRI." In: *NeuroImage* 51, p. 1126.
- Benjamini, Yoav and Yosef Hochberg (1995). "Controlling the False Discovery Rate: A Practical and Powerful Approach to Multiple Testing." In: *J R STAT SOC B (Methodological)* 57.1, p. 289.
- Biswal, B.B., M. Mennes, X.N. Zuo, S. Gohel, C. Kelly, S.M. Smith, C.F. Beckmann, et al. (2010). "Toward discovery science of human brain function." In: *Proc Ntl Acad Sci* 107, p. 4734.
- Biswal, Bharat, F. Zerrin Yetkin, Victor M. Haughton, and James S. Hyde (1995). "Functional connectivity in the motor cortex of resting human brain using echo-planar mri." In: *Magnetic Resonance in Medicine* 34.4, pp. 537–541.
- Borsboom, Denny, Gideon J. Mellenbergh, and Jaap van Heerden (2004). "The Concept of Validity." In: *Psychological Review* 111.4, pp. 1061–1071.
- Breiman, Leo (2001a). "Random Forests." In: *Machine Learning* 45, p. 5.
- (2001b). "Random Forests." In: *Machine Learning* 45.1, pp. 5–32.
- Brier, Matthew R, Anish Mitra, John E McCarthy, Beau M Ances, and Abraham Z Snyder (2015). "Partial covariance based functional connectivity computation using Ledoit–Wolf covariance regularization." In: *NeuroImage* 121, pp. 29–38.
- Brown, Colin J and Ghassan Hamarneh (2016). "Machine Learning on Human Connectome Data from MRI." In: *arXiv:1611.08699*.
- Bullmore, E and O Sporns (2009). "Complex brain networks: graph theoretical analysis of structural and functional systems." In: *Nat Rev Neurosci* 10, p. 186.
- Bzdok, Danilo, Gaël Varoquaux, Olivier Grisel, Michael Eickenberg, Cyril Poupon, and Bertrand Thirion (2016). "Formal Models of the Network Co-occurrence Underlying Mental Operations." In: *PLOS Computational Biology* 12, pp. 1–31.
- Caballero-Gaudes, César and Richard C. Reynolds (2017). "Methods for cleaning the BOLD fMRI signal." In: *NeuroImage* 154, pp. 128–149.
- Calhoun, V. D., T. Adali, G. D. Pearlson, and J. J. Pekar (2001). "A method for making group inferences from fMRI data using independent component analysis." In: *Hum Brain Mapp* 14, p. 140.
- Calhoun, V.D., J. Sui, K. Kiehl, J. Turner, E. Allen, and G. Pearlson (2012). "Exploring the psychosis functional connectome: Aberrant intrinsic networks in schizophrenia and bipolar disorder." In: *Frontiers in Psychiatry*.
- Calhoun, Vince D., Kent A. Kiehl, and Godfrey D. Pearlson (2008). "Modulation of temporally coherent brain networks estimated using

- ICA at rest and during cognitive tasks." In: *Hum Brain Map* 29.7, p. 828.
- Carp, Joshua (2012). "On the plurality of (methodological) worlds: Estimating the analytic flexibility of fMRI experiments." In: *Frontiers in neuroscience* 6.
- Catani, Marco and Michel Thiebaut de Schotten (2012). *Atlas of Human Brain Connections*. Oxford University Press.
- Cattell, Raymond B (1963). "Theory of fluid and crystallized intelligence: A critical experiment." In: *Journal of educational psychology* 54.1, p. 1.
- Cattell, Raymond B and Ivan H Scheier (1961). "The meaning and measurement of neuroticism and anxiety." In:
- Cera, Nicoletta, Armando Tartaro, and Stefano L. Sensi (Sept. 2014). "Modafinil Alters Intrinsic Functional Connectivity of the Right Posterior Insula: A Pharmacological Resting State fMRI Study." In: *PLOS ONE* 9, pp. 1–12.
- Chang, Luke J., Peter J. Gianaros, Stephen B. Manuck, Anjali Krishnan, and Tor D. Wager (2015). "A Sensitive and Specific Neural Signature for Picture-Induced Negative Affect." In: *PLOS Biology* 13, pp. 1–28.
- Chen, Gang, B. Douglas Ward, Chunming Xie, Wenjun Li, Zhilin Wu, Jennifer L. Jones, Małgorzata Franczak, Piero Antuono, and Shi-Jiang Li (2011). "Classification of Alzheimer Disease, Mild Cognitive Impairment, and Normal Cognitive Status with Large-Scale Network Analysis Based on Resting-State Functional MR Imaging." In: *Radiology* 259.1, pp. 213–221.
- Cheng, Wei, Xiaoxi Ji, Jie Zhang, and Jianfeng Feng (2012). "Individual classification of ADHD patients by integrating multiscale neuroimaging markers and advanced pattern recognition techniques." In: *Frontiers in Systems Neuroscience* 6.
- Ciric, Rastko et al. (2017). "Benchmarking of participant-level confound regression strategies for the control of motion artifact in studies of functional connectivity." In: *NeuroImage* 154, pp. 174 –187.
- Colclough, Giles L, Stephen M Smith, Thomas E Nichols, Anderson M Winkler, Stamatios N Sotiroopoulos, Matthew F Glasser, David C Van Essen, and Mark W Woolrich (2017). "The heritability of multimodal connectivity in human brain activity." In: *eLife* 6, e20178.
- Cole, M.W., D.S. Bassett, J.D. Power, T.S. Braver, and S.E. Petersen (2014). "Intrinsic and task-evoked network architectures of the human brain." In: *Neuron* 83, pp. 238–51.
- Collins, Rory (2012). "What makes UK Biobank special?" In: *The Lancet* 379.9822, pp. 1173–1174.
- Conturo, Thomas E., Nicolas F. Lori, Thomas S. Cull, Erbil Akbudak, Abraham Z. Snyder, Joshua S. Shimony, Robert C. McKinstry, Harold Burton, and Marcus E. Raichle (1999). "Tracking neuronal fiber pathways in the living human brain." In: *Proceedings of the National Academy of Sciences* 96, pp. 10422–10427.

- Cover, T. and P. Hart (1967). "Nearest Neighbor Pattern Classification." In: *IEEE Trans. Inf. Theor.* 13, pp. 21–27.
- Cox, SR, SJ Ritchie, C Fawns-Ritchie, EM Tucker-Drob, and IJ Deary (2019). "Structural brain imaging correlates of general intelligence in UK Biobank." In: *Intelligence* 76, p. 101376.
- Craddock, Cameron et al. (2013). "The Neuro Bureau Preprocessing Initiative: open sharing of preprocessed neuroimaging data and derivatives
." In: *Frontiers in Neuroinformatics* 41.
- Craddock, R. Cameron, Rosalia L. Tungaraza, and Michael P. Milham (2015). "Connectomics and new approaches for analyzing human brain functional connectivity." In: *GigaScience* 4, p. 13.
- Craddock, R. Cameron, Paul E. Holtzheimer, Xiaoping P. Hu, and Helen S. Mayberg (2009). "Disease state prediction from resting state functional connectivity." In: *Magnetic Resonance in Medicine* 62, p. 1619.
- Craddock, R Cameron, G Andrew James, Paul E Holtzheimer, Xiaoping P Hu, and Helen S Mayberg (2012). "A whole brain fMRI atlas generated via spatially constrained spectral clustering." In: *Hum brain map* 33, p. 1914.
- Cronbach, Lee J. and Paul E. Meehl (1955). "Construct validity in psychological tests." In: *Psychological Bulletin* 52.4, pp. 281–302.
- Dadi, Kamalaker, Mehdi Rahim, Alexandre Abraham, Darya Chyzhyk, Michael Milham, Bertrand Thirion, and Gaël Varoquaux (2019). "Benchmarking functional connectome-based predictive models for resting-state fMRI." In: *NeuroImage* 192, pp. 115 –134.
- Dadi, Kamalaker, Gaël Varoquaux, Josselin Houenou, Danilo Bzdok, Bertrand Thirion, and Denis Engemann (2020a). "Beyond brain age: Empirically-derived proxy measures of mental health." In: *bioRxiv*. DOI: [10.1101/2020.08.25.266536](https://doi.org/10.1101/2020.08.25.266536).
- Dadi, Kamalaker, Gaël Varoquaux, Antonia Machlouzarides-Shalit, Krzysztof J. Gorgolewski, Demian Wassermann, Bertrand Thirion, and Arthur Mensch (2020b). "Fine-grain atlases of functional modes for fMRI analysis." In: *NeuroImage*, p. 117126. ISSN: 1053-8119.
- Daducci, Alessandro, Erick J. Canales-Rodríguez, Hui Zhang, Tim B. Dyrby, Daniel C. Alexander, and Jean-Philippe Thiran (2015). "Accelerated Microstructure Imaging via Convex Optimization (AMICO) from diffusion MRI data." In: *NeuroImage* 105, pp. 32–44.
- Dalcin, L., R. Bradshaw, K. Smith, C. Citro, S. Behnel, and D. Seljebotn (2011). "Cython: The Best of Both Worlds." In: *Computing in Science & Engineering* 13, pp. 31–39.
- Damoiseaux, J. S., S. A R B Rombouts, F. Barkhof, P. Scheltens, C. J. Stam, S. M. Smith, and C. F. Beckmann (2006). "Consistent resting-state networks across healthy subjects." In: *Proc Natl Acad Sci* 103, p. 13848.
- Delgado, M. R., L. E. Nystrom, C. Fissell, D. C. Noll, and J. A. Fiez (2000). "Tracking the Hemodynamic Responses to Reward and Pun-

- ishment in the Striatum." In: *Journal of Neurophysiology* 84, pp. 3072–3077.
- Desikan R., S. et al. (2006). "An automated labeling system for subdividing the human cerebral cortex on MRI scans into gyral based regions of interest." In: *NeuroImage* 31, p. 968.
- Destrieux, Christophe, Bruce Fischl, Anders Dale, and Eric Halgren (2010). "Automatic parcellation of human cortical gyri and sulci using standard anatomical nomenclature." In: *NeuroImage* 53.1, pp. 1–15.
- Di Martino, Adriana, Chao-Gan Yan, Qingyang Li, Erin Denio, Francisco X Castellanos, Kaat Alaerts, Jeffrey S Anderson, Michal Assaf, Susan Y Bookheimer, Mirella Dapretto, et al. (2014). "The autism brain imaging data exchange: towards a large-scale evaluation of the intrinsic brain architecture in autism." In: *Molecular psychiatry* 19.6, pp. 659–667.
- Diedrichsen, Jörn, Joshua H. Balsters, Jonathan Flavell, Emma Cussans, and Narender Ramnani (2009). "A probabilistic MR atlas of the human cerebellum." In: *NeuroImage* 46.1, pp. 39–46.
- Dodero, Luca, Ha Quang Minh, Marco San Biagio, Vittorio Murino, and Diego Sona (2015). "Kernel-based classification for brain connectivity graphs on the Riemannian manifold of positive definite matrices." In: *International Symposium on Biomedical Imaging (ISBI)*. IEEE.
- Dosenbach, N. U. F. et al. (2010). "Prediction of Individual Brain Maturity Using fMRI." In: *Science* 329.5997, pp. 1358–1361.
- Dubois, Julien C, Paola Galdi, Lynn K Paul, and Ralph Adolphs (2018a). "A distributed brain network predicts general intelligence from resting-state human neuroimaging data." In: *bioRxiv*, p. 257865.
- Dubois, Julien and Ralph Adolphs (2016). "Building a Science of Individual Differences from fMRI." In: *Trends in cognitive sciences* 20.6, pp. 425–443.
- Dubois, Julien, Paola Galdi, Lynn K. Paul, and Ralph Adolphs (2018b). "A distributed brain network predicts general intelligence from resting-state human neuroimaging data." In: *Philosophical Transactions of the Royal Society B: Biological Sciences* 373.1756, p. 20170284.
- Dubois, Julien, Paola Galdi, Yanting Han, Lynn K. Paul, and Ralph Adolphs (2018c). "Resting-State Functional Brain Connectivity Best Predicts the Personality Dimension of Openness to Experience." In: *Personality Neuroscience* 1.
- Duff, Eugene P., Aaron J. Trachtenberg, Clare E. Mackay, Matt A. Howard, Frederick Wilson, Stephen M. Smith, and Mark W. Woolrich (2012). "Task-driven ICA feature generation for accurate and interpretable prediction using fMRI." In: *NeuroImage* 60.1, pp. 189–203.

- Duncan, Keith J, Chotiga Pattamadilok, Iris Knierim, and Joseph T Devlin (2009). "Consistency and variability in functional localisers." In: *Neuroimage* 46, p. 1018.
- Eickhoff, Simon B., B. T. Thomas Yeo, and Sarah Genon (2018). "Imaging-based parcellations of the human brain." In: *Nat Rev Neurosci* 19, p. 672.
- Eickhoff, Simon B, Tomas Paus, Svenja Caspers, Marie-Helene Grosbras, Alan C Evans, Karl Zilles, and Katrin Amunts (2007). "Assignment of functional activations to probabilistic cytoarchitectonic areas revisited." In: *Neuroimage* 36, p. 511.
- Eisenberg, Ian W., Patrick G. Bissett, A. Zeynep Enkavi, Jamie Li, David P. MacKinnon, Lisa A. Marsch, and Russell A. Poldrack (2019). "Uncovering the structure of self-regulation through data-driven ontology discovery." In: *Nature Communications* 10.1, pp. 1–13.
- Elliott, P., T. C Peakman, et al. (2008). "The UK Biobank sample handling and storage protocol for the collection, processing and archiving of human blood and urine." In: *Int J Epidemiology* 37.2, p. 234.
- Engemann, Denis A, Oleh Kozynets, David Sabbagh, Guillaume Lemaître, Gael Varoquaux, Franziskus Liem, and Alexandre Gramfort (2020a). "Combining magnetoencephalography with magnetic resonance imaging enhances learning of surrogate-biomarkers." In: *eLife* 9, e54055.
- Engemann, Denis Alexander, Oleh Kozynets, David Sabbagh, Guillaume Lemaître, Gaël Varoquaux, Franziskus Liem, and Alexandre Gramfort (2020b). "Combining magnetoencephalography with magnetic resonance imaging enhances learning of surrogate-biomarkers." In: *eLife* 9, e54055.
- Enkavi, A Zeynep, Ian W Eisenberg, Patrick G Bissett, Gina L Mazza, David P MacKinnon, Lisa A Marsch, and Russell A Poldrack (2019). "Large-scale analysis of test-retest reliabilities of self-regulation measures." In: *Proceedings of the National Academy of Sciences* 116.12, pp. 5472–5477.
- Esteban, Oscar, Daniel Birman, Marie Schaer, Oluwasanmi O. Koyejo, Russell A. Poldrack, and Krzysztof J. Gorgolewski (2017). "MRIQC: Advancing the automatic prediction of image quality in MRI from unseen sites." In: *PLOS ONE* 12, p. 1.
- Esteban, Oscar, Christopher J Markiewicz, Ross W Blair, Craig A Moodie, A Ilkay Isik, Asier Erramuzpe, James D Kent, Mathias Goncalves, Elizabeth DuPre, Madeleine Snyder, et al. (2019). "fMRIprep: a robust preprocessing pipeline for functional MRI." In: *Nature methods* 16.1, p. 111.
- Evans, Alan C. (2006). "The NIH MRI study of normal brain development." In: *NeuroImage* 30, pp. 184 –202.
- Eysenck, H. J. (1958). "The continuity of abnormal and normal behavior." In: *Psychological Bulletin* 55.6, pp. 429–432.

- Filippini, Nicola, Bradley J. MacIntosh, Morgan G. Hough, Guy M. Goodwin, Giovanni B. Frisoni, Stephen M. Smith, Paul M. Matthews, Christian F. Beckmann, and Clare E. Mackay (2009). "Distinct patterns of brain activity in young carriers of the APOE-ε4 allele." In: *Proceedings of the National Academy of Sciences* 106.17, pp. 7209–7214.
- Fletcher, P.T. and S. Joshi (2007). "Riemannian geometry for the statistical analysis of diffusion tensor data." In: *Signal Processing* 87, p. 250.
- Foerde, Karin, Barbara J. Knowlton, and Russell A. Poldrack (2006). "Modulation of competing memory systems by distraction." In: *Proc Natl Acad Sci* 103.31, p. 11778.
- Fox, M and M Raichle (2007). "Spontaneous fluctuations in brain activity observed with functional magnetic resonance imaging." In: *Nat Rev Neurosci* 8, p. 700.
- Fox, M, A Snyder, J Zacks, and M Raichle (2006). "Coherent spontaneous activity accounts for trial-to-trial variability in human evoked brain responses." In: *Nat Neurosci* 9, p. 23.
- Fox, M.D. and M.D. Greicius (2010). "Clinical applications of resting state functional connectivity." In: *Front Syst Neurosci* 4, p. 19.
- Fox, M.D., A.Z. Snyder, J.L. Vincent, M. Corbetta, D.C. Van Essen, and M.E. Raichle (2005). "The human brain is intrinsically organized into dynamic, anticorrelated functional networks." In: *Proc Ntl Acad Sci* 102, p. 9673.
- Friedman, Jerome, Trevor Hastie, Holger Höfling, and Robert Tibshirani (2007). *Pathwise coordinate optimization*. Tech. rep. Annals of Applied Statistics.
- Friston, K. J., A. P. Holmes, K. J. Worsley, J.-B. Poline, C. Frith, and R. Frackowiak (1995). "Statistical Parametric Maps in Functional Imaging: A General Linear Approach." In: *Hum Brain Mapp*, p. 189.
- Friston, K.J., P. Fletcher, O. Josephs, A. Holmes, M.D. Rugg, and R. Turner (1998). "Event-Related fMRI: Characterizing Differential Responses." In: *NeuroImage* 7.1, pp. 30–40.
- Friston, Karl J. (1994). "Functional and effective connectivity in neuroimaging: A synthesis." In: *Human Brain Mapping* 2.1-2, pp. 56–78.
- (2009). "Modalities, Modes, and Models in Functional Neuroimaging." In: *Science* 326.5951, pp. 399–403.
- Friston, Karl J (2011). "Functional and effective connectivity: a review." In: *Brain connectivity* 1.1, 13–36.
- Gabitov, Ella, David Manor, and Avi Karni (2015). "Patterns of Modulation in the Activity and Connectivity of Motor Cortex during the Repeated Generation of Movement Sequences." In: *J Cog Neurosci* 27, p. 736.
- Glasser, Matthew F. et al. (2016). "A multi-modal parcellation of human cerebral cortex." In: *Nature* 536, pp. 171–178.

- Gorgolewski, Krzysztof J, Amos Storkey, Mark E Bastin, Ian R Whittle, Joanna M Wardlaw, and Cyril R Pernet (2013). "A test-retest fMRI dataset for motor, language and spatial attention functions." In: *GigaScience* 2.1, pp. 2047–217X–2–6.
- Gorgolewski, Krzysztof J. et al. (2015). "NeuroVault.org: a web-based repository for collecting and sharing unthresholded statistical maps of the human brain." In: *Frontiers in Neuroinformatics* 9, p. 8.
- Gorgolewski, Krzysztof, Christopher D. Burns, Cindee Madison, Dav Clark, Yaroslav O. Halchenko, Michael L. Waskom, and Satrajit S. Ghosh (2011). "Nipype: a flexible, lightweight and extensible neuroimaging data processing framework in python." In: *Front Neuroinform* 5, p. 13.
- Gorgolewski, Krzysztof, Oscar Esteban, Schaefer Gunnar, Wandell Brain, and Russell Poldrack (2017). "OpenNeuro – a free online platform for sharing and analysis of neuroimaging data." In: *23rd Annual Meeting of the Organization for Human Brain Mapping*, p. 1677.
- Goutte, Cyril, Peter Toft, Egill Rostrup, Finn A Nielsen, and Lars Kai Hansen (1999). "On clustering fMRI time series." In: *NeuroImage* 9.3, pp. 298–310.
- Greicius, M.D., G. Srivastava, A.L. Reiss, and V. Menon (2004). "Default-mode network activity distinguishes Alzheimer's disease from healthy aging: evidence from functional MRI." In: *Proceedings of the National Academy of Sciences* 101, p. 4637.
- Greicius, M.D., K. Supekar, V. Menon, and R.F. Dougherty (2008). "Resting-state functional connectivity reflects structural connectivity in the default mode network." In: *Cerebral Cortex*.
- Greve, Douglas N. and Bruce Fischl (2009). "Accurate and robust brain image alignment using boundary-based registration." In: *NeuroImage* 48, p. 63.
- Griffanti, Ludovica et al. (2014a). "ICA-based artefact removal and accelerated fMRI acquisition for improved resting state network imaging." In: *NeuroImage* 95, pp. 232 –247.
- Griffanti, Ludovica, Gholamreza Salimi-Khorshidi, Christian F Beckmann, Edward J Auerbach, Gwenaëlle Douaud, Claire E Sexton, Enikő Zsoldos, Klaus P Ebmeier, Nicola Filippini, Clare E Mackay, et al. (2014b). "ICA-based artefact removal and accelerated fMRI acquisition for improved resting state network imaging." In: *Neuroimage* 95, pp. 232–247.
- Groot, Marius de, Meike W. Vernooij, Stefan Klein, M. Arfan Ikram, Frans M. Vos, Stephen M. Smith, Wiro J. Niessen, and Jesper L. R. Andersson (2013). "Improving alignment in Tract-based spatial statistics: Evaluation and optimization of image registration." In: *NeuroImage* 76, pp. 400–411.
- Guo, Hao, Xiaohua Cao, Zhifen Liu, Haifang Li, Junjie Chen, and Kerang Zhang (2012). "Machine learning classifier using abnormal

- brain network topological metrics in major depressive disorder." In: *NeuroReport* 23.17, pp. 1006–1011.
- Hanson, Stephen José, Toshihiko Matsuka, and James V. Haxby (2004). "Combinatorial codes in ventral temporal lobe for object recognition: Haxby (2001) revisited: is there a "face" area?" In: *NeuroImage* 23, pp. 156 –166.
- Harrison, Samuel J., Mark W. Woolrich, Emma C. Robinson, Matthew F. Glasser, Christian F. Beckmann, Mark Jenkinson, and Stephen M. Smith (2015). "Large-scale Probabilistic Functional Modes from resting state fMRI." In: *NeuroImage* 109, pp. 217 –231.
- Hastie, Trevor, Robert Tibshirani, and Jerome Friedman (2009). *The elements of statistical learning*. Springer.
- Haxby, James V., Ida M. Gobbini, Maura L. Furey, et al. (2001). "Distributed and overlapping representations of faces and objects in ventral temporal cortex." In: *Science* 293, p. 2425.
- Haynes, John-Dylan and Geraint Rees (2006). "Decoding mental states from brain activity in humans." In: *Nat. Rev. Neurosci.* 7, p. 523.
- Henri, M. Duvernoy (1999). *The Human Brain: Surface, Three-dimensional Sectional Anatomy with MRI, and Blood Supply*. Springer.
- Hozer, Franz and Josselin Houenou (2016). "Can neuroimaging disentangle bipolar disorder?" In: *Journal of affective disorders* 195, pp. 199–214.
- Hua, Kegang, Jiangyang Zhang, Setsu Wakana, Hangyi Jiang, Xin Li, Daniel S. Reich, Peter A. Calabresi, James J. Pekar, Peter C.M. van Zijl, and Susumu Mori (2008). "Tract probability maps in stereotaxic spaces: Analyses of white matter anatomy and tract-specific quantification." In: *NeuroImage* 39, p. 336.
- Hunter, J. D. (2007). "Matplotlib: A 2D graphics environment." In: *Computing In Science & Engineering* 9.3, pp. 90–95.
- Hyvärinen, A. (1999). "Fast and robust fixed-point algorithms for independent component analysis." In: *IEEE Transactions on Neural Networks* 10.3, pp. 626–634.
- Hyvärinen, A. and E. Oja (2000). "Independent component analysis: algorithms and applications." In: *Neural Networks* 13, p. 411.
- Iannilli, Emilia, Roberto Gasparotti, Thomas Hummel, Silvia Zoni, Chiara Benedetti, Chiara Fedrighi, Cheuk Ying Tang, Christoph Van Thriel, and Roberto G. Lucchini (2016). "Effects of Manganese Exposure on Olfactory Functions in Teenagers: A Pilot Study." In: *PLOS ONE* 11.1, pp. 1–9.
- Iidaka, Tetsuya (2015). "Resting state functional magnetic resonance imaging and neural network classified autism and control." In: *Cortex* 63, pp. 55–67.
- Insel, Thomas R. and Bruce N. Cuthbert (2015). "Brain disorders? Precisely." In: *Science* 348, pp. 499–500.
- Insel, Thomas, Bruce Cuthbert, Marjorie Garvey, Robert Heinssen, Daniel S. Pine, Kevin Quinn, Charles Sanislow, and Philip Wang

- (2010). "Research Domain Criteria (RDoC): Toward a New Classification Framework for Research on Mental Disorders." In: *American Journal of Psychiatry* 167.7, pp. 748–751.
- Jenkinson, Mark and Stephen Smith (2001). "A global optimisation method for robust affine registration of brain images." In: *Medical Image Analysis* 5.2, pp. 143–156.
- Jenkinson, Mark, Peter Bannister, Michael Brady, and Stephen Smith (2002a). "Improved Optimization for the Robust and Accurate Linear Registration and Motion Correction of Brain Images." In: *NeuroImage* 17, pp. 825–841.
- (2002b). "Improved Optimization for the Robust and Accurate Linear Registration and Motion Correction of Brain Images." In: *NeuroImage* 17.2, pp. 825–841.
- Jimura, Koji, Fabienne Cazalis, Elena R. S. Stover, and Russell A. Poldrack (2014). "The neural basis of task switching changes with skill acquisition." In: *Frontiers in Human Neuroscience* 8, p. 339.
- Kahnt, Thorsten, Luke J. Chang, Soyoung Q Park, Jakob Heinze, and John-Dylan Haynes (2012). "Connectivity-Based Parcellation of the Human Orbitofrontal Cortex." In: *Journal of Neuroscience* 18, pp. 6240–6250.
- Kapur, S., A. G. Phillips, and T. R. Insel (2012). "Why has it taken so long for biological psychiatry to develop clinical tests and what to do about it?" In: *Molecular Psychiatry* 17.12, pp. 1174–1179.
- Kelly, A.M. Clare, Lucina Q. Uddin, Bharat B. Biswal, F. Xavier Castellanos, and Michael P. Milham (2008). "Competition between functional brain networks mediates behavioral variability." In: *NeuroImage* 39.1, pp. 527–537.
- Keyes, Katherine M., Jonathan Platt, Alan S. Kaufman, and Katie A. McLaughlin (2017). "Association of Fluid Intelligence and Psychiatric Disorders in a Population-Representative Sample of US Adolescents." In: *JAMA psychiatry* 74.2, pp. 179–188.
- Khandaker, Golam M., Christina Dalman, Nils Kappelmann, Jan Stochl, Henrik Dal, Kyriaki Kosidou, Peter B. Jones, and Håkan Karlsson (2018). "Association of Childhood Infection With IQ and Adult Nonaffective Psychosis in Swedish Men: A Population-Based Longitudinal Cohort and Co-relative Study." In: *JAMA Psychiatry* 75.4, pp. 356–362.
- Kievit, Rogier A., Delia Fuhrmann, Gesa Sophia Borgeest, Ivan L. Simpson-Kent, and Richard N. A. Henson (2018). "The neural determinants of age-related changes in fluid intelligence: a pre-registered, longitudinal analysis in UK Biobank." In: *Wellcome Open Research* 3.
- Kim, Jongwan, Jing Wang, Douglas H. Wedell, and Svetlana V. Shinkareva (2016). "Identifying Core Affect in Individuals from fMRI Responses to Dynamic Naturalistic Audiovisual Stimuli." In: *PLOS ONE* 11.9, pp. 1–21.

- Kiviniemi, V., J.H. Kantola, J. Jauhainen, A. Hyvärinen, and O. Tervonen (2003). "Independent component analysis of nondeterministic fMRI signal sources." In: *Neuroimage* 19, p. 253.
- Kiviniemi, V., T. Starck, J. Remes, X. Long, J. Nikkinen, M. Haapea, J. Veijola, et al. (2009). "Functional segmentation of the brain cortex using high model order group PICA." In: *Hum Brain Map* 30, p. 3865.
- Lahey, Benjamin B (2009). "Public health significance of neuroticism." In: *American Psychologist* 64.4, p. 241.
- Laumann, Timothy O. et al. (2016). "On the Stability of BOLD fMRI Correlations." In: *Cerebral Cortex* 27.10, pp. 4719–4732.
- Ledoit, O and M Wolf (2004a). "A well-conditioned estimator for large-dimensional covariance matrices." In: *J. Multivar. Anal.* 88, p. 365.
- Ledoit, Olivier and Michael Wolf (2004b). "A well-conditioned estimator for large-dimensional covariance matrices." In: *Journal of Multivariate Analysis* 88.2, pp. 365–411.
- Lee, Kangjoo, Sungho Tak, and Jong Chul Ye (2010). "A data-driven sparse GLM for fMRI analysis using sparse dictionary learning with MDL criterion." In: *IEEE Trans Med Imag* 30, p. 1076.
- Lepping, Rebecca J., Ruth Ann Atchley, and Cary R. Savage (2016). "Development of a validated emotionally provocative musical stimulus set for research." In: *Psychology of Music* 44.5, pp. 1012–1028.
- Lepping, Rebecca J., Ruth Ann Atchley, Evangelia Chrysikou, Laura E. Martin, Alicia A. Clair, Rick E. Ingram, W. Kyle Simmons, and Cary R. Savage (2016). "Neural Processing of Emotional Musical and Nonmusical Stimuli in Depression." In: *PLOS ONE* 11.6, pp. 1–23.
- Lerch, J.P., A.J. van der Kouwe, A. Raznahan, T. Paus, H. Johansen-Berg, K.L. Miller, S.M. Smith, B. Fischl, and S.N. Sotiroopoulos (2017). "Studying neuroanatomy using MRI." In: *Nature neuroscience* 20, pp. 314 –326.
- Liem, Franziskus, Gaël Varoquaux, Jana Kynast, Frauke Beyer, Shahrzad Kharabian Masouleh, Julia M Huntenburg, Leonie Lampe, Mehdi Rahim, Alexandre Abraham, R Cameron Craddock, et al. (2017a). "Predicting brain-age from multimodal imaging data captures cognitive impairment." In: *NeuroImage* 148, pp. 179–188.
- Liem, Franziskus et al. (2017b). "Predicting brain-age from multimodal imaging data captures cognitive impairment." In: *NeuroImage* 148, pp. 179–188.
- Liu, Thomas T. (2016). "Noise contributions to the fMRI signal: An overview." In: *NeuroImage* 143, pp. 141 –151.
- Luca, M. De, C.F. Beckmann, N. De Stefano, P.M. Matthews, and S.M. Smith (2006). "fMRI resting state networks define distinct modes of long-distance interactions in the human brain." In: *NeuroImage* 29.4, pp. 1359 –1367.

- Lynn, Richard and Terence Martin (1997). "Gender differences in extraversion, neuroticism, and psychotism in 37 nations." In: *The Journal of social psychology* 137.3, pp. 369–373.
- Maglanoc, Luigi A., Tobias Kaufmann, Dennis van der Meer, Andre F. Marquand, Thomas Wolfers, Rune Jonassen, Eva Hilland, Ole A. Andreassen, Nils Inge Landrø, and Lars T. Westlye (2020). "Brain Connectome Mapping of Complex Human Traits and Their Polygenic Architecture Using Machine Learning." In: *Biological Psychiatry* 87.8, pp. 717–726.
- Mennes, Maarten, Clare Kelly, Stan Colcombe, F. Xavier Castellanos, and Michael P. Milham (2013). "The Extrinsic and Intrinsic Functional Architectures of the Human Brain Are Not Equivalent." In: *Cerebral Cortex* 23.1, pp. 223–229.
- Mensch, Arthur., Gael Varoquaux, and Bertrand Thirion (2016). "Compressed Online Dictionary Learning for Fast Resting-State fMRI Decomposition." In: *Proc. ISBI*, p. 1282.
- Mensch, Arthur, Julien Mairal, Bertrand Thirion, and Gaël Varoquaux (2016). "Dictionary Learning for Massive Matrix Factorization." In: *International Conference on Machine Learning*. Vol. 48. Proceedings of Machine Learning Research, pp. 1737–1746.
- (2018). "Stochastic Subsampling for Factorizing Huge Matrices." In: *IEEE Trans Sig Proc* 66, p. 113.
- Michel, Vincent, Alexandre Gramfort, Gaël Varoquaux, Evelyn Eger, Christine Keribin, and Bertrand Thirion (2012). "A supervised clustering approach for fMRI-based inference of brain states." In: *Pattern Recognition* 45, p. 2041.
- Milazzo, Anna-Clare, Bernard Ng, Heidi Jiang, William Shirer, Gael Varoquaux, Jean Baptiste Poline, Bertrand Thirion, and Michael D Greicius (2014). "Identification of mood-relevant brain connections using a continuous, subject-driven rumination paradigm." In: *Cereb. Cortex* 26.3, pp. 933–942.
- Miller, Karla L, Fidel Alfaro-Almagro, et al. (2016). "Multimodal population brain imaging in the UK Biobank prospective epidemiological study." In: *Nature Neuroscience*.
- Miller, Karla L et al. (2016). "Multimodal population brain imaging in the UK Biobank prospective epidemiological study." In: *Nature neuroscience* 19.11, pp. 1523–1536.
- Moran, Joseph M., Eshin Jolly, and Jason P. Mitchell (2012). "Social-Cognitive Deficits in Normal Aging." In: *J Neurosci* 32, p. 5553.
- Mori, Susumu, Setsu Wakana, Peter CM Van Zijl, and LM Nagae-Poetscher (2005). *MRI atlas of human white matter*. Elsevier.
- Mourão-Miranda, Janaina, Arun L.W. Bokde, Christine Born, Harald Hampel, and Martin Stetter (2005). "Classifying brain states and determining the discriminating activation patterns: Support Vector Machine on functional MRI data." In: *NeuroImage* 28, p. 980.

- Mueller, S.G., M.W. Weiner, L.J. Thal, R.C. Petersen, C. Jack, W. Jagust, J. Q. Trojanowski, A. W. Toga, and L. Beckett (2005). "The alzheimer's disease neuroimaging initiative." In: *Neuroimaging Clinics of North America* 15, p. 869.
- Murphy, Kevin and Michael D Fox (2017). "Towards a consensus regarding global signal regression for resting state functional connectivity MRI." In: *Neuroimage* 154, pp. 169–173.
- Nave, Gideon, Wi Hoon Jung, Richard Karlsson Linnér, Joseph W. Kable, and Philipp D. Koellinger (2018). "Are Bigger Brains Smarter? Evidence From a Large-Scale Preregistered Study:" in: *Psychological Science*.
- Ng, Bernard, Martin Dressler, Gaël Varoquaux, Jean-Baptiste Poline, Michael Greicius, and Bertrand Thirion (2014). "Transport on Riemannian Manifold for Functional Connectivity-based Classification." In: *MICCAI - 17th International Conference on Medical Image Computing and Computer Assisted Intervention*.
- Nielsen, Jared A., Brandon A. Zielinski, P. Thomas Fletcher, Andrew L. Alexander, Nicholas Lange, Erin D. Bigler, Janet E. Lainhart, and Jeffrey S. Anderson (2013). "Multisite functional connectivity MRI classification of autism: ABIDE results." In: *Frontiers in Human Neuroscience* 7.
- O'Toole, Alice J., Fang Jiang, Hervé Abdi, and James V. Haxby (2005). "Partially Distributed Representations of Objects and Faces in Ventral Temporal Cortex." In: *J Cog Neurosci* 17, p. 580.
- Olshausen, B.A. and D.J. Field (1997). "Sparse coding with an overcomplete basis set: A strategy employed by V1?" In: *Vision research* 37, p. 3311.
- Ono, Michio, Stefan Kubik, and Chad D Abernathey (1990). *Atlas of the cerebral sulci*. G. Thieme Verlag.
- Pardoe, Heath R., Rebecca Kucharsky Hiess, and Ruben Kuzniecky (2016). "Motion and morphometry in clinical and nonclinical populations." In: *NeuroImage* 135, pp. 177 –185.
- Patenaude, Brian, Stephen M. Smith, David N. Kennedy, and Mark Jenkinson (2011). "A Bayesian model of shape and appearance for subcortical brain segmentation." In: *NeuroImage* 56.3, pp. 907–922.
- Pedregosa, F., G. Varoquaux, A. Gramfort, et al. (2011). "Scikit-learn: Machine Learning in Python." In: *Journal of Machine Learning Research* 12, p. 2825.
- Pennec, X., P. Fillard, and N. Ayache (2006). "A Riemannian framework for tensor computing." In: *Int J Comp Vision* 66, p. 41.
- Perlberg, Vincent, Pierre Bellec, Jean-Luc Anton, Melanie Pelegrini-Issac, Julien Doyon, and Habib Benali (2007). "CORSICA: correction of structured noise in fMRI by automatic identification of ICA components." In: *Magn Reson Imaging* 25, p. 35.
- Perlis, R. H. (2011). "Translating biomarkers to clinical practice." In: *Molecular Psychiatry* 16.11, pp. 1076–1087.

- Perrot, M., D. Rivière, A. Tucholka, and J.-F. Mangin (2009). "Joint Bayesian Cortical Sulci Recognition and Spatial Normalization." In: *IPMI*.
- Pervaiz, Usama, Diego Vidaurre, Mark W. Woolrich, and Stephen M. Smith (2019). "Optimising network modelling methods for fMRI." In: *bioRxiv*.
- Pinel, P., B. Thirion, S. Meriaux, A. Jobert, J. Serres, D. Le Bihan, J.B. Poline, and S. Dehaene (2007). "Fast reproducible identification and large-scale databasing of individual functional cognitive networks." In: *BMC neuroscience* 8, p. 91.
- Pinho, Ana Luísa, Alexis Amadon, Torsten Ruest, Murielle Fabre, Elvis Dohmatob, Isabelle Denghien, Chantal Ginisty, Séverine Becuwe-Desmidt, Séverine Roger, Laurence Laurier, et al. (2018). "Individual Brain Charting, a high-resolution fMRI dataset for cognitive mapping." In: *Scientific data* 5, p. 180105.
- Poldrack, R. A., J. Clark, E. J. Paré-Blagoev, D. Shohamy, J. Creso Moyano, C. Myers, and M. A. Gluck (2001). "Interactive memory systems in the human brain." In: *Nature* 414, 546–550.
- Poldrack, Russell A, Deanna M Barch, Jason P Mitchell, et al. (2013). "Toward open sharing of task-based fMRI data: the OpenfMRI project." In: *Frontiers in neuroinformatics* 7.
- Poldrack, Russell A and Krzysztof J Gorgolewski (2014). "Making big data open: data sharing in neuroimaging." In: *Nature neuroscience* 17.11, pp. 1510–1517.
- Poldrack, Russell A, Yaroslav O Halchenko, and Stephen José Hanson (2009). "Decoding the large-scale structure of brain function by classifying mental states across individuals." In: *Psychological Science* 20, p. 1364.
- Power, Jonathan D. et al. (2011). "Functional Network Organization of the Human Brain." In: *Neuron* 72, pp. 665–678.
- Power, Jonathan D, Kelly A Barnes, Abraham Z Snyder, Bradley L Schlaggar, and Steven E Petersen (2012). "Spurious but systematic correlations in functional connectivity MRI networks arise from subject motion." In: *Neuroimage* 59, pp. 2142–2154.
- Power, Jonathan D., Mark Plitt, Timothy O. Laumann, and Alex Martin (2017). "Sources and implications of whole-brain fMRI signals in humans." In: *NeuroImage* 146, pp. 609–625.
- Power, Robert A and Michael Pluess (2015). "Heritability estimates of the Big Five personality traits based on common genetic variants." In: *Translational psychiatry* 5.7, e604.
- Pruim, Raimon HR, Maarten Mennes, Jan K Buitelaar, and Christian F Beckmann (2015). "Evaluation of ICA-AROMA and alternative strategies for motion artifact removal in resting state fMRI." In: *Neuroimage* 112, pp. 278–287.

- Qiu, Anqi, Annie Lee, Mingzhen Tan, and Moo K. Chung (2015). "Manifold learning on brain functional networks in aging." In: *Medical Image Analysis* 20.1, pp. 52–60.
- Quercia, Daniele, Michal Kosinski, David Stillwell, and Jon Crowcroft (2011). "Our twitter profiles, our selves: Predicting personality with twitter." In: pp. 180–185.
- Rademacher, J., A. M. Galaburda, D. N. Kennedy, P. A. Filipek, and V. S. Caviness (1992). "Human Cerebral Cortex: Localization, Parcellation, and Morphometry with Magnetic Resonance Imaging." In: *J Cog Neurosci* 4, p. 352.
- Rahim, Mehdi, Bertrand Thirion, and Gaël Varoquaux (2017). "Population-shrinkage of covariance to estimate better brain functional connectivity." In: *International Conference on Medical Image Computing and Computer-Assisted Intervention*. Springer, pp. 460–468.
- Raichle, M.E., A.M. MacLeod, A.Z. Snyder, W.J. Powers, D.A. Gusnard, and G.L. Shulman (2001). "A default mode of brain function." In: *Proceedings of the National Academy of Sciences* 98, p. 676.
- Rashid, Barnaly, Mohammad R. Arbabshirani, Eswar Damaraju, Mustafa S. Cetin, Robyn Miller, Godfrey D. Pearlson, and Vince D. Calhoun (2016). "Classification of schizophrenia and bipolar patients using static and dynamic resting-state fMRI brain connectivity." In: *NeuroImage* 134, pp. 645–657.
- Repovs, Grega and Deanna Barch (2012). "Working memory related brain network connectivity in individuals with schizophrenia and their siblings." In: *Frontiers in Human Neuroscience* 6, p. 137.
- Reuter, Martin, M. Dylan Tisdall, Abid Qureshi, Randy L. Buckner, André J.W. van der Kouwe, and Bruce Fischl (2015). "Head motion during MRI acquisition reduces gray matter volume and thickness estimates." In: *NeuroImage* 107, pp. 107–115.
- Richiardi, J., H. Eryilmaz, S. Schwartz, P. Vuilleumier, and D. Van De Ville (2010). "Decoding brain states from fMRI connectivity graphs." In: *NeuroImage*.
- Rissman, Jesse, Adam Gazzaley, and Mark D'Esposito (2004). "Measuring functional connectivity during distinct stages of a cognitive task." In: *NeuroImage* 23.2, pp. 752–763.
- Ritchie, Stuart J. et al. (2015). "Brain volumetric changes and cognitive ageing during the eighth decade of life." In: *Human Brain Mapping* 36.12, pp. 4910–4925.
- Rizk-Jackson, A., A.R. Aron, and R.A. Poldrack (2011). "Classification learning and stop-signal (1 year test-retest)." In: *Stanford Digital Repository*.
- Romanuk, L, M Pope, K Nicol, D Steele, and J Hall (2016). "Neural correlates of fears of abandonment and rejection in borderline personality disorder." In: *Wellcome Open Research* 1.33.
- Rosa, Maria J, Liana Portugal, Tim Hahn, Andreas J Fallgatter, Marta I Garrido, John Shawe-Taylor, and Janaina Mourao-Miranda (2015).

- "Sparse network-based models for patient classification using fMRI." In: *NeuroImage* 105.
- Roy, Arnab, Rachel A. Bernier, Jianli Wang, Monica Benson, Jerry J. French Jr., David C. Good, and Frank G. Hillary (2017). "The evolution of cost-efficiency in neural networks during recovery from traumatic brain injury." In: *PLOS ONE* 12.4, pp. 1–26.
- Rubinov, Mikail and Olaf Sporns (2010). "Complex network measures of brain connectivity: Uses and interpretations." In: *NeuroImage* 52.3, pp. 1059 –1069.
- (2011). "Weight-conserving characterization of complex functional brain networks." In: *NeuroImage* 56, p. 2068.
- Sala-Llonch, Roser, Stephen M. Smith, Mark Woolrich, and Eugene P. Duff (2019). "Spatial parcellations, spectral filtering, and connectivity measures in fMRI: Optimizing for discrimination." In: *Hum Brain Map* 40, p. 407.
- Saygin, Z.M., D.E. Osher, E.S. Norton, D.A. Youssoufian, S.D. Beach, J. Feather, N. Gaab, J.D. Gabrieli, and N. Kanwisher (2016). "Connectivity precedes function in the development of the visual word form area." In: *Nature neuroscience* 19.
- Schaefer, Alexander, Ru Kong, Evan M Gordon, Timothy O Laumann, Xi-Nian Zuo, Avram J Holmes, Simon B Eickhoff, and B T Thomas Yeo (2017). "Local-Global Parcellation of the Human Cerebral Cortex from Intrinsic Functional Connectivity MRI." In: *Cerebral Cortex* 28.9, pp. 3095–3114.
- Schmahmann, Jeremy D., Julien Doyon, David McDonald, Colin Holmes, Karyne Lavoie, Amy S. Hurwitz, Noor Kabani, Arthur Toga, Alan Evans, and Michael Petrides (1999). "Three-Dimensional MRI Atlas of the Human Cerebellum in Proportional Stereotaxic Space." In: *NeuroImage* 10.3, pp. 233 –260.
- Schonberg, Tom, Craig Fox, Jeanette Mumford, Eliza Congdon, Christopher Trepel, and Russell Poldrack (2012). "Decreasing Ventromedial Prefrontal Cortex Activity During Sequential Risk-Taking: An fMRI Investigation of the Balloon Analog Risk Task." In: *Frontiers in Neuroscience* 6, p. 80.
- Shelton, Jill Talley, Emily M Elliott, Russell A Matthews, BD Hill, WM Gouvier, and others (2010). "The relationships of working memory, secondary memory, and general fluid intelligence: working memory is special." In: *Journal of Experimental Psychology: Learning, Memory, and Cognition* 36.3, p. 813.
- Shen, Hui, Lubin Wang, Yadong Liu, and Dewen Hu (2010). "Discriminative analysis of resting-state functional connectivity patterns of schizophrenia using low dimensional embedding of fMRI." In: *NeuroImage* 49.4, p. 3110.
- Simmons, Joseph P, Leif D Nelson, and Uri Simonsohn (2011). "False-positive psychology: Undisclosed flexibility in data collection and

- analysis allows presenting anything as significant." In: *Psychological science* 22, p. 1359.
- Smith, Rachelle, Kamyar Keramatian, and Kalina Christoff (2007). "Localizing the rostralateral prefrontal cortex at the individual level." In: *NeuroImage* 36, pp. 1387–1396.
- Smith, S.M., P.T. Fox, K.L. Miller, D.C. Glahn, P.M. Fox, C.E. Mackay, et al. (2009). "Correspondence of the brain's functional architecture during activation and rest." In: *Proc Natl Acad Sci* 106, p. 13040.
- Smith, S.M., K.L. Miller, G. Salimi-Khorshidi, M. Webster, C.F. Beckmann, T.E. Nichols, J.D. Ramsey, and M.W. Woolrich (2011). "Network modelling methods for fMRI." In: *Neuroimage* 54, p. 875.
- Smith, Stephen M. (2002). "Fast robust automated brain extraction." In: *Human Brain Mapping* 17.3, pp. 143–155.
- (2012). "The future of FMRI connectivity." In: *NeuroImage* 62.2, pp. 1257–1266.
- Smith, Stephen M. and Thomas E. Nichols (2018). "Statistical Challenges in "Big Data" Human Neuroimaging." In: *Neuron* 97, pp. 263–268.
- Smith, Stephen M., Yongyue Zhang, Mark Jenkinson, Jacqueline Chen, P. M. Matthews, Antonio Federico, and Nicola De Stefano (2002). "Accurate, Robust, and Automated Longitudinal and Cross-Sectional Brain Change Analysis." In: *NeuroImage* 17.1, pp. 479–489.
- Smith, Stephen M. et al. (2006). "Tract-based spatial statistics: Voxel-wise analysis of multi-subject diffusion data." In: *NeuroImage* 31.4, pp. 1487–1505.
- Smith, Stephen M, Thomas E Nichols, Diego Vidaurre, Anderson M Winkler, Timothy EJ Behrens, Matthew F Glasser, Kamil Ugurbil, Deanna M Barch, David C Van Essen, and Karla L Miller (2015). "A positive-negative mode of population covariation links brain connectivity, demographics and behavior." In: *Nature neuroscience* 18.11, pp. 1565–1567.
- Smith, Stephen M, Diego Vidaurre, Fidel Alfaro-Almagro, Thomas E Nichols, and Karla L Miller (2019). "Estimation of brain age delta from brain imaging." In: *NeuroImage*.
- Sporns, O., G. Tononi, and GM Edelman (2000). "Theoretical neuroanatomy: relating anatomical and functional connectivity in graphs and cortical connection matrices." In: *Cereb Cortex* 10, p. 127.
- Sporns, O., G. Tononi, and R. Kotter (2005). "The human connectome: a structural description of the human brain." In: *PLoS Comput Biol* 1, e42.
- Sporns, O., D.R. Chialvo, M. Kaiser, and C.C. Hilgetag (2004). "Organization, development and function of complex brain networks." In: *Trends in Cognitive Sciences* 8, p. 418.
- Stephan-Otto, Christian, Sara Siddi, Carl Senior, Daniel Muñoz-Samons, Susana Ochoa, Ana María Sánchez-Laforga, and Gildas

- Brébion (2017). "Visual Imagery and False Memory for Pictures: A Functional Magnetic Resonance Imaging Study in Healthy Participants." In: *PLOS ONE* 12.1, pp. 1–17.
- Szucs, Denes and John PA Ioannidis (2017). "Empirical assessment of published effect sizes and power in the recent cognitive neuroscience and psychology literature." In: *PLoS biology* 15.3, e2000797.
- Taylor, Jason R., Nitin Williams, Rhodri Cusack, Tibor Auer, Meredith A. Shafto, Marie Dixon, Lorraine K. Tyler, Cam-CAN, and Richard N. Henson (2017). "The Cambridge Centre for Ageing and Neuroscience (Cam-CAN) data repository: Structural and functional MRI, MEG, and cognitive data from a cross-sectional adult lifespan sample." In: *NeuroImage* 144, p. 262.
- Thirion, B., G. Flandin, P. Pinel, A. Roche, P. Ciuciu, and J.B. Poline (2006). "Dealing with the shortcomings of spatial normalization: Multi-subject parcellation of fMRI datasets." In: *Hum brain map* 27, p. 678.
- Thirion, Bertrand, Gael Varoquaux, Elvis Dohmatob, and J Poline (2014). "Which fMRI clustering gives good brain parcellations?" In: *Name: Frontiers in Neuroscience* 8, p. 167.
- Thompson, P.M. et al. (2007). "Tracking Alzheimer's Disease." In: *Annals of the New York Academy of Sciences* 1097, pp. 183–214.
- Trzepacz, Paula T., Peng Yu, Jia Sun, Kory Schuh, Michael Case, Michael M. Witte, Helen Hochstetler, and Ann Hake (2014). "Comparison of neuroimaging modalities for the prediction of conversion from mild cognitive impairment to Alzheimer's dementia." In: *Neurobiology of Aging* 35.1, pp. 143 –151.
- Tyler, Peter, Geoffrey M Reed, and Mike J Crawford (2015). "Classification, assessment, prevalence, and effect of personality disorder." In: *The Lancet* 385.9969, pp. 717–726.
- Tzourio-Mazoyer, N., B. Landeau, D. Papathanassiou, F. Crivello, O. Etard, N. Delcroix, B. Mazoyer, and M. Joliot (2002). "Automated anatomical labeling of activations in SPM using a macroscopic anatomical parcellation of the MNI MRI single-subject brain." In: *NeuroImage* 15, p. 273.
- Uncapher, Melina R., J. Benjamin Hutchinson, and Anthony D. Wagner (2011). "Dissociable Effects of Top-Down and Bottom-Up Attention during Episodic Encoding." In: *Journal of Neuroscience* 31.35, pp. 12613–12628.
- Urchs, Sebastian, Jonathan Armoza, Clara Moreau, Yassine Benhajali, Jolène St-Aubin, Pierre Orban, and Pierre Bellec (2019). "MIST: A multi-resolution parcellation of functional brain networks." In: *MNI Open Research* 1.
- Van Essen, D. C. et al. (2012). "The Human Connectome Project: A data acquisition perspective." In: *NeuroImage* 62, pp. 2222–2231.
- Van Essen, David C, Smith, et al. (2013). "The WU-Minn human connectome project: an overview." In: *Neuroimage* 80, pp. 62–79.

- Varoquaux, G., S. Sadaghiani, P. Pinel, A. Kleinschmidt, J. B. Poline, and B. Thirion (2010a). "A group model for stable multi-subject ICA on fMRI datasets." In: *NeuroImage* 51, p. 288.
- Varoquaux, G., A. Gramfort, J. B. Poline, and B. Thirion (2010b). "Brain covariance selection: better individual functional connectivity models using population prior." In: *NIPS*.
- Varoquaux, G., F. Baronnet, A. Kleinschmidt, P. Fillard, and B. Thirion (2010c). "Detection of brain functional-connectivity difference in post-stroke patients using group-level covariance modeling." In: *MICCAI*.
- Varoquaux, G., A. Gramfort, F. Pedregosa, V. Michel, and B. Thirion (2011). "Multi-subject dictionary learning to segment an atlas of brain spontaneous activity." In: *Inf Proc Med Imag*, p. 562.
- Varoquaux, Gaël (2017). "Cross-validation failure: small sample sizes lead to large error bars." In: *NeuroImage*.
- Varoquaux, Gaël and R Cameron Craddock (2013). "Learning and comparing functional connectomes across subjects." In: *NeuroImage* 80, p. 405.
- Varoquaux, Gaël, Flore Baronnet, Andreas Kleinschmidt, Pierre Fillard, and Bertrand Thirion (2010d). "Detection of brain functional-connectivity difference in post-stroke patients using group-level covariance modeling." In: *Medical image computing and computer-assisted intervention: MICCAI ... International Conference on Medical Image Computing and Computer-Assisted Intervention* 13.Pt 1, pp. 200–208.
- Varoquaux, Gaël, Pradeep Reddy Raamana, Denis A Engemann, Andrés Hoyos-Idrobo, Yannick Schwartz, and Bertrand Thirion (2017). "Assessing and tuning brain decoders: cross-validation, caveats, and guidelines." In: *NeuroImage* 145, pp. 166–179.
- Varoquaux, Gaël (2018). "Cross-validation failure: Small sample sizes lead to large error bars." In: *NeuroImage* 180, pp. 68–77.
- Verstynen, Timothy D. (2014). "The organization and dynamics of corticostriatal pathways link the medial orbitofrontal cortex to future behavioral responses." In: *J Neurophysio* 112, p. 2457.
- Vukasović, Tena and Denis Bratko (2015). "Heritability of personality: a meta-analysis of behavior genetic studies." In: *Psychological bulletin* 141.4, p. 769.
- Ward, Joe H. (1963). "Hierarchical Grouping to Optimize an Objective Function." In: *Journal of the American Statistical Association* 58, p. 236.
- Wolfers, Thomas, Jan K Buitelaar, Christian F Beckmann, Barbara Franke, and Andre F Marquand (2015). "From estimating activation locality to predicting disorder: a review of pattern recognition for neuroimaging-based psychiatric diagnostics." In: *Neuroscience & Biobehavioral Reviews* 57, p. 328.
- Wolpert, David H (1996). "The lack of a priori distinctions between learning algorithms." In: *Neural computation* 8.7, pp. 1341–1390.

- Wong, Eleanor, Jeffrey S Anderson, Brandon A Zielinski, and P Thomas Fletcher (2018). "Riemannian Regression and Classification Models of Brain Networks Applied to Autism." In: *International Workshop on Connectomics in Neuroimaging*. Springer, pp. 78–87.
- Woo, Choong-Wan, Luke J. Chang, Martin A. Lindquist, and Tor D. Wager (2017). "Building better biomarkers: brain models in translational neuroimaging." en. In: *Nature Neuroscience* 20.3, pp. 365–377.
- Xue, Gui, Adam R. Aron, and Russell A. Poldrack (2008). "Common Neural Substrates for Inhibition of Spoken and Manual Responses." In: *Cerebral Cortex* 18.8, pp. 1923–1932.
- Xue, Gui and Russell A. Poldrack (2007). "The Neural Substrates of Visual Perceptual Learning of Words: Implications for the Visual Word Form Area Hypothesis." In: *J Cog Neurosci* 19, p. 1643.
- Yarkoni, Tal (2015). "Neurobiological substrates of personality: A critical overview." In: *APA handbook of personality and social psychology* 4, pp. 61–83.
- Yeo, B.T.T., F.M. Krienen, J. Sepulcre, M.R. Sabuncu, et al. (2011). "The organization of the human cerebral cortex estimated by intrinsic functional connectivity." In: *J Neurophysio* 106, p. 1125.
- Youyou, Wu, Michal Kosinski, and David Stillwell (2015). "Computer-based personality judgments are more accurate than those made by humans." In: *Proceedings of the National Academy of Sciences* 112.4, pp. 1036–1040.
- Zalesky, Andrew, Alex Fornito, Ian H. Harding, Luca Cocchi, Murat Yücel, Christos Pantelis, and Edward T. Bullmore (2010). "Whole-brain anatomical networks: Does the choice of nodes matter?" In: *NeuroImage* 50, pp. 970–983.
- Zhang, Hui, Torben Schneider, Claudia A. Wheeler-Kingshott, and Daniel C. Alexander (2012). "NODDI: Practical in vivo neurite orientation dispersion and density imaging of the human brain." In: *NeuroImage* 61.4, pp. 1000–1016.
- Zhang, Y., M. Brady, and S. Smith (2001). "Segmentation of brain MR images through a hidden Markov random field model and the expectation-maximization algorithm." In: *IEEE Transactions on Medical Imaging* 20.1, pp. 45–57.
- Zhu, Daqiang, Kaiming Li, Douglas P. Terry, A. Nicholas Puente, Lihong Wang, Dinggang Shen, L. Stephen Miller, and Tianming Liu (2013). "Connectome-scale assessments of structural and functional connectivity in MCI." In: *Human Brain Mapping* 35.7, pp. 2911–2923.

APPENDICES

A | REVIEW OF PREDICTIVE METHODS

A.1 PRACTICES FOR IMAGING-BASED DIAGNOSIS

Reference	Clinical question	#Subjects	Functional matrix	# Nodes	Classifier
	& Accuracy			(type of nodes)	
Nielsen et al., 2013	ASD 60%	964	Pearson's correlation	7266 (coordinates)	SVM
Abraham et al., 2017	ASD 67%	811	Tangent-space parametrization	84 (data-driven)	SVM- ℓ_2
Iidaka, 2015	ASD 90%	640	Pearson's correlation	90 (anatomical)	KDA
Dodero et al., 2015	ASD 60.76%	94	graph Laplacian	264 (coordinates)	Kernel SVM- ℓ_2
Anderson et al., 2014	ADHD 67%	730	Graph Networks	90 (data-driven)	Decision trees
Cheng et al., 2012	ADHD 76%	730	Pearson's correlations	90 (anatomical)	Kernel SVM- ℓ_2
Rashid et al., 2016	Schizo 59.12%	273	Full correlation	100 (data-driven)	SVM
Bassett et al., 2012	Schizo 75%	58	Graph Networks	90 (anatomical)	SVM- ℓ_2
Shen et al., 2010	Schizo 92%	52	Pearson's correlation	116 (anatomical)	C-means
Guo et al., 2012	MDD 79%	76	Graph & Networks	90 (anatomical)	RBF-SVM
Craddock et al., 2009	MDD 95%	40	Pearson's correlation	15 (coordinates)	SVM- ℓ_1
Rosa et al., 2015	MDD 85%	38	Inverse covariance	137 (pre-defined)	SVM- ℓ_1
Chen et al., 2011	AD 87%	55	Pearson's correlation	116 (anatomical)	LDA
Zhu et al., 2013	MCI 96%	28	Pearson's correlation	358 (coordinates)	SVM- ℓ_2

B | TANGENT-SPACE

Most of the methods that we study are readily-available in several computing environments, including Matlab and Python with a variety of well-maintained implementations. However, the only library that provides the tangent-space parametrization of covariance matrices is the Nilearn Python library ¹. To facilitate reproducing our analysis in different environments, we describe here how to compute this parametrization with a few simple formulas. The computation is made of two step: First a group average covariance matrix Σ_* is computed from the covariances of the training subjects: $\{\Sigma_i, i \in \text{Train}\}$. Second, it is used to transform covariance matrices, in the train set or the test set.

B.1 COMPUTING THE TANGENT-SPACE GROUP AVERAGE

As with any analysis based on covariance or correlation matrices, it is preferable to compute individual covariances from time series with an estimator that ensures well-conditioned matrices. The Ledoit and Wolf, 2004a estimator is a good default choice (Brier et al., 2015; Varoquaux and Craddock, 2013).

Strictly speaking, the group average should be computed according to the geometry of covariance matrices (Pennec, Fillard, and Ayache, 2006; Varoquaux et al., 2010c). This is a Frechet mean, which is computed by minimizing a cost function for instance using algorithm 3 of Fletcher and Joshi, 2007. A simpler approach relies on using the Euclidean mean, which we found to give almost the same predictive performance. In this case, the formula of the mean is the standard one:

$$\text{Euclidean mean : } \Sigma_* = \frac{1}{n_{\text{train}}} \sum_{i \in \text{Train}} \Sigma_i \quad (\text{B.1})$$

¹ <http://nilearn.github.io/>

B.2 TRANSFORMING COVARIANCE MATRICES

Given the group reference covariance matrix Σ_* , covariance matrices are transformed in the tangent-space representation by whitening them as follows (Varoquaux et al., 2010c). Computations are easily written with eigenvalues decompositions²: given a subject's covariance matrix Σ_i ,

1. Compute the whitened matrix $\tilde{\Sigma}_i = \Sigma_*^{-1/2} \Sigma_i \Sigma_*^{-1/2}$:

$$\tilde{\Sigma}_i \leftarrow \mathbf{U}^T \Delta^{-\frac{1}{2}} \mathbf{U} \Sigma_i \mathbf{U}^T \Delta^{-\frac{1}{2}} \mathbf{U} \quad (\text{B.2})$$

where $\mathbf{U}^T \Delta \mathbf{U} = \Sigma_*$ by eigen-value decomposition, and operations on the diagonal matrix Δ are element-wise operation applied to the diagonal.

2. Compute the matrix logarithm $\logm \tilde{\Sigma}_i$:

$$\logm(\tilde{\Sigma}_i) = \tilde{\mathbf{U}}^T \log(\tilde{\Delta}_i) \tilde{\mathbf{U}} \quad (\text{B.3})$$

where $\tilde{\Sigma}_i = \tilde{\mathbf{U}}^T \tilde{\Delta}_i \tilde{\mathbf{U}}$ and the logarithm is applied to the diagonal elements of $\tilde{\Delta}_i$.

Finally, the resulting matrix is turned to a vector and its entries are used as features for the classifier.

The motivation from these transformations arises from the fact that covariance matrices –or correlations matrices– form a specific manifold of the $\mathbb{R}^{p \times p}$ matrices. Their structure is broken by standard additive arithmetic's: the difference of two covariances may create a matrix that does not correspond to the covariance matrix of a signal. Optimal statistical analysis calls for following the structure of the manifold (Pennec, Fillard, and Ayache, 2006). The tangent-space parametrization is a simple way to approximate this structure by Euclidean geometry, in which standard additions and subtractions can be used (Varoquaux et al., 2010c).

With regards to statistical analysis, the structure of covariance matrices appears as constraints, or dependencies, between the coefficients of the matrix. As a result, these coefficients alone form a poor representation for second-level statistical analysis. The tangent-space approximation yields a parametrization of the problem in which features are independent identically distributed (i.i.d.) (Varoquaux et al., 2010c). Such a parametrization is optimal for statistical learning. In addition, as discussed in Varoquaux et al. (2010c), this parametrization also gives good edge-level tests for instance see [Figure B.1](#). Hence, the weight vectors of the classifiers can be interpreted as edge-level weights.

² All covariance matrices are symmetric definite positive, and well-conditioned if estimated with the Ledoit-Wolf approach

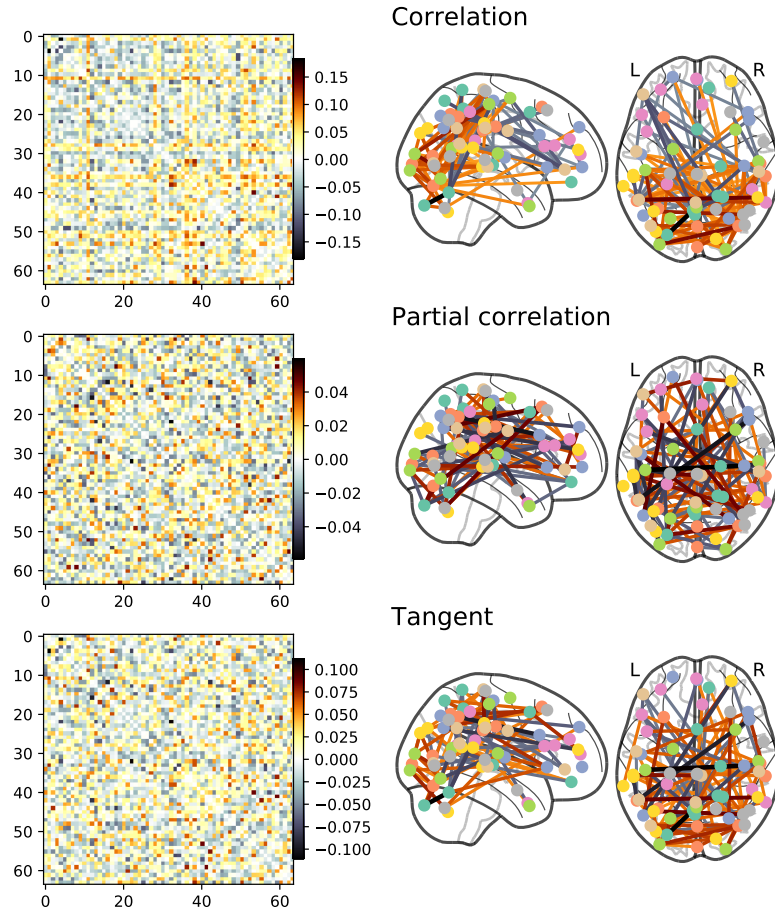


Figure B.1: Difference between mean of MCI and AD group connectivity matrices: We show the connectivity matrices from the ADNI dataset (Mueller et al., 2005) computed on samples diagnosed as Mild Cognitive Impairment (MCI) and Alzheimer’s disease (AD). As can be seen, tangent-space parametrized connections are interpretable and positions in between correlation and partial correlation in terms of connectivity differences. We show the matrices estimated using timeseries extracted with pre-computed MODL dict. learning atlas of $n=64^a$.

^a Pre-computed sparse dictionaries with the MODL approach of Mensch et al., 2016 are available from https://team.inria.fr/parietal/files/2018/10/MODL_rois.zip

C | IMAGING-BASED PREDICTIVE MODELS

C.1 REPRODUCED ON HIGH-QUALITY DATASETS

To investigate the consistency of analytics choices for higher-quality datasets, we perform extra benchmarks including the HCP dataset to probe different setting: data with longer acquisitions. Due to the data size, we limit the benchmarks here to pre-computed atlases. We share the resulting time-series and scripts to reproduce our analysis¹.

HCP DATASET AND A PHENOTYPE STUDIED HCP contains imaging and behavioral data of healthy subjects (Van Essen and Smith, 2013). We use preprocessed rfMRI data from HCP900 release (Van Essen et al., 2012) to discriminate individuals with high vs low intelligence score by splitting the data into 3 groups according to quantiles 0.333 and 0.666. The subjects in the middle group are excluded to make the prediction in a binary classification setup.

Dataset	Prediction task	Groups
HCP	High IQ vs Low IQ	213/230

Table C.1: HCP dataset and prediction task, as well as the number of subjects in each group. HCP - 443. IQ represents fluid intelligence; 788 subjects had an IQ score in the HCP900 release. Table 2.1 denotes other datasets and prediction tasks.

Figure C.1 summarizes the impact of method choice on the prediction accuracy for all six different cohorts. This experiment outline similar tradeoffs as the others: functional atlas pre-computed with dictionary learning (here MODL or SOMF, from Mensch et al., 2016, 2018), tangent-space parametrization, and ℓ_2 -regularized classifiers are preferable. This experiment is not as systematic as the other, as a very large dataset like HCP would require much more computing power to study region extraction². Yet, even for region-definition methods, it outlines similar trends than when tuning the regions to the data at hand.

¹ github.com/KamalakerDadi/benchmark_rsfMRI_prediction

² To ensure a correct nested cross-validation and avoid circularity (overfitting), data-driven region-extraction methods must be run on each fold, hence several hundred time for each pipeline configuration.

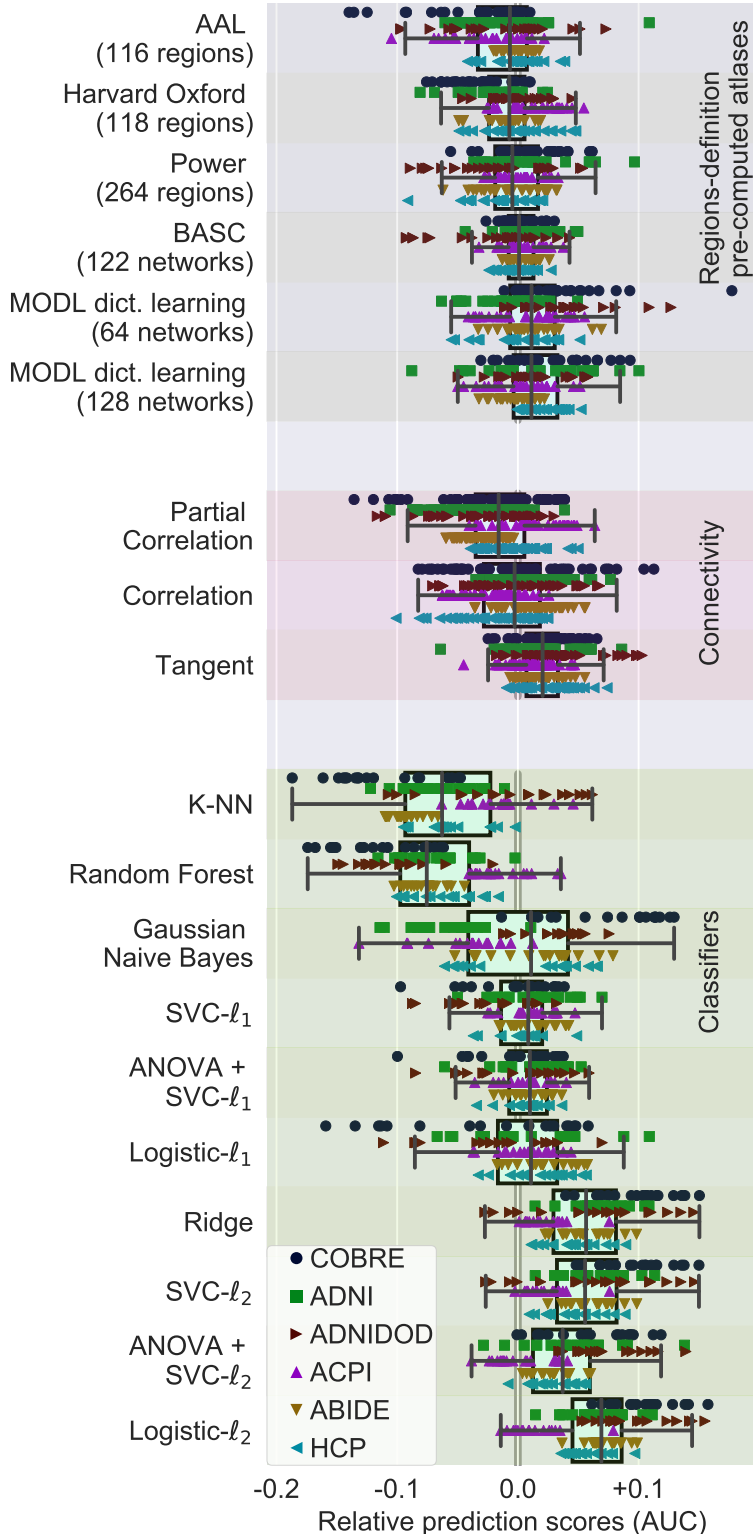


Figure C.1: Pipelining choices with precomputed regions, across six datasets: Marginal distribution of relative prediction scores, using only pre-computed atlases for regions definition, where MODL is a parcellation built using a form of Online dictionary learning. Restricting to pre-computed regions and adding a different dataset (HCP) gives results consistent with Figure 2.5, 2.4, and 2.3: best choices are regions defined functionally, with decomposition methods (MODL) followed by clustering methods (BASC), tangent-space parametrization of connectivity, and ℓ_2 -regularized logistic regression. The box displays the median and quartiles, while the whiskers give the 5th and 95th percentiles.

D | DIFUMO EXTRACTION

D.1 IMPLEMENTATION DETAILS: MODEL PARAMETERS

To run the SOMF algorithm, we relied on the open-source Python package readily available at <https://arthurmensch.github.io/modl/>. The MODL package is implemented using Cython (Dalcin et al., 2011), *scikit-learn* (Pedregosa, Varoquaux, and Gramfort, 2011) and *nilearn* (Abraham et al., 2014b).

We use a coordinate descent algorithm (Friedman et al., 2007) to solve for the inner ℓ_1 regularization problems with positivity constraints. Setting optimum λ for DiFuMo extraction is a challenging task as the DiFuMo extraction is an unsupervised learning problem. On one hand the number of modes extracted should approximately cover the whole brain; on the other hand the overlap should be minimal between the modes. As can be seen from [Table D.1](#), higher λ gives a lower brain coverage whereas lower value has 100% coverage starting from low-dimensions. Yet lower λ creates overlap between the modes as shown on [Figure D.1](#). We set $\lambda = 0.001$ as it provides a good compromise in between modes overlap and brain coverage, as summarized on [Figure D.2](#). It gives full brain coverage for high-order atlases.

Following Mensch et al. (2018), we access a random fraction of each record at each iteration to accelerate training. We use a subsampling ratio value $r = 12$, run the algorithm on a single epoch, and use a learning rate $\beta = 0.92$, as empirically proposed by Mensch et al. (2016). We compute a brain mask that intersect the signal from all the resampled images, using Nilearn (Abraham et al., 2014b). DiFuMo atlases are learned using this mask. The training scripts are available at https://github.com/KamalakerDadi/DiFuMo_analysis_scripts.

D.2 INPUT FMRI DATA

This section gives complementary details to Section 3.3.2. Table D.2 lists the corresponding fMRI data which we relied upon for DiFuMos extraction. The data includes BOLD timeseries from different cognitive tasks and resting-state based studies, the combination of task+rest give 2192 recording sessions to fit the model.

Dimension	λ	Non-zero voxels (%)
64	0.01	12%
	0.001	59%
	0.0001	100%
128	0.01	21%
	0.001	77%
	0.0001	100%
256	0.01	34%
	0.001	98%
	0.0001	100%
512	0.01	51%
	0.001	100%
	0.0001	100%
1024	0.01	73%
	0.001	100%
	0.0001	100%

Table D.1: Coverage of the whole brain (%) as a function of dimension and range of λ in DiFuMo model. While the higher dimension 1024 of DiFuMo maps yields a coverage of the whole brain, other DiFuMo atlases with smaller dimensions do not have such coverage. We recommend the optimum trade-off value as $\lambda = 0.001$ by analysing both the degree of overlap between modes as shown on [Figure D.1](#) and non-zero voxels. A lower λ gives full coverage of the whole brain but suffers from strong overlap between modes whereas higher λ has lost the brain coverage. The values are reported based on union of all modes per dimension.

We also consider extracting DiFuMo from resting-state and task data separately. This is to evaluate the impact of learning functional atlases separately on task and rest fMRI data and compare them to using both data types in the training dataset. For this, we separate the training dataset ([Table D.2](#)) into task fMRI studies and resting-state studies (adding each up to 1970 and 222 fMRI recording sessions respectively). We train DiFuMo atlases (of all dimensions) on each data corpus separately, and compare the performance of the obtained atlases with the atlases trained on both datasets used jointly.

[Figure D.3](#) compares the performance of atlases trained on rest, task and rest+task data, for predicting mental states across 6 task fMRI studies (see [Table D.4](#) for the details about the studies) and predicting traits from connectomes across 7 different cohorts (see [Table D.3](#) for the list of cohorts). Overall, it reveals that using functional modes learnt from both data types – task and rest – marginally improves brain signal extraction.

We do not observe a significant impact of using task-specific modes for predicting traits from functional connectomes. Previous work have established a strong correspondance between resting-state and task

fMRI study	#Subjects	#Sessions	#Runs
(Schonberg et al., 2012)	16	—	3
(Aron, Gluck, and Poldrack, 2006)	17	—	2
(Xue and Poldrack, 2007)	13	—	
(Jimura et al., 2014)	14	2	6
(Xue, Aron, and Poldrack, 2008)	20	—	2
(Aron et al., 2007)	14	—	3
(Foerde, Knowlton, and Poldrack, 2006)	14	—	2
(Rizk-Jackson, Aron, and Poldrack, 2011)	8	2	3
(Alvarez and Poldrack, 2011)	13	—	8
(Poldrack et al., 2001)	14	—	2
(Mennes et al., 2013)	21	—	2
(Kelly et al., 2008)	26	—	2
(Haxby, Gobbini, and Furey, 2001)	6	—	12
(O'Toole et al., 2005)			
(Hanson, Matsuka, and Haxby, 2004)			
(Duncan et al., 2009)	49	—	2
(Moran, Jolly, and Mitchell, 2012)	36	—	2
(Uncapher, Hutchinson, and Wagner, 2011)	18	—	10
(Gorgolewski et al., 2013)	10	2	—
(Repovs and Barch, 2012)	1	—	—
(Cera, Tartaro, and Sensi, 2014)	26	2	3
(Verstynen, 2014)	28	—	—
(Gabitov, Manor, and Karni, 2015)	15	—	3
(Lepping et al., 2016)	39	—	5
(Lepping, Atchley, and Savage, 2016)			
(Iannilli et al., 2016)	1	—	—
(Stephan-Otto et al., 2017)	26	—	2
(Kim et al., 2016)	11	—	2
(Romaniuk et al., 2016)	40	—	—
(Roy et al., 2017)	26	2	—

Table D.2: Large-scale fMRI datasets downloaded from OpenNeuro to build our multi-dimensional DiFuMo atlases. Data are pre-processed using *fMRIprep*. The corpus is 2.4TB in total.

Rest-fMRI	Prediction groups	Samples
HCP900	High IQ vs Low IQ 213/230	443 subjects
ABIDE	Autism vs control 402/464	866 subjects
ACPI	Marijuana use vs control 62/64	126 subjects
ADNI	Alzheimers vs MCI 40/96	136 subjects
ADNIDOD	PTSD vs control 89/78	167 subjects
COBRE	Schizophrenia vs control 65/77	142 subjects
CamCAN	Age 24 – 86	626 subjects

Table D.3: Resting-state fMRI datasets used in the pipeline described on Section 3.4.3 for predicting phenotypic labels from functional connectomes. In CamCAN, age is predicted using ridge regression. The groups from other datasets are predicted using logistic regression. IQ - Fluid intelligence, PTSD, MCI.

functional networks (Bzdok et al., 2016; Smith et al., 2009). This can explain the little difference observed when appending resting-state data to the training corpus.

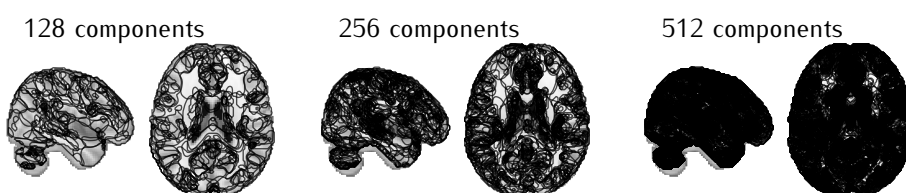


Figure D.1: Overlap between maps with $\lambda = 0.0001$ in DiFuMo model, for DiFuMo dimensionality 64, 256, and 512. As dimensionality increases, subdivisions are strongly overlapped lacking clear delineation across brain regions. [Table D.1](#) gives details about the percentage of non-zero voxels covering whole brain for $\lambda = 0.01, 0.001, 0.0001$

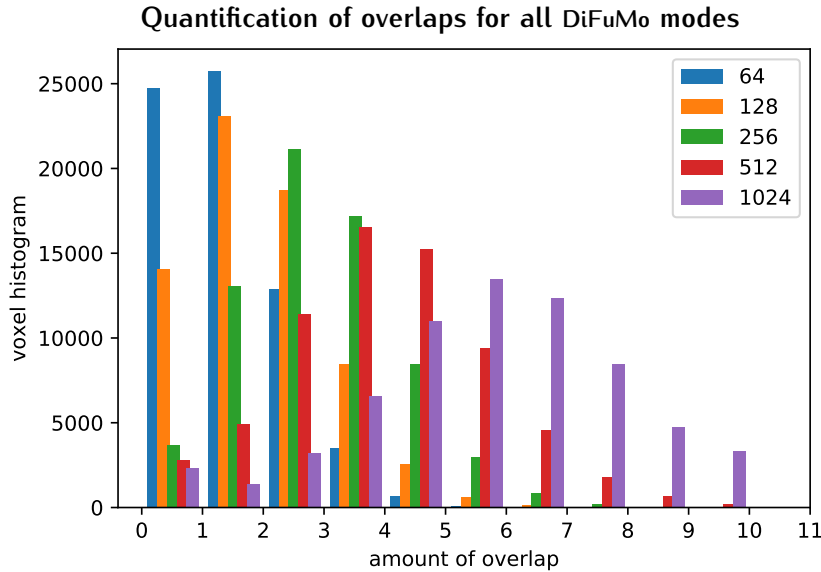


Figure D.2: Comparison of modes overlap for all proposed DiFuMo atlases.

The y-axis shows how many voxels are at the intersect of exactly n modes (x-axis), without thresholding the modes. On average, at least two modes are shared between voxels. Coverage (i.e. low number of voxel at the intersect of 0 mode) is higher for finer grain atlases, at the cost of larger overlap. Note that the overlaps often comprises voxels with small values, and may thus be weak.

Task-fMRI	Prediction task	# maps
NV503: Emotion	Rating:1,2,3,4,5	4924
NV504: Pain	Sensitivity: 1,2,3	84
HCP: Working mem.	face vs place	3140
HCP: Gambling	loss vs reward	1574
HCP: Relational	relational vs matching	1572
IBC: Archi standard	left vs right hand	1040

Table D.4: Dataset, prediction tasks and dataset size for each of the 6 decoding tasks we consider in Section 3.4.2. z-maps from HCP and IBC were computed using the GLM, while NeuroVault directly provided the β -maps for Emotion and Pain. NV: NeuroVault.

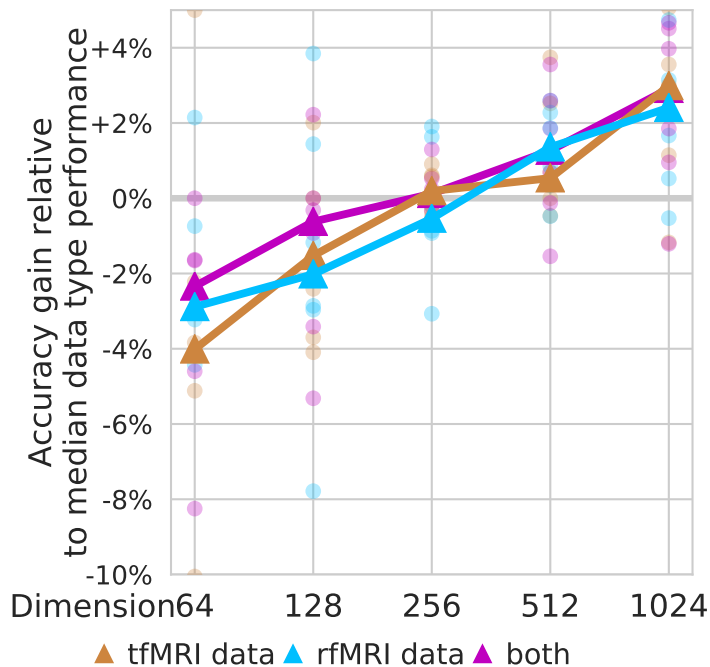
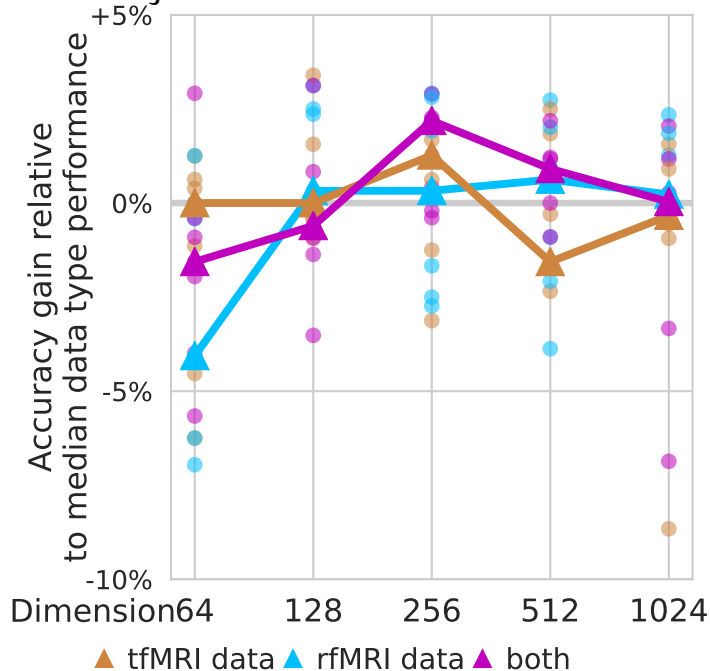
a. Predicting mental tasks**b. Predicting traits from functional connectomes**

Figure D.3: Impact of the choice of DiFuMo atlases training data on decoding and functional connectomes. Each point gives the relative prediction score, over 6 different task fMRI experiments. The thick lines give the median relative score per type of data in task, rest and combination of both. Using the combination of both is marginally better than using task data alone to learn parcellations. We observe no crucial dominance of task-dependent variance in dictionaries in decoding performance.

E | IMAGE-DERIVED PROXY MEASURES

E.1 DATA ACQUISITION DETAILS ON UKBB SAMPLES

Here we detail about data acquisition parameters of multi-modalities of MRI images that we use in our study at Chapter 4.

Non-imaging data were acquired through different assessment procedures across multiple sites¹. Cognitive functioning of each participant was assessed with self-report measures administered through touchscreen questionnaires, complemented by verbal interviews, physical measures, biological sampling and imaging data. Here we focused on the following categories of measures provided by the UKBB: Sociodemographics, Lifestyle and environment, Early life factors, Psychosocial factors and many others. MRI data² were acquired in Manchester with Siemens Skyra 3T using a standard Siemens 32-channel RF receiver head coil (Alfaro-Almagro et al., 2018). We considered three MR imaging modalities as each of them potentially captures unique neurobiological details: sMRI, resting-state functional MRI rfMRI and dMRI. Briefly, the acquisition parameters used for each modality are described here. For additional technical details, refer (Miller et al., 2016).

E.1.1 T1 weighted MRI or structural MRI

We relied on T1-weighted MR sequences used for acquiring high-resolution brain 3D brain volumes. In UKBB, brain volumes were extracted from high-resolution T1 images acquired using a Magnetization-Prepared Rapid Acquisition with Gradient Echo (MPRAGE) sequence at spatial resolution of 1x1x1 mm.

E.1.2 Resting-state functional MRI

Resting-state functional MR images capture low-frequency fluctuations in blood oxygenation that can reveal ongoing neuronal large-scale interactions in distinct brain networks (Biswal et al., 1995). Resting state was acquired using EPI sequences with multi-band acceleration

¹ Details about multiple sites <http://biobank.ctsu.ox.ac.uk/crystal/field.cgi?id=54>

² Details about MRI acquisition and image processing pipelines http://biobank.ctsu.ox.ac.uk/showcase/showcase/docs/brain_mri.pdf

at resolution 2.4x2.4x2.4 mm and repetition time (TR) of 0.735s. As a result 3D volumes were acquired every 0.735s during 6 minutes resulting in 490 brain volumes in time (4D image). All images were acquired in Anterior-Posterior phase encoding direction. For this purpose, participants were instructed to keep their eyes fixated on a crosshair and to “think of nothing in particular.”

E.1.3 Diffusion MRI

Diffusion-weighted imaging is used to measure the local structures in-vivo by tracking the movement of the water molecules along fibre tracts. dMRI were acquired using EPI sequences at resolution 2x2x2 mm with 50 diffusion-encoding directions by varying the field strength b-value=1000, b-value=2000.

E.2 DATA PROCESSING DETAILS ON UKBB SAMPLES

All the MR data preprocessing steps described here were carried out by UKBB brain imaging team³ using software tool called FSL⁴. Briefly, we walk through the steps for each modality.

E.2.1 Structural MRI

After de-identification of faces on raw T1 images, further processing on de-faced T1 images included field distortion correction, reduction of Field of View (FoV) and skull stripping using Brain Extraction Tool (BET) (Smith, 2002) followed by registration to MNI152 T1 template space using (FLIRT) (Jenkinson and Smith, 2001; Jenkinson et al., 2002b). The images were then warped to MNI152 template using non-linear registration method (FNIRT) (Andersson et al., 2007) and segmented into most prominent tissue types such as Gray Matter (GM), White Matter (WM) and Cerebro-Spinal Fluid (CSF) volumes using FAST segmentation method (Zhang, Brady, and Smith, 2001). This whole process yielded a full bias field corrected T1 images which were then further processed to generate IDPs. The IDPs based on sMRI are volumes of 157 grey matter cortical and subcortical anatomical structures⁵, in total modelled with SIENAX (Smith et al., 2002) and FIRST (Patenaude et al., 2011) tools.

³ MR data processing details http://biobank.ctsu.ox.ac.uk/showcase/showcase/docs/brain_mri.pdf

⁴ <https://fsl.fmrib.ox.ac.uk/fsl/fslwiki>

⁵ The ROIs are the combinations from several atlases: Harvard-Oxford cortical and subcortical atlases, and Diedrichsen cerebellar atlas.

E.2.2 Diffusion MRI

The preprocessing of diffusion weighted images includes: correction for eddy current distortions, head motion and removal of image slices lying outside the brain (Andersson and Sotropoulos, 2015). These corrected images were followed by gradient distortion correction. The preprocessed images were then further processed for IDPs. For this purpose, images were separately fed into Diffusion Tensor Imaging (DTIFIT) tool to model the 50 diffusion directions to generate IDPs, e.g. FA, MO, MD and NODDI (Neurite Orientation Dispersion and Density Imaging) estimates using AMICO (Accelerated Microstructure Imaging via Convex Optimization) (Daducci et al., 2015; Zhang et al., 2012). This also enabled modeling the biological properties of fiber tracts visible in the form of IDPs, ICVF, ISOVF and OD. In order to facilitate cross-subject comparisons on fiber tract based IDPs, all the outputs need to be aligned to common space. This was achieved using an approach called tract-based spatial statistics (TBSS) (Smith et al., 2006). For more details on the technical aspects like cross-alignment procedures can be found in (Alfaro-Almagro et al., 2018; Groot et al., 2013).

E.2.3 Resting-state fMRI

We applied the following pre-processing pipeline on rfMRI data before processing for IDPs. The pipeline started with motion correction using MCFLIRT (Jenkinson et al., 2002b), grand-mean intensity normalisation and high-pass temporal filtering (Gaussian-weighted least-squares straight line fitting, with sigma=50.0s) including the unwarping of EPI and co-registration to T1 template and GDC. Finally, structured artefacts were removed by ICA followed by FIX cleaning (FMRIB's ICA-based X-noiseifier). After pre-processing, the next step was to identify the resting-state networks (RSN) on a group of subjects using linear decomposition method called ICA (Hyvärinen, 1999) implemented with MELODIC tool (Beckmann and Smith, 2004b). Group-PCA algorithm was then applied on the preprocessed rfMRI images as a dimensionality reduction step before feeding into MELODIC ICA to identify RSN at higher resolution i.e. 100 ICA components. These ICA components were quality-checked and 45 components were identified as artifactual components (components of no interest). The remaining 55 components were used for further processing to get IDPs. The 55 ICA components are identified on group of 4100 UKBB rfMRI images and easily accessible at this location. The next step is to extract subject-specific time series signals by projecting ICA components onto each individual raw rfMRI images. In total, 55 signals per subject were extracted using the first stage in the dual regression analysis (Filippini et al., 2009). We then estimated connectivity matrices on the ensuing time series based

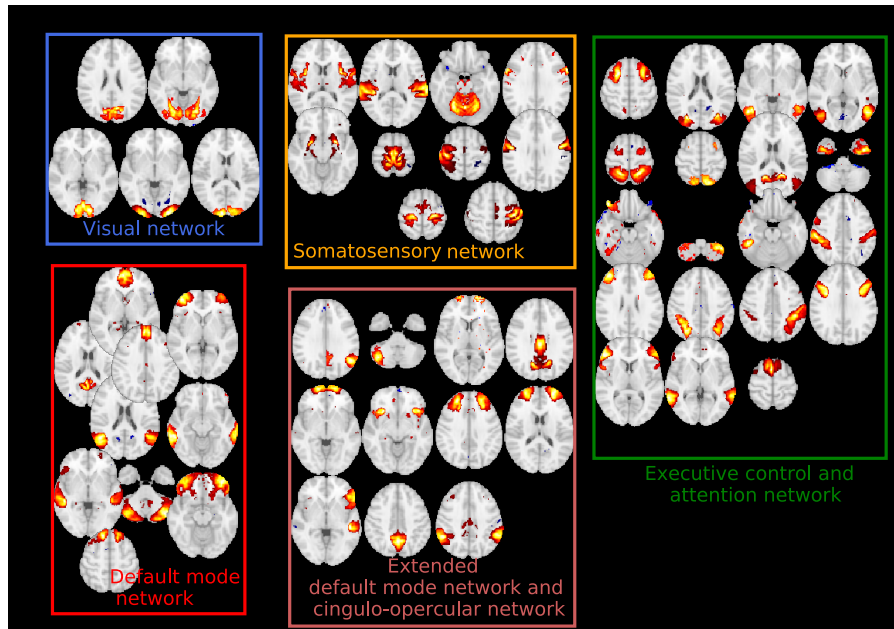


Figure E.1: ICA components (n=55) on UKBB resting-state fMRI data. Resting-state functional connectivity features are estimated from these wide-range of functional brain networks.

Group	eid	Variables
1: Age, Sex	31-0.0	Sex
	34-0.0	Year of birth
	52-0.0	Month of birth
	21022-0.0	Age at recruitment
	21003-2.0	Age when attended assessment centre

Table E.1: List of 5 baseline variables grouped into Age, Sex.

on a regularized covariance estimate (Ledoit and Wolf, 2004b). We then mapped the covariance matrices into a Euclidean representation based on the Riemannian tangent space embedding as proposed in (Varoquaux et al., 2010d). We then vectorized the connectivity matrices by extracting the lower triangular part and used them as the rfMRI features for supervised learning. The tangent space parametrization was implemented with Nilearn (Abraham et al., 2014a).

E.3 MORE EXPERIMENTS

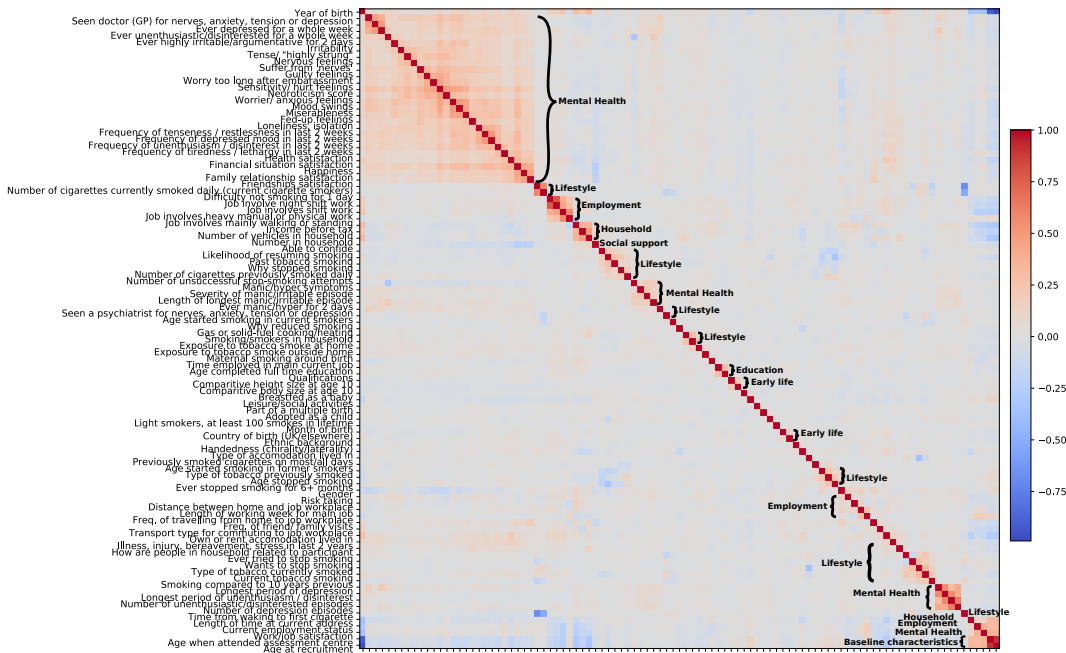


Figure E.2: Pearson's correlation coefficients across non-imaging UKBB variables. The coefficients are reordered to form a block-like structure easy to form 5 groups where each group is assigned to correlated variables.

Group	eid	Variables
3: Education	6138-2.0	Qualifications
	845-2.0	Age completed full time education

Table E.2: List of 2 variables grouped into Education.

Group	eid	Variables
2: Early life	1647-2.0	Country ogf birth (UK/elsewhere)
	1677-2.0	Breastfed as a baby
	1687-2.0	Comparative body size at age 10
	1697-2.0	Comparative height size at age 10
	1707-2.0	Handedness (chirality/laterality)
	1767-2.0	Adopted as a child
	1777-2.0	Part of a multiple birth
	1787-2.0	Maternal smoking around birth

Table E.3: List of 9 non-imaging variables grouped into Early life.

Group	eid	Variables
4: Lifestyle	670-2.0	Type of accommodation lived in
	680-2.0	Own or rent accommodation lived in
	6139-2.0	Gas or solid-fuel cooking/heating
	699-2.0	Length of time at current address
	709-2.0	Number in household
	6141-2.0	How are people in household related to participant
	728-2.0	Number of vehicles in household
	738-2.0	Income before tax
	796-2.0	Distance between home and job workplace
	757-2.0	Time employed in main current job
	767-2.0	Length of working week for main job
	777-2.0	Freq. of travelling from home to job workplace
	6143-2.0	Transport type for commuting to job workplace
	6142-2.0	Current employment status
	806-2.0	Job involves mainly walking or standing
	816-2.0	Job involves heavy manual or physical work
	826-2.0	Job involves shift work
	3426-2.0	Job involves night shift work
	1031-2.0	Freq. of friend / family visits
	6160-2.0	Leisure/social activities
	2110-2.0	Able to confide
	1239-2.0	Current tobacco smoking
	1249-2.0	Past tobacco smoking
	1259-2.0	Smoking/smokers in household
	1269-2.0	Exposure to tobacco smoke at home
	1279-2.0	Exposure to tobacco smoke outside home
	2644-2.0	Light smokers, at least 100 smokes in lifetime
	2867-2.0	Age started smoking in former smokers
	2877-2.0	Type of tobacco previously smoked
	2887-2.0	Number of cigarettes previously smoked daily
	2897-2.0	Age stopped smoking
	2907-2.0	Ever stopped smoking for 6+ months
	2926-2.0	Number of unsuccessful stop-smoking attempts
	2936-2.0	Likelihood of resuming smoking

Table E.4: List of non-imaging variables grouped into Lifestyle.

Group	eid	Variables
4: Lifestyle	3436-2.0	Age started smoking in current smokers
	3446-2.0	Type of tobacco currently smoked
	3456-2.0	Number of cigarettes currently smoked daily (current cigarette smokers)
	3466-2.0	Time from waking to first cigarette
	3476-2.0	Difficulty not smoking for 1 day
	3486-2.0	Ever tried to stop smoking
	3496-2.0	Wants to stop smoking
	3506-2.0	Smoking compared to 10 years previous
	5959-2.0	Previously smoked cigarettes on most/all days
	6157-2.0	Why stopped smoking
	6158-2.0	Why reduced smoking

Table E.5: Continuation to previous Table E.4 non-imaging lifestyle variables.

Group	eid	Variables
5: Mental Health	2040-2.0	Risk taking
	4526-2.0	Happiness
	4537-2.0	Work/job satisfaction
	4548-2.0	Health satisfaction
	4559-2.0	Family relationship satisfaction
	4570-2.0	Friendships satisfaction
	4581-2.0	Financial situation satisfaction
	4598-2.0	Ever depressed for a whole week
	4609-2.0	Longest period of depression
	4620-2.0	Number of depression episodes
	4631-2.0	Ever unenthusiastic/disinterested for a whole week
	4642-2.0	Ever manic/hyper for 2 days
	4653-2.0	Ever highly irritable/argumentative for 2 days
	2050-2.0	Frequency of depressed mood in last 2 weeks
	2060-2.0	Frequency of unenthusiasm / disinterest in last 2 weeks
	2070-2.0	Frequency of tenseness / restlessness in last 2 weeks

Table E.6: List of 16 mental health variables from a total of 25.

Group	eid	Variables
5: Mental Health	2080-2.0	Frequency of tiredness / lethargy in last 2 weeks
	2090-2.0	Seen doctor (GP) for nerves, anxiety, tension or depression
	2100-1.0	Seen a psychiatrist for nerves, anxiety, tension or depression
	5375-2.0	Longest period of unenthusiasm / disinterest
	5386-2.0	Number of unenthusiastic/disinterested episodes
	5663-2.0	Length of longest manic/irritable episode
	5674-2.0	Severity of manic/irritable episode
	6145-2.0	Illness, injury, bereavement, stress in last 2 years
	6156-2.0	Manic/hyper symptoms

Table E.7: Remaining list mental health variables from a total of 25.
[Linked to Table E.6](#)

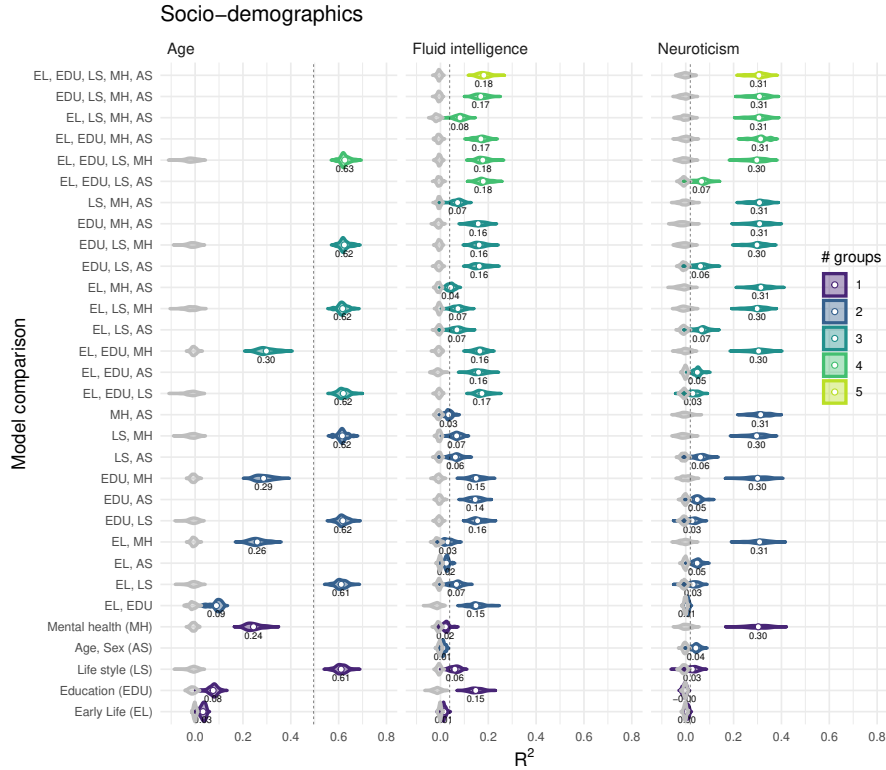


Figure E.3: Prediction of individual differences from socio-demographic data. Prediction of age, fluid intelligence and neuroticism based from 86 socio-demographic variables ordered from lower to higher i.e. a single group to 5 groups as introduced on Table E.8. Models are based on non-exhaustive combinations of variables related to early life factors (EL), education (EDU), life-style (LS) and measures related to age and sex (AS). Color indicates the number of blocks of variables per model. We used the R^2 score to facilitate comparisons across prediction targets. The estimated null-distribution is depicted by gray violin plots. The expected prediction performance is depicted by colored violin plots. Vertical dotted lines indicate the average performance of the full MRI model introduced in Fig. 4.4. For convenience, the mean performance is annotated for each plot. One can readily see that prediction with socio-demographics was markedly stronger than with the brain-based model for all three targets. Education related variables explains most of fluid intelligence prediction and similarly mental health for neuroticism prediction. On the other hand, lifestyle showed impact on age prediction when socio-demographic variables are considered. This plot is related to the simplified plot in Fig. 4.2. Overall, considering full socio-demographics (5 groups = 86 variables) explains better predictions significance of additive learning effects.

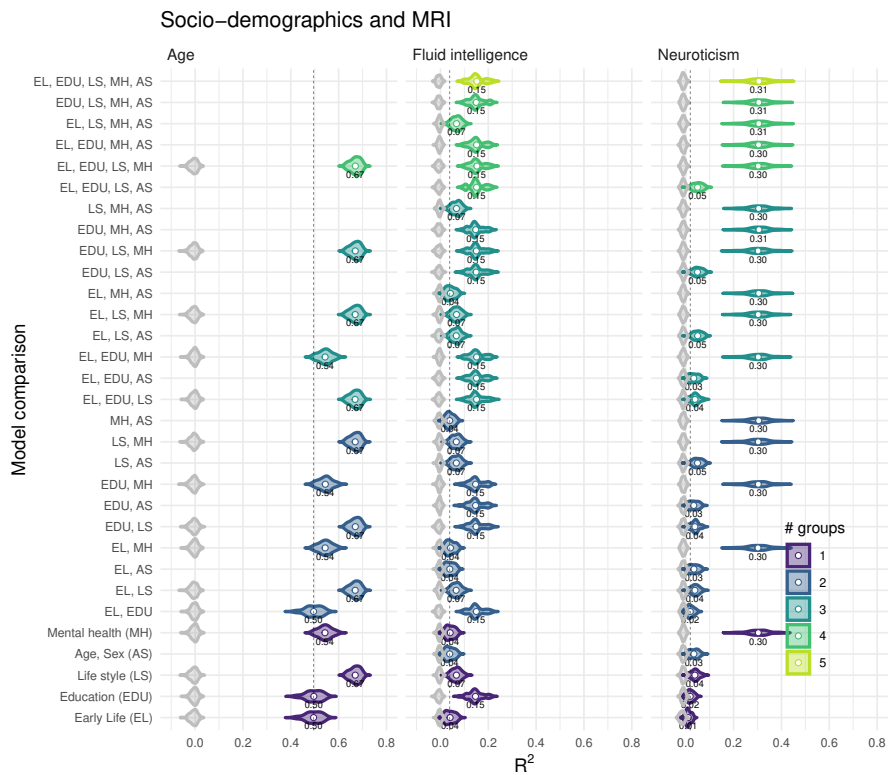


Figure E.4: Prediction of individual differences from imaging and socio-demographic data. Prediction of age, fluid intelligence and neuroticism based from 86 socio-demographic variables Table E.8 and the 2074 variables included in the full-MRI model from Fig. 4.4. Rules for graphical display as in Fig. E.3. One can see that the effect of combining socio-demographics with brain-data depended on the prediction target. For age, overall performance improved beyond the previous analyses. The picture was less consistent for fluid intelligence and neuroticism.

Index	Name	# variables	# groups
1	EL, EDU	11	2
2	EL, LS	54	2
3	EL, AS	14	2
4	EL, MH	34	2
5	EDU, LS	47	2
6	EDU, AS	7	2
7	EDU, MH	27	2
8	LS, AS	50	2
9	LS, MH	70	2
10	MH, AS	30	2
11	EL, EDU, LS	56	3
12	EL, EDU, AS	16	3
13	EL, EDU, MH	36	3
14	EL, LS, AS	59	3
15	EL, LS, MH	79	3
16	EL, MH, AS	39	3
17	EDU, LS, AS	52	3
18	EDU, LS, MH	72	3
19	EDU, MH, AS	32	3
20	LS, MH, AS	75	3
21	EL, EDU, LS, MH	81	4
22	EL, EDU, LS, AS	61	4
23	EL, EDU, MH, AS	41	4
24	EL, LS, MH, AS	84	4
25	EDU, LS, MH, AS	77	4
26	EL, EDU, LS, MH, AS	86	5

Table E.8: More non-imaging baseline models, a progressive extension of models reported on Table 4.2. These models are based on the combination of two or more groups: Early Life (EL), Education (EDU), Life style (LS), Mental health (MH), Age, Sex (AS). Random forest model paramters tuned with in-built cross-validation Number of trees is set by stabilization of out-of-bag (OOB) error rate after trying from a range of values in 250, 350, 500, 800, 1000, 2000, 3000, 5000.

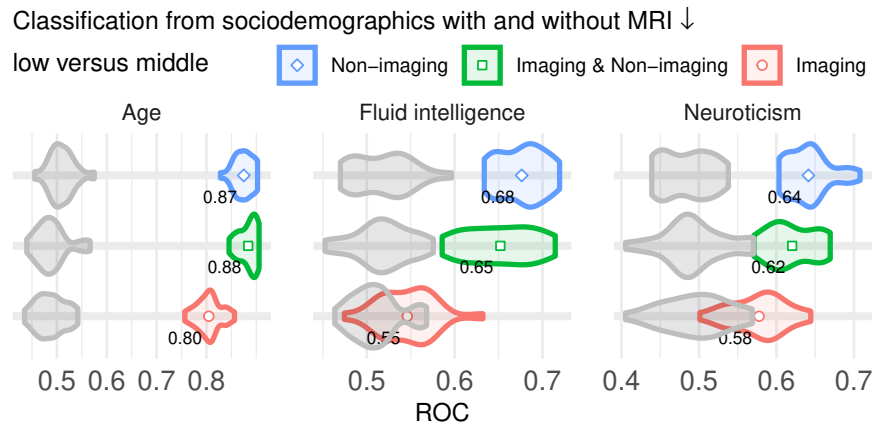


Figure E.5: Classification analysis from imaging, socio-demographics and combination of both data of low versus middle groups on the basis of age, fluid intelligence and neuroticism scores. This analysis reveals model comparison outputs in contrast to the predictions on Figs. 4.3 and E.6. Shape and color indicates the type of data used for model comparison on these binary groups. We report the accuracy in AUC. The estimated null-distribution is shown in gray violin plots whereas colored violin plots depict the distribution of classification accuracies per model. The mean value is shown on each violin plot to facilitate easy comparisons across classification groups. We observe low classification accuracies using these groups while comparing to classification accuracies with low vs high groups as on Fig. 4.3. Overall, the model comparisons showed consistency with low vs high groups i. e. socio-demographics data gave better prediction performance than imaging with fluid intelligence and neuroticism as proxy measures. Adding brain imaging to socio-demographics improves age prediction than socio-demographics or imaging alone.

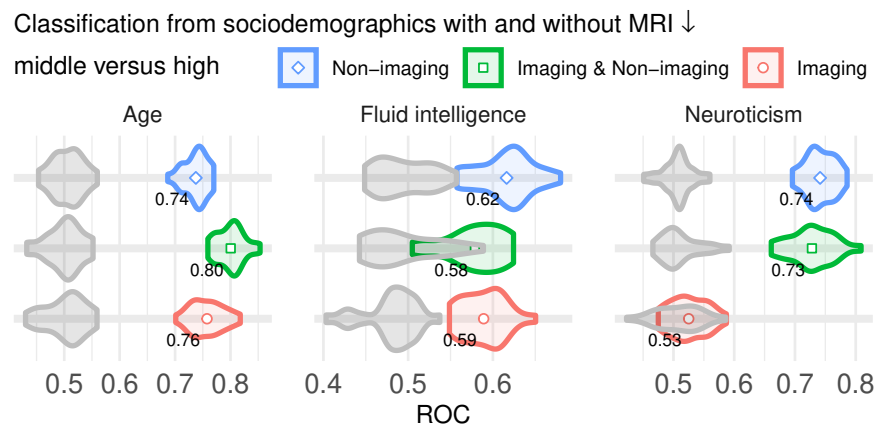


Figure E.6: Classification analysis from imaging, socio-demographics and combination of both data of middle vs high groups on the basis of age, fluid intelligence and neuroticism scores. This analysis reveals model comparison outputs in contrast to the predictions on Figs. 4.3 and E.5. Shape and color indicates the type of data used for model comparison on these binary groups. We report the accuracy in AUC. The estimated null-distribution is shown in gray violin plots whereas colored violin plots depict the distribution of classification accuracies per model. The mean value is shown on each violin plot to facilitate easy comparisons across classification groups. We observe low classification accuracies using these groups while comparing to classification accuracies with low vs high groups as on Fig. 4.3. Overall, the model comparisons showed socio-demographics data gave better prediction performance than imaging with fluid intelligence and neuroticism while brain-imaging brings in additive predictive effects for age prediction.

Titre: Apprentissage statistique sur l'imagerie de population pour la santé mentale

Mots clés: Apprentissage statistique, imagerie cérébrale, psychiatrie

Résumé: Les troubles mentaux présentent une grande hétérogénéité entre les individus. Une difficulté fondamentale pour étudier leurs manifestations ou leurs facteurs de risque est que le diagnostic des conditions mentales pathologiques est rarement disponible dans les grandes cohortes de santé publique. Ici, nous cherchons à développer des biomarqueurs, signatures cérébrales de troubles mentaux. Pour cela, nous utilisons l'apprentissage automatique pour prédire les résultats de santé mentale grâce à l'imagerie de population, en se basant sur l'imagerie cérébrale (imagerie par résonance magnétique (IRM)). Compte tenu des évaluations comportementales ou cliniques, l'imagerie de population peut relier les caractéristiques uniques des variations cérébrales à ces mesures autodéclarées non cérébrales basées sur des questionnaires. Ces mesures non cérébrales fournissent une description unique des différences psychologiques de chaque individu qui peuvent être liées à la psychopathologie à l'aide de méthodes statistiques. Cette thèse de doctorat examine le potentiel d'apprentissage de tels résultats basés sur l'imagerie pour analyser la santé mentale. En utilisant des méthodes d'apprentissage automatique, nous effectuons une évaluation, à la fois complète et robuste, des mesures de population pour guider des prévisions de haute qualité des résultats pour la santé.

Cette thèse est organisée en trois parties principales: premièrement, nous présentons une étude approfondie des biomarqueurs du connectome, deuxièmement, nous proposons une réduction significative des données qui facilite les études d'imagerie de population à grande échelle, et enfin nous introduisons des mesures indirectes pour la santé mentale.

Nous avons d'abord mis en place une étude approfondie des connectomes d'imagerie afin de prédire les phénotypes cliniques. Avec l'augmentation des images cérébrales de haute

qualité acquises en l'absence de tâche explicite, il y a une demande croissante d'évaluation des modèles prédictifs existants. Nous avons effectué des comparaisons systématiques reliant ces images aux évaluations cliniques dans de nombreuses cohortes pour évaluer la robustesse des méthodes d'imagerie des populations pour la santé mentale. Nos résultats soulignent la nécessité de fondations solides dans la construction de réseaux cérébraux entre les individus. Ils décrivent des choix méthodologiques clairs.

Ensuite, nous contribuons à une nouvelle génération d'atlas fonctionnels du cerveau pour faciliter des prédictions de haute qualité pour la santé mentale. Les atlas fonctionnels du cerveau sont en effet le principal goulot d'étranglement pour la qualité de la prédiction. Ces atlas sont construits en analysant des volumes cérébraux fonctionnels à grande échelle à l'aide d'un algorithme statistique évolutif, afin d'avoir une meilleure base pour la prédiction des résultats. Après les avoir comparés avec des méthodes de pointe, nous montrons leur utilité pour atténuer les problèmes de traitement des données à grande échelle.

La dernière contribution principale est d'étudier les mesures de substitution potentielles pour les résultats pour la santé. Nous considérons des comparaisons de modèles à grande échelle utilisant des mesures du cerveau avec des évaluations comportementales dans une cohorte épidémiologique d'imagerie, le UK Biobank. Dans cet ensemble de données complexe, le défi consiste à trouver les covariables appropriées et à les relier à des cibles bien choisies. Cela est difficile, car il y a très peu de cibles pathologiques fiables. Après une sélection et une évaluation minutieuses du modèle, nous identifions des mesures indirectes qui sont en corrélation avec des conditions non pathologiques comme l'état de sommeil, la consommation d'alcool et l'activité physique. Ceux-ci peuvent être indirectement utiles pour l'étude épidémiologique de la santé mentale.

Title: Machine Learning on Population Imaging for Mental Health

Keywords: Statistical learning, brain imaging, psychiatry

Abstract: Mental disorders display a vast heterogeneity across individuals. A fundamental challenge to studying their manifestations or risk factors is that the diagnosis of mental pathological conditions are seldom available in large public health cohorts. Here, we seek to develop brain signatures, biomarkers, of mental disorders. For this, we use machine learning to predict mental-health outcomes through population imaging i. e. with brain imaging (Magnetic Resonance Imaging (MRI)). Given behavioral or clinical assessments, population imaging can relate unique features of the brain variations to these non-brain self-reported measures based on questionnaires. These non-brain measurements carry a unique description of each individual's psychological differences which can be linked to psychopathology using statistical methods. This PhD thesis investigates the potential of learning such imaging-based outcomes to analyze mental health. Using machine-learning methods, we conduct an evaluation, both a comprehensive and robust, of population measures to guide high-quality predictions of health outcomes.

This thesis is organized into three main parts: first, we present an in-depth study of connectome biomarkers, second, we propose a meaningful data reduction which facilitates large-scale population imaging studies, and finally we introduce proxy measures for mental health.

We first set up a thorough benchmark for imaging-connectomes to predict clinical phenotypes. With the rise in the high-quality brain images acquired without tasks, there is an increasing demand in evaluation of existing mod-

els for predictions. We performed systematic comparisons relating these images to clinical assessments across many cohorts to evaluate the robustness of population imaging methods for mental health. Our benchmarks emphasize the need for solid foundations in building brain networks across individuals. They outline clear methodological choices.

Then, we contribute a new generation of brain functional atlases to facilitate high-quality predictions for mental health. Brain functional atlases are indeed the main bottleneck for prediction. These atlases are built by analyzing large-scale functional brain volumes using scalable statistical algorithm, to have better grounding for outcome prediction. After comparing them with state-of-the-art methods, we show their usefulness to mitigate large-scale data handling problems.

The last main contribution is to investigate the potential surrogate measures for health outcomes. We consider large-scale model comparisons using brain measurements with behavioral assessments in an imaging epidemiological cohort, the United Kingdom (UK) Biobank. On this complex dataset, the challenge lies in finding the appropriate covariates and relating them to well-chosen outcomes. This is challenging, as there are very few available pathological outcomes. After careful model selection and evaluation, we identify proxy measures that display distinct links to socio-demographics and may correlate with non-pathological conditions like the condition of sleep, alcohol consumption and physical fitness activity. These can be indirectly useful for the epidemiological study of mental health.